UNIVERSIDAD AUTÓNOMA DE MADRID

Departamento de Física de la Materia Condensada

EMERGENT GAUGE FIELDS AND TOPOLOGICAL EFFECTS IN DIRAC MATTER

Tesis doctoral presentada por
Yago Ferreirós Bas

Programa de Doctorado de Física de la Materia Condensada y Nanotecnología

---

Directores:
Alberto Cortijo
María Ángeles Hernández Vozmediano

Tutor:
Nicolás Agraït

Madrid, Junio 2016

Agradecimientos

Esta tesis no hubiera sido posible sin el incondicional apoyo de muchas personas. El principal motivo de que yo esté en este momento escribiendo estas líneas, es el apoyo de Geli y Alberto, mis tutores de tesis. Siempre estaré agradecido por la manera en la que me han apoyado, y por todo el tiempo que han dedicado para ayudarme en mi formación como científico, así como en otros aspectos de la vida. Trabajar con ellos ha sido todo un placer, a la vez que un bonito reto, y cualquier logro que esté por venir en mi carrera se lo deberé a ambos. Quiero dar las gracias también a Tony, uno de los mejores físicos que he conocido y una pieza fundamental en mi formación, y a Nicolás por haber accedido a tutelar esta tesis y haberse mostrado tan accesible.

Durante el transcurso de la tesis, he tenido el honor de colaborar con grandísimos científicos. La sabiduría y claridad de ideas de Karl ha sido un ejemplo para mí, y los consejos de Fito, Fernando y Héctor, tanto de física como de otros aspectos de la vida investigadora, han supuesto una ayuda inestimable. He podido aprender mucho de Paco, uno de los grandes, en especial de su inigualable intuición para la física, así como de Belén, Rafa y Pablo. My stay in Nijmegen was a fantastic experience, and I want to really thank Misha for his hospitality, his time to discuss physics with me, and specially for making a fruitful scientific collaboration possible. I really enjoyed the discussions with Frank, and the warm atmosphere at the department: Zhenya, Guus, Hylke... all very nice people.

La agradable vida en el ICMM ha contribuído a que todo fuera más fácil. Agradezco a todos los compañeros del grupo, o que alguna vez lo fueron, por el magnífico tiempo que hemos pasado juntos, especialmente durante las comidas: Ángel, Jose, Francesca, Luca, Bruno, Nacho, Laura, Mauricio, Vincenzo, Vicente, Raquel... He de dar las gracias también a mis compañeros de despacho, Mónica, Fernando y Jose Carlos, por contribuir a crear un ambiente agradable, en el cual me he sentido realmente a gusto.

No podría dejar de agradecer el apoyo y el tiempo pasado con los compañeros de las mesas. Gracias a Peibol, Edu, Paula, Miguel, Manuela, Paloma, Clara, Luis, Drino, Emilio y todos aquellos que estuvieron presentes durante los años de universidad. Quiero hacer también una mención especial a los amigos de la infancia en el colegio,

cuya amistad he mantenido hasta hoy, y que han contribuído a moldear la persona en la que me he convertido: Pelu, Galla, Frodo, Íñigo, Marcos y Román. En especial a uno de ellos, Pelu, le estaré siempre agradecido por saber que siempre va a estar ahí, tanto en los buenos como en los malos momentos.

Para ir terminando, quiero agradecer a mis padres su apoyo infinito y su dedicación absoluta. Es sobre todo gracias a ellos que he encontrado la fuerza necesaria para acometer este desafiante reto. Es realmente tranquilizador saber que siempre estarán ahí, apoyando mi carrera.

Por último, quiero dedicar unas palabras a Tamara. Nunca he tenido más tranquilidad y convicción para llevar a buen puerto mi carrera investigadora como desde que estamos juntos. Es el motor que me impulsa, nada de esto sería posible sin ella.

Publication list

The research performed during the development of this thesis has led to the following publications:

1. *Domain wall motion in junctions of thin-film magnets and topological insulators.*
   Yago Ferreiros, Alberto Cortijo,
   Phys. Rev. B 89, 024413 (2014).

2. *Large conduction band and Fermi velocity spin splitting due to Coulomb interactions in single-layer MoS_2.*
   Yago Ferreiros, Alberto Cortijo,
   Phys. Rev. B 90, 195426 (2014).

3. *Dirac electrons and domain walls: a realization in junctions of ferromagnets and topological insulators.*
   Yago Ferreiros, Frank Buijnsters, M. I. Katsnelson,
   Phys. Rev. B 92, 085416 (2015).

4. *Elastic gauge fields in Weyl semimetals.*
   Alberto Cortijo, Yago Ferreiros, Karl Landsteiner, Maria A. H. Vozmediano,
   Phys. Rev. Lett. 115, 177202 (2015).

5. *Visco elasticity in 2D materials.*
   Alberto Cortijo, Yago Ferreiros, Karl Landsteiner, Maria A. H. Vozmediano,
   2D Mater. 3 011002 (2016).

6. *Unconventional electromagnetic mode in neutral Weyl semimetals.*
   Yago Ferreiros, Alberto Cortijo,
   Phys. Rev. B 93, 195154 (2015).

Other publications during this period:

- *Quantum corrections to vortex masses and energies.*
  Yago Ferreiros, Antonio Gonzalez-Arroyo,
  Phys. Rev. D 90, 025004 (2014).

- *Chirality-dependent transmission of spin waves through domain walls.* Frank Buijnsters, Yago Ferreiros, A. Fasolino, M. I. Katsnelson, Phys. Rev. Lett. 116, 147204 (2016).

Abstract

In this thesis we deal with systems hosting Dirac quasiparticles. The main focus is put on the physics arising from the interplay of non trivial topology and the emergence of gauge fields, stemming from the interaction of electrons with either magnetic and elastic degrees of freedom. The investigation relies on tools from quantum field theory, in particular the theory of quantum anomalies and topological field theory. The physical systems involved are two dimensional Dirac materials, like graphene and single layer transition metal dichalcogenide semiconductors; three dimensional time reversal invariant topological insulators, from which we focused on the two dimensional physics occurring at the edge; and Weyl semimetals. Under certain conditions, all these materials can be expected to be in a topological phase of matter, denoted quantum Hall state. Most of the results derived in this thesis are consequences of the special properties of this state of matter.

Resumen

En esta tesis tratamos con sistemas que albergan quasipartículas de Dirac. La atención se centra en la física que surge de la interrelación entre la topología y los campos gauge emergentes en ciertos materiales, derivados de la interacción de los electrones con los grados de libertad magnéticos y elásticos. La investigación se soporta en las herramientas de la teoría cuántica de campos, en particular en la teoría de anomalías cuánticas y la teoría de campos topológica. Los sistemas físicos tratados son materiales de Dirac en dos dimensiones, como el grafeno y semiconductores dicalcogenuros de metales de transición; aislantes topológicos tridimensionales, en los cuales nos centramos en la física bidimensional de su superficie; y semimetales de Weyl. Bajo ciertas condiciones, se puede esperar que estos materiales se encuentren en una fase topológica de la materia, llamada estado Hall cuántico. La mayoría de los resultados obtenidos en esta tesis son consecuencia de las propiedades especiales de este estado de la materia.

Introduction

Dirac matter refers to those materials whose low energy electronic quasiparticle excitations behave as Dirac fermions. The most popular example of a gapless 2D Dirac material is graphene[1, 2], in which the spin of the Dirac spinor is not the real spin, but a pseudospin related to the sublattice degrees of freedom. Beyond graphene, other important materials hosting 2D Dirac pseudospinors are the transition metal dicalcogenide (TMD) semiconductors [3, 4] which, unlike graphene, have a gaped spectrum which could be important for technological applications. With the emergence of 3D topological insulators (TI)[5, 6, 7], a new realization of 2D Dirac fermions arises as gapless excitations localized on the boundary of a 3D material, as a consequence of the topology of the bulk. The spinorial degree of freedom of these boundary fermions is the real spin of the electrons, and their gapless nature implies that their spin orientation is aligned with their propagation direction. This maximizes the effects of spin-orbit coupling which is very valuable for spintronic applications[8].

More recently, new materials hosting gapless Dirac fermions have been discovered in 3D, which are called Dirac semimetals[9]. In those Dirac semimetals having inversion or time reversal (**T**) symmetry broken, the four component spinor splits into two two component Weyl spinors, separated in four-momentum space. These are called Weyl semimetals (WSMs), which were first proposed to occur in a class of iridate materials[10], and their experimental realization during the last year[11, 12, 13, 14, 15] has given rise to an intense theoretical and experimental activity associated to new material types, and to the possibility of exploring the exotic physics associated to chiral matter.

An important aspect of Weyl fermions in quantum field theory is the presence of quantum anomalies. They are produced when a symmetry transformation of a classical system, either external (space-time transformations like translations or rotations) or internal (like global phase or gauge transformations), is broken by quantum fluctuations. The most prominent example is the chiral anomaly of Weyl fermions in even space-time dimensions, which represents a non conservation of chiral charge at the quantum level, but there are others equally sound like the gravitational anomaly or the trace anomaly (see for example [16]). With the advent of Dirac matter, the

possible experimental consequences of the physics of anomalies has become a very active subject in condensed matter physics.

When 2D Dirac fermions are gaped, **T** symmetry is broken and their quantum effective electromagnetic behavior is described by a topological field theory (TFT), characterized by a Chern-Simons (CS) term[17, 18]. A similar thing happens in 3D, where a new scale in the system can be introduced, inducing a separation of the two chiral projections of the Dirac fermion in momentum space. This results in a **T** breaking WSM, which supports also a CS topological effective action. When real materials are considered, boundaries have to be taken into account. It so happens that, in the presence of a boundary, the CS term breaks gauge invariance of the action and, as a result, the electric charge conservation is challenged in the bulk of the material. This violation of charge conservation is compensated by 1D chiral fermions living on the boundary, which are anomalous themselves, in such a way that gauge invariance of the whole system is guaranteed[19]. This relation between bulk and edge effective theories is usually called bulk-edge correspondence.

Contrary to the 2D case, massless 3D Dirac fermions are intrinsically chiral anomalous. The 3D chiral anomaly implies that when non orthogonal electric and magnetic fields are switched on, chiral charge is no longer conserved and a charge imbalance between the two chiralities is generated. A very exotic property of 3D Dirac fermions is the so called chiral magnetic effect, by which a current is generated proportional to an applied magnetic field whenever there is an imbalance of chiral charge[20]. The two effects combine so that the net effect is a current proportional to the electric field, with a resistance which is inversely proportional to the squared magnetic field. This negative magnetoresistance has recently been experimentally observed in Dirac and Weyl semimetals[21, 22, 23]. However, there still exist discussions on whether the observed effects are entirely due to the chiral anomaly, as other mechanisms can also contribute to a negative magnetoresistance.

Some degrees of freedom couple to Dirac fermions in a way that resembles the coupling of a gauge field. The two cases we treat in the thesis are magnetization and elasticity. It happens that magnetic degrees of freedom couple to the spin of the surface states of 3D TI[24], via an exchange interaction, in such a way that the in-plane magnetization is seen as an emergent gauge field from the surface states point of view. Meanwhile, elastic deformations in systems which host Dirac cones at non equivalent points of the Brillouin zone, couple also minimally to the electrons in the low energy limit, generating emergent elastic gauge fields[25, 26]. In the case of graphene, the elastic gauge fields have given rise to spectacular experimental consequences, as for example the measurement of pseudo magnetic fields arisen from strain of the order of hundreds of Tesla[27]. The physics of emergent gauge fields in Dirac matter is yet to be fully explored, and this is one main goal of this thesis.

Goals and layout of the Thesis

The goal of the thesis is primarily to study the interplay of topology and emergent gauge fields in systems hosting Dirac fermions, focusing on its effects on physical observables. We study emergent gauge fields, arising from the coupling of electrons to magnetization on the surface of 3D TIs coated with magnetically active materials, and to elasticity in materials hosting Weyl cones at non-equivalent points of the Brillouin zone, which we call Weyl crystals. Beyond the physics of emergent gauge fields, but still related to the physics of Dirac matter, we also investigate the propagation of light in WSMs and the effect of coulomb interactions on the band structure of TMD semiconductors. In what follows, we will briefly describe the motivation and goals of each publication included in the thesis.

Publications A and B study the effect of the topological fermions at the surface of a 3D TI on the dynamics of an out of plain domain wall. Domain walls are magnetic configurations which can be considered as topological defects in the magnetic texture, they can move under the action of electromagnetic fields and applied currents, and are used in race-track technology. The motivation of this work was the possibility to act on this motion using the properties of TI surface states. Out-of-plane magnetization transforms the surface of the TI into a realization of a Chern insulator, with Chern number of opposite sign to either side of the DW. It turns out that the chiral edge state localized at the DW (where the magnetization changes sign) has some interesting properties, as for example supporting dissipationless currents, which are worth to be studied in relation to the motion of the DW.

Articles C and D study a topological response of the quantum Hall (QH) state, the Hall viscosity, which arises as a response of the stress tensor to time dependent shape deformations in time reversal broken systems. The analysis of this response in electronic systems requires the coupling of the electronic degrees of freedom to either lattice deformations (phonon Hall viscosity) or to a geometrical distortion in continuum models which used the formalism of QFT in curved space. The main idea underlying articles C and D is the realization, taken from graphene, that elastic deformations couple to Weyl systems as elastic gauge fields. The presence of elastic gauge fields defines an elastic coupling which is not captured by the curved spacetime or standard lattice formalism. We investigate the consequences of this coupling for the Hall viscosity response. Perhaps the most important aspect of these works is the derivation done in article D of that elastic gauge fields will also be present in 3D Weyl semimetals.

In publication E, we investigate the electromagnetic properties of a $\mathbf{T}$ breaking WSM, specifically the effect of the low energy electronic structure on light propagation. We wondered how the interplay of non trivial topology and different velocity scales for electrons (Fermi velocity) and light, could affect the dispersion relation and

attenuation of electromagnetic modes.

In article F, a study of the effect of Coulomb interactions on the low energy band structure of single layer TMD semiconductors was carried on. The goal was to see how the gap, the Fermi velocities for each spin configuration, and the splitting of the valence and conduction bands are affected by interactions. In a field were numeric DFT and GW calculations are the dominant approach, we wanted to do a semi-analytic study based on the low energy continuum model, to have a better understanding on the mechanisms at work, specially on the renormalization of the spin-orbit coupling which gives the splitting of the conduction and valence bands.

Discussion of the results

In this section we will discuss the results and comment on future projections of the work done in this thesis.

Articles A and B

In these two articles it is shown how 3D TI surface states have a very interesting effect on the DW dynamics. The setup is basically a thin film ferromagnet, hosting an out-of-plane magnetic DW, deposited on top of a 3D TI. The magnetization couples to the electron spin of the TI surface states via an exchange interaction, so that the in-plane components couple to the electrons minimally, in a similar way as a gauge field. The electronic chiral edge state living at the DW supports dissipationless currents, which can be triggered by doping the system with electrons or holes, or by applying a voltage difference between the end points of the DW. The equations underlying the physics of the edge mode are precisely those describing the chiral anomaly in 1D. This chiral current exerts a torque on the magnetization, trying to drive the internal angle of the DW from a Bloch configuration towards a Néel configuration. In addition, the quantum fluctuations of the chiral edge state generate an in-plane (or hard-axis) effective anisotropy energy, which competes with the chiral current. The relative values of the current and the generated anisotropy energy define the internal angle of the DW, so that it can be externally manipulated by doping with a gate or applying a voltage difference between the end points of the DW. Tuning the edge current and making use of an external perpendicular magnetic field, one can even reverse the chirality of the DW in a controllable manner, driving the system from a given Bloch configuration to the opposite Bloch configuration.

The effective in-plane anisotropy energy stabilizes the internal angle of the DW, so that for ferromagnetic films with very week intrinsic hard-axis anisotropy, DW motion can still be achieved without suffering from an extremely early Walker breakdown. We studied DW dynamics both under applied perpendicular magnetic fields and external currents through the ferromagnet. The maximum terminal velocities that can be achieved are highly sensitive to the exchange coupling (go with the square of the

exchange coupling), which defines the effective in-plane anisotropy energy. It seems that to obtain high enough velocities valid for practical applications, the exchange coupling should be of the order of hundreds of meV, which probably is far from being experimentally reachable at the moment. This is not the whole story though, as there is a way to further stabilize the internal angle and delay the appearance of Walker breakdown. It turns out that the torque exerted by the edge current flowing along the DW does exactly this. The application of an edge current can significantly increase the achievable terminal velocities.

In my opinion, the most important aspect of this work is the possibility of controlling and stabilizing the internal angle of the DW, both by applying a gate voltage and by applying an electric field. This has a potential influence on future investigations of TI for spintronic applications, specially those searching for efficient ways of achieving DW motion and manipulation. In fact, this work has already influenced later publications following these lines[28, 29, 30, 31].

Article C

In this work we show how those 2D Dirac materials hosting emergent elastic gauge fields, present a Hall viscosity response as a counterpart of the Hall conductivity. Graphene and TMD semiconductors are the principal candidates, both in their monolayer and multilayer realizations. When **T** symmetry is broken, the low energy electromagnetic physics of Dirac fermions is described by a topological Chern-Simons term in the effective action. This term gives a Hall conductivity response. When elasticity is considered, there is also a Chern-Simons term for the elastic gauge fields. Contrarily to the electromagnetic case, this term does not give a contribution to the electric current, but it gives a **T** breaking contribution to the stress tensor proportional to the strain rate, which is precisely the Hall viscosity. One can break **T** either with or without a magnetic field, so one is in the QH or anomalous QH state, respectively. In both cases, there is a non zero Hall conductivity and, as a consequence a non zero Hall viscosity. This is in contrast with the traditional Hall viscosity response, which is proportional to the electron density and is zero in the anomalous QH state.

The Hall viscosity arising from the elastic gauge fields is proportional to the inverse of the squared lattice spacing, as opposed to the traditional response which is proportional to the inverse of the squared magnetic length. This means that the elastic gauge field Hall viscosity is three or four orders of magnitude bigger than the traditional one, for magnetic fields of 10 T and 1 T respectively. This really increases the chances to experimentally detect the Hall viscosity.

Article D

The principal requisite for a 2D Dirac material to support elastic gauge fields, is to have Dirac cones located at non equivalent points of the Brillouin zone. In this article we prove that WSMs, which are 3D materials with Weyl cones at non equivalent points of the Brillouin zone, support elastic gauge fields in analogy to the 2D and layered cases. The elastic gauge fields couple axially (with opposite sign to the two chiralities) to the electrons, so they can be considered as emergent axial fields. This result opens the field of straintronics in WSMs, making it a real possibility to realize all the physics associated to the axial anomaly by strain engineering. This could provide a realization of the axial magnetic effect, which gives a current proportional to the chemical potential and the axial magnetic field. These axial magnetic fields will arise from strain generated by deformations of the samples.

In addition, as a consequence of having elastic gauge fields and following the reasoning of article C, we show that the **T** breaking WSM presents a Hall viscosity response. It is associated with the triangle diagram with three axial fields (AAA), which is weighted by a factor of 1/3 with respect to the axial-vector-vector (AVV) diagram that is responsible of the Hall conductivity. This work is interesting to both, condensed matter and high energy communities. In condensed matter it opens an entire new field of research, and from the quantum field theory point of view it might prove the 1/3 relation.

Summarizing, the two most important aspects of works C and D combined, are the recognition that the elastic gauge fields known in graphene will also be present in most of the Weyl/Dirac materials, and the enhancement of the Hall viscosity improving the chances to observe this elusive response.

Article E

In this work we consider the minimal model for a **T** breaking WSM, with the Fermi level lying at the Weyl nodes, and compute the quantum corrections to the photon propagator to 1-loop level. The polarization function consists on a parity-even and a parity-odd contribution. The first one is analogous to the polarization function of massless electrodynamics, while the second one comes from the Chern-Simons term and is of topological origin. This last contribution is known to gap one of the two independent electromagnetic modes and induce gyrotropy, so that left- and right-handed polarized light propagate at different speeds. The critical point of a solid state realization of a WSM, however, is that the velocity of propagation of light is different from the Fermi velocity of the electrons, which we show that in addition to the non trivial topology encoded in the Chern-Simons term, results in an unusual

behavior of light propagation.

Our first finding is that due to the mismatch of the light and Fermi velocities, light is attenuated when propagating through a WSM. This property is shared by Dirac semimetals as well, because it is not related to the non trivial topology. The second and most important finding, is that the electromagnetic mode that is supposed to be gaped due to the Chern-Simons term, actually splits into two branches: the traditional gaped one plus a new gapless excitation. The gapless branch is overdamped in some regimes, but in other regimes its attenuation is weak. For a realistic situation where light is collimated along the direction of the separation of the Weyl nodes, but still with small deviation in the perpendicular direction, it shows up as a well defined and damped peak in the spectral function. Perhaps the most intriguing result, at low frequencies (near the electron-hole continuum threshold) this gapless excitation has a velocity similar to the Fermi velocity, representing a photon traveling coherently with the electrons. In the other limit of the spectrum however, the behavior approaches that of a massive damped photon with velocity close to the speed of light. This novel optical excitation could provide a new and clean signature for WSMs, and could be detected in experiments as an additional resonance on the transmission coefficient of light. It is important to stress that for the new gapless excitation to be observed, the Fermi level has to lie at the Weyl nodes, other ways the electromagnetic modes would acquire a gap induced by the plasma frequency. This could make the experimental observation more difficult, as in general the Fermi level of Weyl semimetals is well above/below the Weyl points.

The finding that the mismatch of light and Fermi velocities, together with topological characteristics of a material, can give rise to unusual electromagnetic excitations could open a line of research for characterizing topological matter. We suspect that a similar splitting of an electromagnetic mode into two branches could happen also in the bulk of 3D topological insulators. If this is proven to be right, novel electromagnetic propagation could happen in other topological materials as well.

Article F

In this article we study the effect of coulomb interactions in the low energy band structure of single layer TMD semiconductors. We make use of an effective low energy continuum model, and obtain the electron self energy self-consistently using the Schwinger-Dyson equation for the propagator. We obtain the corrected values for the gaps and Fermi velocities for each spin, as well as the spin splitting of the conduction and valence bands, all as a function of the renormalized coupling constant and the lattice cut-off. We take the specific case of MoS_2 and impose, as a renormalization condition, the measured optical absorption energies of the excitonic peaks A, B. This

way we impose agreement with the experiment. The conduction band spin splitting is generally found to be quite large, indeed much larger than that obtained from first principle calculations in the literature. For a coupling constant of $g = 2$, we obtain a conduction band splitting of the order of $70meV$. Contrarily, the valence band splitting is compatible with first principle calculations.

From our semi-analytic approach, it is easy to see that the big renormalization of the band splittings comes from the difference in the value of the gaps for each spin polarization, product of the spin-orbit interaction, which is big even in the limit of very weak interactions. From this point of view the big values of the conduction band spin splitting are unavoidable, so one wonders where the discrepancy with first principles calculations comes from. It might be that higher energy bands not included in our model conspire to suppress the renormalization of the spin-orbit interaction, or it could be that previous first principles calculations could be underestimating it. Whatever scenario is right, we feel that our work indeed gives insight into the effect of interactions on the spin-orbit coupling and band structure, and opens a debate on how first principle calculations give such small values of the conduction band splitting. Is it the higher energy bands that conspire? We believe the question remains open.

Conclusions

In this thesis we have contributed to develop novel lines of research, opening the path for future investigations. Among the achievements, we have contributed to the understanding of the role of topology on the magnetization dynamics on the surface of TI, a result which could be of interest for both the fundamental point of view and for spintronic applications; to the discovery of a new type of Hall viscosity response, which greatly improves the chances of experimental observation of this elusive phenomenon; or to the understanding of the coupling of elasticity and electrons in WSMs, and more generally in Weyl crystals, for which we proved the existence of elastic gauge fields. Perhaps this last result is the most important of all, as it really opens a new path for strain engineering in WSMs. In general, we believe that the results of this thesis can be of interest not only to condensed matter researchers, but also to other fields with a focus on technological applications. Looking to the future, we believe that the physics related to topological phases of matter is one of the most promising lines of research, both for the understanding of physics at a fundamental level, and for experimental and technological applications. In these lines, this thesis has answered several questions, but most importantly has also opened important opportunities for theoretical and experimental research.

Conclusiones

En esta tesis hemos contribuído a desarrollar nuevas líneas de investigación, abriendo el camino a futuros trabajos científicos. Entre otros logros, hemos contribuído al entendimiento del papel de la topología en la dinámica de la magnetización en la superficie de aislantes topológicos, con resultados que pueden ser de interés tanto desde un punto de vista fundamental como para aplicaciones en espintrónica; al descubrimiento de un nuevo tipo de viscosidad Hall, que aumenta en gran manera las posibilidades de observar este elusivo fenómeno; o al entendimiento del acoplo de la elasticidad y los electrones en semimetales de Weyl y, de manera más genérica, en cristales de Weyl, para los cuales hemos demostrado la existencia de los campos gauge elásticos. Posiblemente este último resultado sea el más importante de todos, debido a que abre todo un campo relacionado con la ingeniería de deformaciones en semimetales de Weyl. En general, creemos firmemente que los resultados de esta tesis pueden ser de interés no sólo para investigadores de materia condensada, sino también para otros campos centrados en aplicaciones tecnológicas. Mirando al futuro, creemos que la física de las fases topológicas de la materia es una de las líneas de investigación más prometedoras, tanto para el entendimiento de la física al nivel más fundamental, como para aplicaciones tecnológicas y experimentales. En este contexto, esta tesis ha respondido varias preguntas, pero también ha abierto oportunidades importantes para investigaciones tanto a nivel teórico como experimental.

Bibliography

[1] K. S. Novoselov et al. "Electric Field Effect in Atomically Thin Carbon Films". In: *Science* 306.5696 (2004), pp. 666–669.

[2] A. H. Castro Neto et al. "The electronic properties of graphene". In: *Rev. Mod. Phys.* 81 (1 2009), pp. 109–162.

[3] Kin Fai Mak et al. "Atomically Thin MoS_2: A New Direct-Gap Semiconductor". In: *Phys. Rev. Lett.* 105 (13 2010), p. 136805.

[4] Di Xiao et al. "Coupled Spin and Valley Physics in Monolayers of MoS_2 and Other Group-VI Dichalcogenides". In: *Phys. Rev. Lett.* 108 (19 2012), p. 196802.

[5] Liang Fu, C. L. Kane, and E. J. Mele. "Topological Insulators in Three Dimensions". In: *Phys. Rev. Lett.* 98 (10 2007), p. 106803.

[6] M. Z. Hasan and C. L. Kane. "*Colloquium* : Topological insulators". In: *Rev. Mod. Phys.* 82 (4 2010), pp. 3045–3067.

[7] Xiao-Liang Qi and Shou-Cheng Zhang. "Topological insulators and superconductors". In: *Rev. Mod. Phys.* 83.4 (2011), pp. 1057–1110.

[8] Dmytro Pesin and Allan H. MacDonald. "Spintronics and pseudospintronics in graphene and topological insulators". In: *Nat Mater* 11.5 (May 2012), pp. 409–416.

[9] Z. K. Liu et al. "A stable three-dimensional topological Dirac semimetal Cd3As2". In: *Nat Mater* 13.7 (July 2014), pp. 677–681.

[10] Xiangang Wan et al. "Topological semimetal and Fermi-arc surface states in the electronic structure of pyrochlore iridates". In: *Phys. Rev. B* 83 (20 2011), p. 205101.

[11] Su-Yang Xu et al. "Discovery of a Weyl fermion semimetal and topological Fermi arcs". In: *Science* 349.6248 (2015), pp. 613–617. ISSN: 0036-8075.

[12] B. Q. Lv et al. "Experimental Discovery of Weyl Semimetal TaAs". In: *Phys. Rev. X* 5 (3 2015), p. 031013.

[13] B. Xu et al. “Optical spectroscopy of the Weyl semimetal TaAs”. In: *Phys. Rev. B* 93 (12 2016), p. 121110.

[14] J. Y. Liu et al. “Discovery of a topological semimetal phase coexisting with ferromagnetic behavior in Sr1-yMnSb2 (y˜0.08)”. In: *ArXiv e-prints* (July 2015).

[15] S. Borisenko et al. “Time-Reversal Symmetry Breaking Type-II Weyl State in YbMnBi2”. In: *ArXiv e-prints* (July 2015).

[16] Reinhold A. Bertlmann. *Anomalies in Quantum Field Theory*. 1996.

[17] A. N. Redlich. “Parity violation and gauge noninvariance of the effective gauge field action in three dimensions”. In: *Phys. Rev. D* 29.10 (1984), pp. 2366–2374.

[18] M Nakahara. *Geometry, Topology and Physics*. 2003.

[19] C. G. Callan and J. A. Harvey. “Anomalies and fermion zero modes on strings and domain walls”. In: *Nuclear Physics B* 250.14 (1985), pp. 427 –436.

[20] Kenji Fukushima, Dmitri E. Kharzeev, and Harmen J. Warringa. “Chiral magnetic effect”. In: *Phys. Rev. D* 78 (7 2008), p. 074033.

[21] Hui Li et al. “Negative magnetoresistance in Dirac semimetal Cd3As2”. In: *Nat Commun* 7 (Jan. 2016).

[22] Frank Arnold et al. “Negative magnetoresistance without well-defined chirality in the Weyl semimetal TaP”. In: *Nat Commun* 7 (May 2016).

[23] Cheng-Long Zhang et al. “Signatures of the Adler-Bell-Jackiw chiral anomaly in a Weyl fermion semimetal”. In: *Nat Commun* 7 (Feb. 2016).

[24] Yaroslav Tserkovnyak and Daniel Loss. “Thin-Film Magnetization Dynamics on the Surface of a Topological Insulator”. In: *Phys. Rev. Lett.* 108 (18 2012), p. 187201.

[25] J. L. Mañes. “Symmetry-based approach to electron-phonon interactions in graphene”. In: *Phys. Rev. B* 76 (4 2007), p. 045430.

[26] M.A.H. Vozmediano, M.I. Katsnelson, and F. Guinea. “Gauge fields in graphene”. In: *Physics Reports* 496.45 (2010), pp. 109 –148. ISSN: 0370-1573.

[27] N. Levy et al. “Strain-Induced Pseudo–Magnetic Fields Greater Than 300 Tesla in Graphene Nanobubbles”. In: *Science* 329.5991 (2010), pp. 544–547. ISSN: 0036-8075.

[28] Jacob Linder. “Improved domain-wall dynamics and magnonic torques using topological insulators”. In: *Phys. Rev. B* 90 (4 2014), p. 041412.

[29] Ryohei Wakatsuki, Motohiko Ezawa, and Naoto Nagaosa. “Domain wall of a ferromagnet on a three-dimensional topological insulator”. In: *Scientific Reports* 5 (Sept. 2015), 13638 EP –.

[30] P. Upadhyaya and Y. Tserkovnyak. “Domain Wall in a Quantum Anomalous Hall Insulator as a Magnetoelectric Piston”. In: *ArXiv e-prints* (Dec. 2015).

[31] S. Rex, F. S. Nogueira, and A. Sudbo. “Topological magnetic dipolar interaction and non-local electric magnetization control in topological insulator heterostrucutres”. In: *ArXiv e-prints* (Feb. 2016).

Publications

Article A

Domain wall motion in junctions of thin-film magnets and topological insulators

PHYSICAL REVIEW B **89**, 024413 (2014)

Domain wall motion in junctions of thin-film magnets and topological insulators

Yago Ferreiros* and Alberto Cortijo†
Instituto de Ciencia de Materiales de Madrid, CSIC, Cantoblanco, 28049 Madrid, Spain
(Received 24 July 2013; revised manuscript received 25 November 2013; published 17 January 2014)

We derive the equations of motionof a domain wall in a thin-film magnet coupled to the surface states of a topological insulator, in the presence of both an electric field along the domain wall and a magnetic field perpendicular to the junction. We show how the electric field acts as a chirality stabilizer holding off the appearance of Walker breakdown and enhancing the terminal velocity of the wall. We also propose a mechanism to reverse the domain wall chirality in a controllable manner, by tuning the chiral current flowing through the wall. An input from a weak perpendicular magnetic field is required in order to break the reflection symmetry that protects the degeneracy of the chirality vacuum.

DOI: 10.1103/PhysRevB.89.024413 PACS number(s): 75.60.−d, 75.78.Fg, 03.65.Vf, 85.75.−d

I. INTRODUCTION

Within the field of spintronics, the electric control of magnetic domain wall (DW) motion holds one of the prominent places. It is of considerable interest both from fundamental as from the perspective of applied science, and this is so since the experimental realization of the magnetic "race-track" technology [1,2]. Traditionally, there were two main ways of acting on a magnetic DW: the application of an external magnetic field and the interaction with an electronic current which is spin polarized and is hosted by the ferromagnet. As it is well known since the early studies of DWs in the presence of an external magnetic field, the DW motion is severely reduced when the magnetic field exceeds some critical value and the system enters in the so-called region of Walker breakdown [3], caused by DW structural instabilities, setting a limitation for actual high speed operation devices. Trying to stabilize the internal structure of the DW, so higher velocities can be reached, has become an important task [4]. In this context the presence of the spin-torque field, while still suffering from the upper Walker breakdown bound, significantly enlarges the DW velocity [5]. There has been recent experimental success on delaying the appearance of Walker breakdown in the context of current-induced motion, by Rashba field mediated chirality stabilization [6]. Also, recent experimental progress has been done in controlling the DW motion by using external electric fields. The strategies in this case consist of changing the carrier density by field effect and thus controlling the spin-torque effect [7], or modifying the perpendicular anisotropy by electric fields [8].

In this context, three-dimensional topological insulators (TI) provide a new spectrum of possibilities regarding DW motion. An interesting aspect of the surface states of three-dimensional TI is that external magnetic agents can modify their spectrum [9] and electronic transport properties [10], and conversely, the dynamics of magnets coupled to these surface states can be severely modified [11–14]. Specifically, the question of how the presence of these surface states influences the dynamics of a DW has been recently addressed in the literature [12,14]. We will go further by bringing into play an out-of-plane magnetic field, and show how magnetic field generated DW velocity can be significantly increased by holding off the appearance of Walker breakdown via an external electric field, and how the macroscopic DW chirality can be controlled by the presence of the TI surface state. In this way, previous unnoticed terms in the DW effective action will be obtained.

The paper is organized as follows: In Sec. II we present the model for both the magnetic thin film and the TI surface states. The DW solution is presented together with the description of the coupling between the DW and the TI surface states. In Sec. III we obtain the effective action and equations of motion of the DW in terms of collective coordinates by integrating out the fermionic degrees of freedom. In Sec. IV we describe how the presence of both magnetic and electric fields can stabilize the DW motion delaying the appearance of the Walker breakdown. In Sec. V we describe how the DW chirality can be tuned at will by manipulating the electric and magnetic fields. At the end, in Sec. VI we present a brief summary of the results obtained in this work.

II. THE MODEL

To be specific we will consider an insulating ferromagnetic thin film, hosting a DW with an out-of-plane magnetization (see Fig. 1), deposited on top of the surface of a three dimensional TI. The continuum Hamiltonian for the surface states of the TI, coupled by exchange interaction to the magnetic thin film, takes the standard form ($\hbar = 1$ will be used):

$$H_{TI}^{\pm} = \int d^2x (v_F \psi^+ \hat{\mathbf{x}}_3 \cdot (i\nabla \times \boldsymbol{\sigma})\psi \pm \Delta \mathbf{m}(\mathbf{x},t) \cdot \psi^+ \boldsymbol{\sigma} \psi), \quad (1)$$

where Δ is the exchange coupling between the magnet and the surface states (it is definite positive) and the total magnetization $\mathbf{M}(\mathbf{x},t)$ relates with $\mathbf{m}(\mathbf{x},t)$ as $\mathbf{M}(\mathbf{x},t) = \gamma_{MI}/a^3 \mathbf{m}(\mathbf{x},t)$. Here $\gamma_{MI} = \mu_B g_{MI}$ is the gyromagnetic ratio of the magnetic insulator (μ_B is the Bohr magneton and g_{MI} is the Landé factor of the magnetic insulator). It is useful to write $\mathbf{m}(\mathbf{x},t)$ in spherical coordinates:

$$\mathbf{m}(\mathbf{x},t) = S(\sin\theta\cos\phi, \sin\theta\sin\phi, \cos\theta) \quad (2)$$

*yago.ferreiros@csic.es
†alberto.cortijo@csic.es

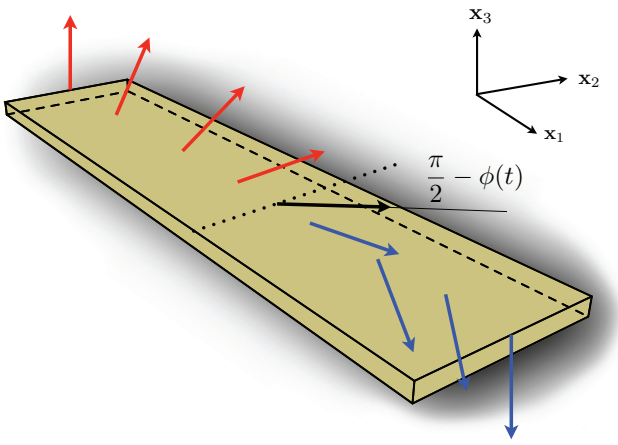

FIG. 1. (Color online) Artistic image of the DW considered in the text. The dotted line defines $X(t)$ and the continuous line defines $\phi(t)$. Red (light) color means a positive out-of-plane magnetization while blue (dark) color means a negative out-of-plane magnetization. The black arrow indicates a magnetization pointing in the $\mathbf{x}_1$-$\mathbf{x}_2$ plane.

The signs + and − in $H_{TI}^{\pm}$ correspond to antiferromagnetic and ferromagnetic exchange coupling, respectively. Regarding the external electromagnetic fields, we will analyze the effect of a magnetic field B pointing along the $\hat{\mathbf{x}}_3$ direction, and an electric field E pointing along the direction defined by the DW. These fields will couple to the TI surface states not only through the electromagnetic vector field A_μ but also through a Zeeman coupling $H_z = -\int d^2x \gamma_{TI} B \psi^+ \sigma_z \psi$, being $\gamma_{TI} = \mu_B g_{TI}$ the gyromagnetic ratio for the topological insulator. For the magnetic layer, we will assume that its dynamics are conveniently described by an anisotropic Heisenberg model with an easy axis along $\hat{\mathbf{x}}_3$ and a hard axis on the $\hat{\mathbf{x}}_1$-$\hat{\mathbf{x}}_2$ plane [3,5]:

$$H_{MI} = \frac{1}{2}\int \frac{d^3x}{a^3}\big(J(\nabla \mathbf{m})^2 + K_{x_1}^{\perp} m_1^2 + K_{x_2}^{\perp} m_2^2 - K m_3^2 - \gamma_{MI} B m_3\big), \tag{3}$$

where J stands for the stiffness constant, and K, $K_{x_1,x_2}^{\perp}$ are the easy and hard axis anisotropies, respectively. The full Lagrangian includes the dynamical term generated by the Berry phase of the spins [3,5]:

$$\mathcal{L}_{MI} = \int \frac{d^3x}{a^3} \dot{\phi} S(\cos\theta - 1) - H_{MI}. \tag{4}$$

It is well known that the equations of motion derived from (4) support static extended solutions in the form of DWs [15]. Also in this situation, the excitation spectrum of the magnetic layer consists of gapped spin waves together with two zero energy modes. The latter are related to invariance under translations of the DW center and rotations of the azimuthal angle that describes the DW chirality. Actually, the excitation associated with the azimuthal angle is a zero mode only if the hard axis anisotropy is zero, however one can consider small anisotropies so that it effectively decouples from the other massive excitations and still describes correctly the low energy dynamics [3,5]. To study the DW dynamics at low energies the zero modes are promoted to dynamical variables with finite kinetic energy. When the magnetic field is switched on or other external elements like electric field or the TI surface states are present, these dynamical variables are no longer zero modes, and become gapped excitations. Still, similar to the case with the hard axis anisotropy, they correctly describe the low energy dynamics if the energy remains smaller than that of the gapped excitation spectrum.

The time evolution of the DW can be described in terms of the two variables $X(t)$ and $\phi(t)$, representing translations and rotations of the azimuthal angle. The x_3 component of the magnetization takes the following form:

$$m_3^{DW} = -S \tanh\left(\frac{x_1 + X(t)}{\delta}\right), \tag{5}$$

where $\delta = \sqrt{J/K}$ is the DW width and S is the maximum value of the magnetization. The in-plane components of $\mathbf{m}$ will be

$$\mathbf{m}_\perp = S\,\mathrm{sech}\left(\frac{x_1 + X(t)}{\delta}\right)(\cos\phi(t), \sin\phi(t), 0). \tag{6}$$

In order to find the effective theory describing the time evolution of the coordinates $X(t)$ and $\phi(t)$ we integrate out the fermionic degrees of freedom in the presence of the background field m_3^{DW}. To do this we use the fermionic spectrum which has been extensively discussed in the literature [16,17]. It is important to note that, besides the third component of the magnetization acting as a mass for the TI surface states, we also have two other components for $\mathbf{m}^{DW}$. These components are coupled to the other two Pauli matrices in the fermionic action (1), which of course do not commute with σ_3 and thus induce couplings between the fermionic eigenstates previously calculated. The technical details of this derivation are presented in Appendices A–C; here we will comment on the most salient features of the calculation. First of all, the presence of an external magnetic field B pointing along the perpendicular direction to the TI surface states completely changes the fermionic spectrum (and hence the effective action) depending on if $|B|$ is larger or smaller than $S\Delta/\gamma_{TI}$. The reason is mainly the appearance in the latter case of a fermionic chiral state where the mass $m \equiv \Delta m_3^{DW} + \gamma_{TI} B$ changes sign. In this regard we can define two regimes:

(i) *Chiral regime*. It occurs when $|B| < S\Delta/\gamma_{TI}$, so the mass changes sign. The fermionic spectrum consists of a chiral massless state bound to (localized on) the wall, plus massive scattering (extended) states. There can appear massive bound states too. Specifically, the number of bound states (taking into account also the chiral state) is going to be the largest integer less than $\Delta\delta S/(2v_F) + 1$ (see Appendix A).

(ii) *Nonchiral regime*. It occurs when $|B| > S\Delta/\gamma_{TI}$, so the mass does not change sign. As a consequence there is no chiral massless state. The spectrum consists of massive scattering states and, depending on the slope of m_3^{DW}, massive bound states.

The computation of the exact spectrum for a mass of the type $\tanh(x)$, and for any values of Δ, S, δ, and v_F, is a formidable task, and closed solutions are known only for special values of the parameters [17]. To obtain a solution for generic values, we will follow an approximate but much simpler route [18]. We will approximate m_3^{DW} to a straight line to obtain and integrate out the bound fermionic spectrum,

while we will rely on an adiabatic approximation to integrate out the scattering states.

III. EFFECTIVE ACTION FOR THE DW DYNAMICS

By integrating out the fermionic degrees of freedom (both massless and massive) up to one loop level and adding the part coming from the isolated MI, we obtain the effective action for the collective coordinates $X(t)$ and $\phi(t)$ (see Appendices A–C for details on the computation):

$$\Gamma^{\pm}_{DW} = \Gamma_{MI} + \Gamma^{\pm}_{TI}. \tag{7}$$

The MI part is

$$\Gamma_{MI} = S\mathcal{N}\int dt \int_{-\frac{L_2}{2}}^{\frac{L_2}{2}} dx_2 \left\{ \frac{\dot{X}}{\delta}\phi - \frac{K^{\perp}_{x_1} S}{2}\cos^2\phi - \frac{K^{\perp}_{x_2} S}{2}\sin^2\phi + \gamma_{MI} B \frac{X}{\delta} \right\}, \tag{8}$$

where $\mathcal{N}$ is the number of spins in the wall divided by L_2. For the TI part, the calculation is different depending whether we are in the chiral or nonchiral regime. We shall present the results separately for both situations.

A. Effective action in the chiral regime

In this regime $|B| < S\Delta/\gamma_{TI}$. Setting $S = 1$, an exchange coupling of $\Delta = 0.1$ eV, a Landé factor for the topological insulator of $g_{TI} = 100$, and restoring $\hbar$ we find that this regime is defined for values of B up to $|B| < 17$ T (the reason for quite such a big, although still realistic, exchange coupling will be transparent in Sec. IV). For such large magnetic fields we should consider both the orbital coupling that originates the formation of Landau levels (LL) and the Zeeman coupling, which generates a splitting of these levels. The stronger the magnetic field, the more important the Zeeman mass term is in comparison with the energy of the first nonzero LL, which scales with the magnetic field as $B^{1/2}$. In typical 3D TIs, however, the Zeeman splitting remains much smaller than the energy separation of the LL even for quite big fields. As an example, the Zeeman splitting is negligible for fields up to at least $B = 11$ T in Bi_2Se_3 [19].

At low fields, far from the formation of LL, we can treat the orbital coupling perturbatively. In this situation the Zeeman coupling will contribute to a parity breaking mass term of the form $m = \Delta m_3^{DW} + \gamma_{TI} B$, which will give rise to a quantum anomalous hall effect (QAHE) with a topological Chern-Simons term [20,21].

For fields larger than $B \approx 2$ T the LL formation becomes relevant [19]. At these fields, in order to obtain the effective action at low energies it is enough to consider the ultra quantum limit, where only the lowest LL is populated and inter-Landau-level transitions are neglected. In this situation the mass term will be equal to that of the QAHE just described $m = \Delta m_3^{DW} + \gamma_{TI} B$, but now we are in the scenario of a normal quantum hall effect (QHE). As long as we only consider the zero LL, the filling factor is just 1, and a Chern-Simons term analogous to that of the QAHE is obtained [22].

We conclude that the same effective field theory describes both situations of small and large magnetic fields. We have to stress that these considerations have to do only with the massive scattering fermions, which live in $(2+1)$ dimensions. The chiral state is not modified when changing the magnetic field due to its chiral nature. The massive bound states, however, change when varying B, but they do not generate a topological response. So for the bound states a perturbative treatment of the orbital contribution is justified, as in the case of a weak magnetic field.

All considered, after computing the spectrum for the corresponding mass term and integrating out the fermions we arrive to (in real time):

$$\Gamma^{\pm}_{TI} = S\int dt \int_{-\frac{L_2}{2}}^{\frac{L_2}{2}} dx_2 \left\{ -\frac{\Delta}{v_F} J^{EM}_{2,\pm}\cos\phi - \frac{\mathcal{N}K^{\perp}_0 S}{2}\cos^2\phi - \frac{\mathcal{N}K^{\perp}_m S}{2}\sin^2\phi \pm \gamma_{\text{eff}}\delta B E \sin\phi \right\}. \tag{9}$$

It is worth pointing out that terms 2, 3, and 4 of the r.h.s. of Eq. (9) are new, in the sense that they were not previously reported in the literature. The one-dimensional (integrated over x_1) electromagnetic current density flowing along the DW, $J^{EM}_{2,\pm}$, is (see Appendix D)

$$J^{EM}_{2,\pm} = \frac{v_F}{2\pi}\frac{1}{\partial_0 \pm v_F\partial_2}E. \tag{10}$$

Notice that $J^{EM}_{2,\pm}$ is written in terms of the integral operator $1/(\partial_0 \pm v_F\partial_2)$. An specific form of the electromagnetic current has to be obtained by fixing the boundary conditions, in order to study the physics in the chiral regime (Appendix D). $K^{\perp}_0 = \Delta^2/(2\pi\mathcal{N}v_F)$ and $\gamma_{\text{eff}} = \gamma_{TI}/(2\pi v_F S)$, and we do not have an exact value for $K^{\perp}_m$, although we know it is of the order of $K^{\perp}_0$ (see Appendix A). $K^{\perp}_0$ and $K^{\perp}_m$ renormalize the MI hard axis anisotropies $K^{\perp}_{x_1}$ and $K^{\perp}_{x_2}$ respectively, however their value is going to be considerably smaller than their MI counterparts. Hence the uncertainty in the value of $K^{\perp}_m$ will have no impact on the final results. It is worth it to notice that $K^{\perp}_0$ is generated by the chiral mode, while $K^{\perp}_m$ is generated by the coupling between the chiral and massive modes.

We see that the fermionic fluctuations contribute with a torque term proportional to $\cos\phi J^{EM}_{2,\pm}$ generated by the coupling with the chiral mode. This torque can be understood in terms of the nonconservation of the one-dimensional chiral current flowing along the DW. According to the Callan-Harvey mechanism [16] the nonconservation of the chiral current is compensated by a charge inflow from the two-dimensional bulk. The spin of the chiral state, being perpendicular to the current motion, is forced to lie on the $\mathbf{x}_1$-$\mathbf{x}_2$ plane. However, the current flowing from the bulk is spin polarized, and its polarization in the third direction is proportional to the sign of the induced mass. So the inflow current must change its spin polarization when reaching the chiral current, changing its total angular momentum. This excess of angular momentum is absorbed by the magnetic moments of the DW, generating the torque term.

We see also that when both magnetic and electric fields are switched on, the scattering fermions generate a term $\pm\gamma_{\text{eff}}\delta B E \sin\phi$ which stems from the Chern-Simons term. Finally and for completeness, we point out that the anisotropy term $K^{\perp}_m$ is renormalized as the number $\theta = \Delta\delta S/(2v_F)$

increases, this is whenever an additional massive bound state appears. This renormalization is discontinuous, as for $0 < \theta \leqslant 1$ the number of massive bound states N is zero, for $1 < \theta \leqslant 2$ $N = 1$, and so on (see Appendix A for details). For given TI and MI materials, massive bound states appear as the DW width δ increases. But as we already said, the exact value of $K_m^\perp$ is going to be irrelevant for us, as it is going to be small compared to $K_{x_1}^\perp$ and $K_{x_2}^\perp$.

The equations of motion are readily obtained from Eq. (9) in this regime. After fixing the electromagnetic current configuration (see Appendix D) and incorporating Gilbert damping [3] we have:

$$\dot{\phi} = \frac{\gamma_{MI} B}{1+\alpha^2} + \frac{\alpha}{\mathcal{N}(1+\alpha^2)}\left(\frac{\Delta I_\pm}{v_F}\sin\phi - \frac{\mathcal{N}K^\perp S}{2}\sin 2\phi \pm \gamma_{\text{eff}}\delta B E\cos\phi\right), \tag{11}$$

$$\dot{X} = \frac{\delta\gamma_{MI}}{\alpha}B - \frac{\delta}{\alpha}\dot{\phi}, \tag{12}$$

where $I_\pm$ is the static (and spatially averaged) electromagnetic current configuration flowing along the DW, α is the Gilbert damping constant, and $K^\perp = K_{x_2}^\perp + K_m^\perp - K_{x_1}^\perp - K_0^\perp$.

B. Effective action in the nonchiral regime

In this regime $|B| > S\Delta/\gamma_{TI}$, which is reached for values of $|B| > 17$ T for typical values of $\Delta \sim 0.1$ eV. However, for materials with exchange couplings two orders of magnitude smaller ($\Delta \approx 1$ meV) this regime would become experimentally important ($|B| > 0.17$ T). Hence we will present the computation of the effective action in the nonchiral regime also for completeness.

The same analysis done in the previous section can be done here. The only difference is now the absence of the chiral state. After doing the corresponding computation (see Appendix C) we get:

$$\Gamma_{TI}^\pm = \pm\int dt \int_{-\frac{L_2}{2}}^{\frac{L_2}{2}} dx_2 \, \frac{\Delta S\delta \, Sign(B)}{4v_F} E\sin\phi. \tag{13}$$

We see that all the terms where the chiral fermions were involved disappear, and the only term remaining is the topological Chern-Simons term, but with a different value than in the chiral regime. This is so because in the chiral regime the mass changes sign at some point on the $\hat{\mathbf{x}}_1$ axis, while in the nonchiral regime the mass sign depends only on the sign of B (see Appendix C).

The equations of motion now read:

$$\dot{\phi} = \frac{\gamma_{MI} B}{1+\alpha^2} + \frac{\alpha}{\mathcal{N}(1+\alpha^2)}\left(-\frac{\mathcal{N}K^\perp S}{2}\sin 2\phi \pm \frac{\Delta\delta \, Sign(B)}{4v_F}E\cos\phi\right), \tag{14}$$

$$\dot{X} = \frac{\delta\gamma_{MI}}{\alpha}B - \frac{\delta}{\alpha}\dot{\phi}, \tag{15}$$

with $K^\perp = K_{x_2}^\perp - K_{x_1}^\perp$.

IV. ELECTRIC FIELD MEDIATED DW CHIRALITY STABILIZATION

If we turn off the electric field, both in the chiral and nonchiral regime the equations of motion are equivalent to those of a DW in a MI in the presence of an easy-axis magnetic field, with well known solutions [3]. For magnetic fields smaller than a critical field $B_c = \alpha K^\perp S/(2\hbar\gamma_{MI})$, the time-averaged terminal velocity of the wall is $\langle\dot{X}\rangle = \mu B$, where μ is the mobility and its value is $\mu = \delta\gamma_{MI}/\alpha$. When B reaches B_c Walker breakdown (WB) occurs and ϕ starts to precess decreasing the terminal velocity as B increases. If B continues growing there is a point where the terminal velocity starts to increase linearly again but with considerably lower mobility [3]. Thus being able to stabilize the chirality ϕ avoiding this WB regime is essential to maintain the high initial mobility $\mu = \delta\gamma_{MI}/\alpha$ and hence to reach high velocities.

As we pointed out in Sec. III, for values of $\Delta = 0.1$ eV and $g_{TI} = 100$, the chiral regime extends up to fields of $B = 17$ T so we will always be in this regime. After switching on the electric field, the picture is modified with respect to that of an isolated MI as two new terms appear in the equations of motion [terms 2 and 4 of the r.h.s of Eq. (11)]. These new terms will act as chirality stabilizers, delaying the appearance of WB. The equations of motion for the chiral regime can be written in a more manageable form:

$$\dot{\phi}' = \frac{B}{B_c} - \sin 2\phi \mp \frac{I}{I^*}\sin\phi \pm r\frac{I}{I^*}\frac{B}{B_c}\cos\phi, \tag{16}$$

$$\dot{X} = \mu B - \frac{\delta}{\alpha}\dot{\phi}, \tag{17}$$

with:

$$I = -\frac{e^2}{2h}V; \quad I^* = \frac{\mathcal{N}v_F e K^\perp S}{2\Delta} \tag{18}$$

$$\phi' = \frac{2\hbar(1+\alpha^2)}{\alpha K^\perp S}\phi \tag{19}$$

$$r = \frac{2\hbar\gamma_{TI}\delta B_c}{L_2\Delta S}. \tag{20}$$

V is the voltage between both sides of the magnetic strip [14] (see Appendix D). Notice that we reintroduced $\hbar$ and e.

To make a quantitative analysis, we need to give values to the different parameters appearing in the model. For a permalloy MI strip, we can set a DW width of $\delta = 10$ nm, a Gilbert damping constant of $\alpha = 0.01$, a Landé factor of $g_{MI} = 2$, a strip thickness of 1 nm, a lattice constant $a = 0.35$ nm, and we do $S = 1$. The density of spins of the wall in the $\hat{\mathbf{x}}_2$ direction is $\mathcal{N} = 2.3 \times 10^{11} m^{-1}$. For the hard axis anisotropy energy we set [3] $K^\perp = 1\kappa_B 1K$. On the other hand, for the TI we set a Fermi velocity of $v_F = 5 \times 10^5$. The TI Landé factor and the exchange coupling energy have been already introduced.

For these values of the parameters we have $I^* = 8 \times 10^{-6} A$, $B_c = 3.8 \times 10^{-3} T$, $\mu = 1.9 \times 10^5 T^{-1} m/s$, and $r = 4.4 \times 10^{-12}/L_2$. Such a small value for r means that for strip widths down to $L_2 \sim 1$ μm, the last term of the right hand side of equation (16) can be neglected for all possible values

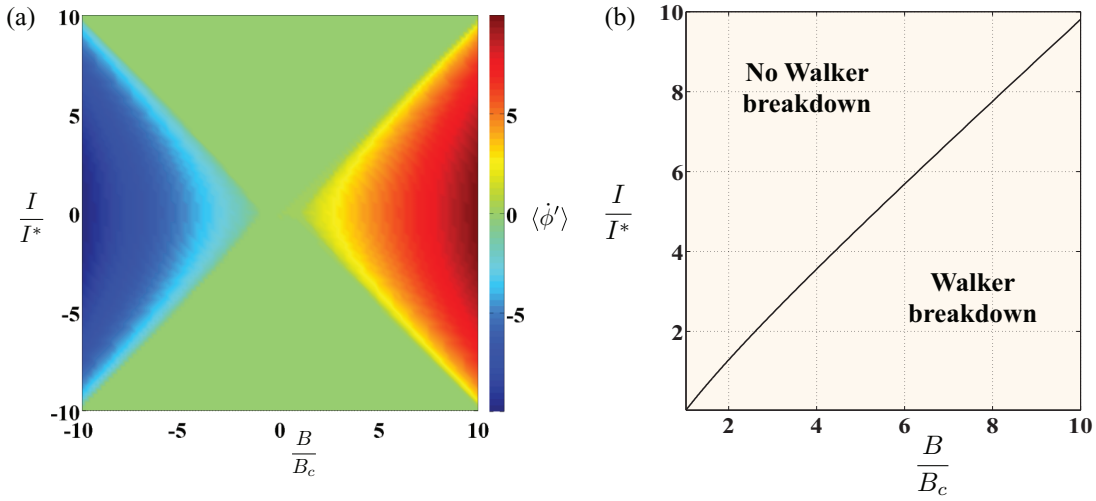

FIG. 2. (Color online) (a) $\langle\dot{\phi}'\rangle$ as a function of I/I^* and B/B_c, valid for both ferro and antiferro exchange couplings. In the green flat region where $\langle\dot{\phi}'\rangle = 0$ WB is absent. In the two triangular regions with $\langle\dot{\phi}'\rangle \neq 0$ WB occurs. (b) WB frontier as a function of I/I^* and B/B_c. Again valid for both ferro and antiferro exchange couplings.

of the field up to which the chiral regime extends, and the chirality stabilization is mediated by the chiral current (third term) rather than by the topological response generated by the extended $(2+1)$ dimensional states (last term).

We plot in Fig. 2(a) the averaged terminal precession velocity $\langle\dot{\phi}'\rangle$, obtained by numerically solving Eq. (16), as a function of B/B_c and I/I^*. The green (light) region indicates zero average precession velocity corresponding to the non-WB regime. In Fig. 2(b) we plot the border between the two regimes for positive I and B for which the magnetic field acquires its critical value $B = B_c$. It is apparent how B_c increases with I with a close to linear behavior, so we face a scenario where the corresponding high mobility μ of the non-WB region is extended to higher fields. This way high velocities can be achieved with relatively low magnetic fields. We stress that the behavior is the same with both ferro- and antiferromagnetic exchange couplings.

Let us take a look to the value of the current I^*. If we set a magnetic strip width of $L_2 = 100\ \mu$m, this current would give rise to a current density of $8 \times 10^{-2} A/m$. This is approximately an order of magnitude smaller than the value at which the breakdown of the dissipationless current occurs $(\sim 1 A/m)$ [23,24]. Looking at Fig. 2, for a magnetic strip 100 μm wide it would be challenging to stay in the non-WB region for fields higher than $B = 10B_c$, as one would need currents of at least $I \sim 10I^*$, which equals to $0.8A/m$ or higher. The wider the strip, the lower the current density corresponding to the current I^*, so the situation improves for wider strips. For a field $B = 10B_c$ and a current density of $0.8A/m$, a velocity of $\dot{X} = 7.2 \times 10^3 m/s$ is achieved for a strip 100 μm wide, an order of magnitude higher than that at B_c, which is a promising result.

V. CURRENT INDUCED DW CHIRALITY REVERSAL AND MACROSCOPIC QUANTUM COHERENCE OF CHIRALITY

In this section we will consider again the chiral sector, initially at zero magnetic field. Solving the equation for ϕ we find that as t increases $\dot{\phi}$ tends to zero and the angle ϕ stabilizes. There are two cases to consider, $sign(K^\perp) = \pm 1$, which give qualitatively different potential energies. The case of interest for us is $sign(K^\perp) = -1$ occurring when $K^\perp_{x_2} = 0$ and assuming that $K^\perp_{x_1}$ is much larger than the anisotropies generated by the fermionic fluctuations. In this case, the potential energy density is:

$$\mathcal{V}(\phi) = \frac{S\mathcal{N}K^\perp_{x_1}}{2}\left(\cos^2\phi + \frac{I_\pm}{I^*}\cos\phi\right). \tag{21}$$

We see that the vacuum is degenerate. If $|I_\pm| \geqslant 2I^*$ the vacuum is given by $\phi = 2n\pi$ for $I_\pm < 0$ and $\phi = (2n+1)\pi$ for $I_\pm > 0$. On the other hand, if $|I_\pm| < 2I^*$ a splitting occurs so there are two minima $\phi_\pm$ for each integer n at $\phi_\pm = 2n\pi \pm \arccos[-I_\pm/(2I^*)]$ for $I_\pm < 0$ and $\phi_\pm = (2n+1)\pi \pm \arccos[-I_\pm/(2I^*)]$ for $I_\pm > 0$. These two minima are separated by a potential barrier whose height increases as $|I_\pm|$ decreases towards zero. In Fig. 3, the potential is plotted for different values of $I_\pm$ (see the cases with $B = 0$ only).

There is a way to flip the chirality of the wall with the help of a weak magnetic field. It is schematically shown in Fig. 3. The idea is to start with a wall configuration in the absence of current, sitting at $\phi = \pi/2$ which is a minimum of the potential for $I_\pm = 0$. Then we switch on a current and slowly increase it up to $-2I^*$, flipping the angle ϕ in the process down to zero. At this point, we introduce a small magnetic field in the $\hat{\mathbf{x}}_3$ direction, and start to decrease the current towards zero. An extra term $\pm\gamma_{\text{eff}}\delta B E \sin\phi$ is generated [see Eq. (9)], such that the reflection symmetry protecting the degeneracy of the two minima ϕ_+ and ϕ_- is broken. Now by choosing the correct sign for B, ϕ will fall to ϕ_-, and one can turn off the magnetic field again. Continuing to decrease the current, we finally end up at $\phi = -\pi/2$ when $I_\pm = 0$. This way we have flipped the chirality of the DW in a totally controlled manner.

Assuming that this flip is performed adiabatically (with a sufficiently slowly varying current), in the process the wall

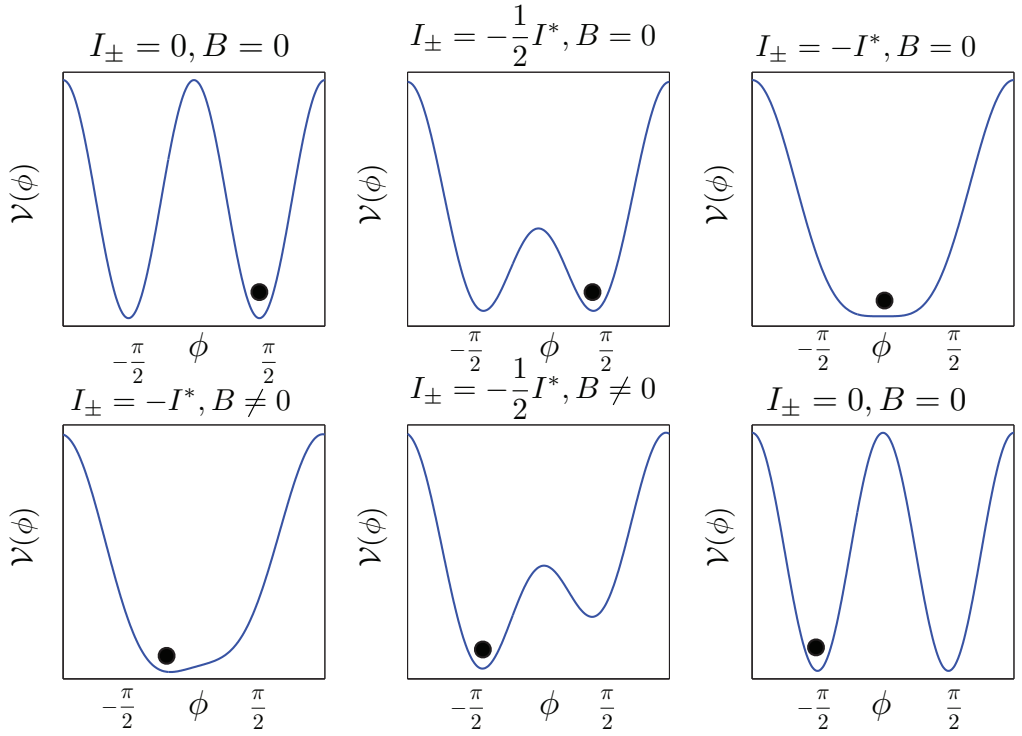

FIG. 3. (Color online) Schematic sequence of chirality reversal (from left to right and top to bottom). The black point represents the actual DW chirality.

performs a displacement of $\Delta X = \pi\delta/\alpha$. This displacement would be an experimental signature of the chirality reversal [6].

Let us now introduce a strong enough pinning potential so we can integrate out the coordinate X and treat ϕ as a particle moving in the potential given by Eq. (21). Quantum tunneling of chirality between different vacua is possible. The frequency of the quantum coherent oscillation between two first neighbor vacua has been obtained before, for a DW in a ferromagnet with finite hard axis anisotropy [25]. Their configuration is analogous to ours if we do $I_\pm = 0$, the two vacua corresponding to $\phi = \pi/2$ and $\phi = -\pi/2$. In Ref. [25] it is found that strong pinning and weak hard axis anisotropy favor the quantum coherence between the two chiralities. In our configuration, the potential barrier that separates the two $\phi_\pm$ vacua decreases as the absolute value of the current is increased towards $2I^*$, and disappears when it reaches $2I^*$. As the probability of quantum tunneling decreases exponentially with the height of the barrier, the quantum coherence between ϕ_+ and ϕ_- can be significantly enhanced by the application of a current. This way one can significantly rise the frequency for the quantum coherent oscillation between positive and negative chiralities, making this phenomenon easier to be observed.

VI. CONCLUSIONS

In the present work we have obtained the equations of motion for a DW coupled both to the surface states of a TI and to external electromagnetic fields. The external electric field acts on the DW via the chiral state through a new type of spin-torque mechanism. By controlling both the electric and magnetic fields the appearance of the Walker breakdown can be held off significantly increasing the terminal velocity of the DW. Also through the appropriate tuning of the electromagnetic fields one can reverse the DW chirality in a controllable manner. This control can be of use to design future logic gates.

ACKNOWLEDGMENTS

The authors gratefully acknowledge M. A. H. Vozmediano for valuable comments and suggestions. This research is partially supported by CSIC JAE-doc fellowship program and the Spanish MECD Grants No. FIS2011-23713 and No. PIB2010BZ-00512.

APPENDIX A: CONTRIBUTION OF THE FERMIONIC BOUND STATES TO THE EFFECTIVE ACTION FOR $B = 0$

Here we show how the computation of the contribution of the fermionic bound states is done, in the absence of magnetic field and for ferromagnetic coupling (it is straightforward to change the calculation for antiferromagnetic coupling). Next we will do the computation for the scattering states, which will give a $(2 + 1)$ dimensional topological Chern-Simons term as we will see. The remaining part would be the contribution of the terms arising from the coupling between the scattering and bound states, but its computation is much more involved and we will skip it. To do so we acknowledge that the scattering states renormalize all terms generated by the massive bound states (via scattering-scattering and scattering-bound states couplings), or in other words the massive bound states can not

generate terms additional to those generated by the scattering states. However, this is not true the other way around, that is, the massive bound states do not renormalize all terms generated by the scattering states. There is one term that is specific from the $(2+1)$ dimensional extended states, which is the topological Chern-Simons term.

Then as we said, the coupling between the scattering and bound states is going to renormalize the terms generated by the bound states alone. By taking into account only the bound state contribution plus the $(2+1)$ Chern-Simons term, we are going to obtain all the possible terms generated by the massive states, but are going to miss the renormalization to the nontopological terms coming from the scattering-bound states coupling. However, this will not be important and will not have an appreciable impact on the final results, as we point out in Sec. III.

As the bound states are localized around $x=-X$, let us expand $\mathbf{m}^{DW}(x_1+X)$ around this point up to the linear term [18]. For the electromagnetic field we choose the gauge $A_1=0$ and $A_i=A_i(t,x_2)$, so we explore the effect of an electric field E pointing along the $\hat{\mathbf{x}}_2$ direction and zero magnetic field B. Under these assumptions, and from the continuum Hamiltonian for the surface states of the TI (see main text), we can write the fermionic action as (all computations in the Appendix will be done in imaginary time, except those in Appendix D):

$$\mathcal{S}_{TI}^{bs}=\int dtd^2x\overline{\Psi}(D_1(x_1)+D_2(t,x_2))\Psi, \quad \text{(A1a)}$$

$$D_1(x_1)=-v_F\sigma_1\partial_1-\Delta S\frac{x_1+X}{\delta}, \quad \text{(A1b)}$$

$$D_2(t,x_2)=\sigma_3(\partial_0-iA_0)-v_F\sigma_2(\partial_2-iA_2')+iv_F\sigma_1A_1', \quad \text{(A1c)}$$

with $A_1'=-\Delta S\sin\phi/v_F$, $A_2'=A_2+\Delta S\cos\phi/v_F$ and $\overline{\Psi}=\Psi^\dagger\sigma_3$. Notice that we did $A_\mu\to A_\mu/e$.

We will exactly compute the spectrum of the operator (A1b) and use it as a basis for the fermion fields. To this end we can express D_1 in terms of creation and annihilation operators of the harmonic oscillator and *chiral* projectors:

$$D_1=\sqrt{\frac{2\Delta Sv_F}{\delta}}(aP_R+a^\dagger P_L), \quad \text{(A2)}$$

where

$$a=-\sqrt{\frac{\delta}{2\Delta Sv_F}}\left(v_F\partial_1+\frac{\Delta S}{\delta}(x_1+X)\right), \quad \text{(A3a)}$$

$$a^\dagger=\sqrt{\frac{\delta}{2\Delta Sv_F}}\left(v_F\partial_1-\frac{\Delta S}{\delta}(x_1+X)\right), \quad \text{(A3b)}$$

$$P_R=\frac{1}{2}(1+\sigma_1),\quad P_L=\frac{1}{2}(1-\sigma_1). \quad \text{(A3c)}$$

a and $a^\dagger$ fulfill the commutation relation $[a,a^\dagger]=1$.

D_1 is not a Hermitian operator, so we diagonalize $D_1^\dagger D_1$ instead and obtain:

$$\Psi(t,x_1,x_2)=\sum_{n=0}^{\infty}\left\{\rho_n(x_1+X)\Psi_R^n(t,x_2)+\rho_{n-1}(x_1+X)\Psi_L^n(t,x_2)\right\}, \quad \text{(A4a)}$$

$$\overline{\Psi}(t,x_1,x_2)=\sum_{n=0}^{\infty}\left\{\overline{\Psi}_R^n(t,x_2)\rho_n^*(x_1+X)+\overline{\Psi}_L^n(t,x_2)\rho_{n-1}^*(x_1+X)\right\}, \quad \text{(A4b)}$$

with $\Psi_{R,L}^{(n)}=P_{R,L}\Psi^{(n)}$ and $\overline{\Psi}_{R,L}^{(n)}=\Psi^{(n)}P_{L,R}$. The functions ρ_n are defined through ($\int dx\rho_{n'}^*\rho_n=\delta_{n'n}$):

$$a^\dagger a\rho_n=n\rho_n, aa^\dagger\rho_n=(n+1)\rho_n, \quad \text{(A5a)}$$

$$a^\dagger\rho_n=\sqrt{n+1}\rho_{n+1}, a\rho_n=\sqrt{n}\rho_{n-1}. \quad \text{(A5b)}$$

From the standard knowledge of the theory of the harmonic oscillator, we know that there is always a zero mode $D_1^\dagger D_1\Psi_0=0$ with $\Psi_0=\rho_0\psi_R^0(t,x_2)$ being chiral.

So far we have calculated the eigenstates linearizing $\tanh(\frac{x_1+X}{\delta})$, and we have an infinite discrete Hilbert spectrum. The linear approximation should only be valid in the region $|x_1+X|<\delta/2$. Beyond this point, the spectrum already calculated differs substantially to the real one, which is known to consist of a finite number of bound states and the continuum (scattering states), so we have to impose a cutoff in n. There are two equivalent ways of doing it. One is to compute the spatial dispersion of each eigenstate in the coordinate x_1 and assume that it must be smaller than the DW width. The other possibility is to impose that the masses of the bound states have to be smaller than the asymptotic mass of the scattering states. Following the second route, we have that the highest value of n is reached when:

$$\sqrt{D_1^\dagger D_1}\rho_N<\Delta S\rho_N, \quad \text{(A6)}$$

so

$$N<\frac{\Delta S\delta}{2v_F}\equiv\theta. \quad \text{(A7)}$$

Taking into account the (massless) zero mode, the total number of bound states is $N+1$, N being the largest integer smaller than θ. To illustrate the effect of having more bound states than the chiral one, we will restrict ourselves to calculate the effective action for the two illustrative cases of $N=0$ (just the chiral zero mode) and $N=1$ (one massive bound state apart of the chiral zero mode).

At this point, it is convenient to explicitly decompose the bispinor $\Psi^n=(\alpha^n,\chi^n)$ in its chiral parts:

$$\Psi_R^n=\psi_R^n\frac{1}{\sqrt{2}}\begin{pmatrix}1\\1\end{pmatrix},\Psi_R^n=\psi_R^n\frac{1}{\sqrt{2}}\begin{pmatrix}1\\-1\end{pmatrix} \quad \text{(A8a)}$$

$$\psi_R^n=\frac{1}{\sqrt{2}}(\alpha^n+\chi^n),\quad \psi_L^n=\frac{1}{\sqrt{2}}(\alpha^n-\chi^n). \quad \text{(A8b)}$$

Now, substituting in (A1a) the eigenmode expansion (A4), using the decomposition (A8) and integrating over the spatial coordinate x_1, we arrive at the following $(1+1)$ action:

$$\mathcal{S}^{bs}_{TI} = \mathcal{S}^0 + \mathcal{S}^1 + \mathcal{S}^{01}, \tag{A9a}$$

$$\mathcal{S}^0 = \int dtdx_2 \psi^{0+}_R(\hat{\partial} - i\hat{A})\psi^0_R, \tag{A9b}$$

$$\mathcal{S}^1 = \int dtdx_2 \Big\{ \psi^{1+}_R(\hat{\partial} - i\hat{A})\psi^1_R + \psi^{1+}_L(\hat{\partial}^* + i\hat{A}^*)\psi^1_L + \sqrt{\frac{2\Delta S v_F}{\delta}}\left(\psi^{1+}_R\psi^1_L + \psi^{1+}_L\psi^1_R\right)\Big\}, \tag{A9c}$$

$$\mathcal{S}^{01} = \int dtdx_2 \Big\{ i v_F\left(\psi^{1+}_L A_1'\psi^0_R - \psi^{0+}_R A_1'\psi^1_L\right) + \sqrt{\frac{\Delta S}{2v_F\delta}}\left(\psi^{1+}_R \dot{X}\psi^0_R - \psi^{0+}_R\dot{X}\psi^1_R\right)\Big\}, \tag{A9d}$$

where we have defined the *chiral* operators $\hat{\partial} = \partial_0 + i v_F \partial_2$ and $\hat{A} = A_0 + i v_F A_2'$, and $\dot{X} = \partial_0 X$. It is important here to note that when $N = 0$ $(0 < \theta \leqslant 1)$ only the chiral mode is present so $\mathcal{S}^1$ and $\mathcal{S}^{01}$ are absent.

In order to get the effective action in terms of the variables $X(t)$ and $\phi(t)$, and the external electric field, we integrate out the fermions in the corresponding functional integral and find, to 1-loop order:

$$\Gamma^{bs}_{TI} = \Gamma^{bs}_{A'} + \Gamma^{bs}_X + \Gamma^{bs}_{||}, \tag{A10a}$$

$$\Gamma^{bs}_{A'} = -\frac{1}{2}Tr\Big\{\hat{\partial}^{-1}\hat{A}\hat{\partial}^{-1}\hat{A} + (\hat{\partial} g_0 \hat{A}^* \hat{\partial} g_0 \hat{A}^* + c.c.) + \frac{4\Delta S v_F}{\delta} g_0 \hat{A} g_0 \hat{A}^*\Big\}, \tag{A10b}$$

$$\Gamma^{bs}_X = -i\frac{\Delta S v_F}{\delta} Tr\{g_0 A_1' \hat{\partial}^{-1}\dot{X} + \hat{\partial}^{-1} A_1' g_0 \dot{X}\}, \tag{A10c}$$

$$\Gamma^{bs}_{||} = -v_F^2 Tr\left\{\frac{2\Delta S v_F}{\delta}\hat{\partial} g_0 A_1' \hat{\partial}^{-1} g_0 A_1' - \hat{\partial} g_0 A_1' \hat{\partial}^* g_0 A_1'\right\}, \tag{A10d}$$

where Tr is the trace and $g_0 = (\hat{\partial}\hat{\partial}^* - 2\Delta S v_F/\delta)^{-1}$. The evaluation of the integrals in (A10) is tedious but standard. We are interested in the low energy dynamics of the effective action so we will keep terms up to order $O(\frac{p^2}{\Delta^2 S^2})$ in the expansion parameter $p/\Delta S$. The final result reads [26]

$$\Gamma^{bs}_{A'} = \frac{1}{4\pi v_F}\int dtdx_2 A_a'\left\{\delta_{ab} - \frac{\partial_a\partial_b}{\partial^2} - \frac{i}{2\partial^2}(\epsilon_{cb}\partial_a\partial_c - \epsilon_{ad}\partial_d\partial_b)\right\}A_b', \tag{A11a}$$

$$\Gamma^{bs}_{||} = \frac{\Delta^2 S^2}{4\pi v_F}\int dtdx_2\left(\gamma + \ln\left(\frac{\theta^{-1}}{8\pi}\right)\right)\sin^2\phi, \tag{A11b}$$

and $\Gamma^{bs}_X = 0$. Now we have $\partial_a = (\partial_0, v_F\partial_2)$, $A_a' = (A_0, v_F A_2 + \Delta S\cos\phi)$, and remember that $\theta = \Delta S\delta/(2v_F)$. The contribution (A11a) is generated by the chiral state alone, and its gauge variation is not zero, revealing the anomalous nature of the chiral $(1+1)$ theory [27] living in the wall. On the other hand (A11b) is generated by the coupling between the chiral and massive bound states. This term is renormalized by the corresponding term coming from the coupling between the chiral and scattering states, but as we said at the beginning of this section we are not going to compute the former, as the computation would be much more involved. We argue in Sec. III that this will not affect our final results. Finally the massive-massive coupling does not contribute to this order $O(\frac{p^2}{\Delta^2 S^2})$.

We can be more explicit and split $\Gamma^{bs}_{A'}$ in its two contributions coming from the gauge field A_a and the part depending on the collective coordinate $\phi(t)$, $\Gamma^{bs}_{A'} = \Gamma^{bs}_A + \Gamma^{bs}_\phi$:

$$\Gamma^{bs}_A = \frac{1}{4\pi v_F}\int dtdx_2 A_a\left(\delta_{ab} - \frac{\partial_a\partial_b}{\partial^2} - \frac{i}{2\partial^2}(\epsilon_{cb}\partial_a\partial_c - \epsilon_{ad}\partial_d\partial_b)\right)A_b, \tag{A12a}$$

$$\Gamma^{bs}_\phi = \frac{\Delta S}{4\pi}\int dtdx\left(2\cos\phi\frac{1}{\partial_0 + i v_F\partial_2}E + \frac{\Delta S}{v_F}\cos^2\phi - i\frac{1}{v_F}A_0\cos\phi\right), \tag{A12b}$$

where $E = \partial_0 A_2 - \partial_2 A_0$. The terms that violate gauge invariance are the last terms in the integrand of both (A12a) and (A12b). Let us stress that the expression (A11b) is valid only at order $O(\frac{p^2}{\Delta^2 S^2})$, while expressions (A12a) and (A12b) are exact.

APPENDIX B: CONTRIBUTION OF THE FERMIONIC SCATTERING STATES TO THE EFFECTIVE ACTION FOR $B = 0$

The propagating states of the fermionic spectrum could potentially contribute to the effective action of the DW, but we will see that their contribution to the $(1+1)$ effective action is going to be zero up to order $O(\frac{p^2}{\Delta^2 S^2})$. However, despite having a null $(1+1)$ contribution, the scattering states generate a $(2+1)$ Chern-Simons term that is essential to restore the gauge invariance that was lost in the isolated $(1+1)$ chiral theory [16].

To avoid computing the exact form of the fermionic spectrum we can resort on the adiabatic approximation [28] assuming that the scattering states for a *tanh* type of mass are asymptotically equal to the scattering states for a *constant* mass. This approximation turns out to be valid in the low energy limit where $p \ll |\Delta S|$. We start from the Hamiltonian for the surface states of the TI and write the fermionic action. As we are now not computing the exact fermionic spectrum (in which case it emerges naturally), it is important to notice that, as the magnetization is translated by $-X(t)$, so have to

be the fermions: $\Psi = \Psi(t,x_1 + X(t),x_2)$. We have:

$$\mathcal{S}_{TI} = \int dtd^2x\overline{\Psi}(t,x_1,x_2)(\sigma_3(\partial_0 + \dot{X}\partial_1) - i\sigma_3 A_0' - v_F\sigma_1(\partial_1 - iA_1') - v_F\sigma_2(\partial_2 - iA_2') + m)\Psi(t,x_1,x_2), \tag{B1}$$

where $A_0' = A_0$, $A_1' = -\Delta S\,\mathrm{sech}(x_1/\delta)\sin\phi/v_F$, $A_2' = A_2 + \Delta S\,\mathrm{sech}(x_1/\delta)\cos\phi/v_F$, $m = -\Delta S\tanh(x_1/\delta)$ (we are taking again a ferromagnetic exchange coupling) and we did a change of variables $x_1 \to x_1 - X$. The strategy is to integrate out the fermions with a constant mass m, so a Chern-Simons term is obtained, and then substitute m by $-\Delta S\tanh(x_1/\delta)$, arriving to (in imaginary time):

$$\Gamma_{TI}^{\text{scatt}} = \frac{i}{8\pi}\int dtd^2x\,sign(x_1)\epsilon_{\mu\rho\nu}A_\mu'\partial_\rho A_\nu'. \tag{B2}$$

If we integrate over x_1, $\Gamma_{TI}^{\text{scatt}}$ vanishes (except a term needed to restore gauge invariance, as we will see in a moment). But the crucial point is that despite its contribution to the $(1+1)$ effective action being zero, its gauge variation is finite. If we substitute the explicit value of A_μ' in (B2) we get a standard Chern-Simons term for A_a (with $a = 0,2$), but with a mass that changes sign, and a contribution mixing the components of the gauge field A_a and the collective coordinate ϕ. The gauge variation of the Chern-Simons term cancels exactly the gauge variation of the anomalous chiral $(1+1)$ effective action (A12a). On the other hand, the mixed term, when integrated over x_1, exactly cancels the last term in Eq. (A12b). So the scattering states do not contribute to the effective action of the DW (for $B = 0$), but are crucial to restore gauge invariance.

APPENDIX C: PRESENCE OF A PERPENDICULAR MAGNETIC FIELD *B*

When an external magnetic field is applied perpendicular to the sample, new contributions to the effective action appear. The first thing to note is that the magnetic field B couples to the fermions both through the gauge field A_μ (orbital contribution) and through a Zeeman term. For small magnetic fields a perturbative treatment of the orbital coupling is justified, but for big fields LL formation becomes relevant and this is no longer the case. However, as explained in the main text, whichever the magnitude of the field the topological response of the $(2+1)$ scattering states is going to be the same.

Regarding the chiral state, it will not see the magnetic field due to its chiral nature. Then the only contribution will be the Chern-Simons term generated by the scattering states (it was zero in the case $B = 0$, but it will be finite for finite B). Of course this is not completely true, because the coupling between the chiral and the massive states could give new contributions also. We can check if this is the case by doing the computation with the bound states, as we did in Appendix A. To do it, we can treat the orbital coupling perturbatively, as bound states live in $(1+1)$ and the magnetic field is not going to generate a topological nonperturbative response, as is the case in $(2+1)$ with the QHE. Doing the computation one finds that new terms do not appear up to order $O(\frac{p^2}{\Delta^2 S^2})$.

Then the only contribution is the topological Chern-Simons term generated by the scattering states. So we can directly import the expression (B2) and substitute $\mathrm{sign}(x_1)$ by $sign(m)$, with m being:

$$m = -\Delta S\tanh\left(\frac{x_1}{\delta}\right) + \gamma_{TI}B. \tag{C1}$$

For the chiral regime we can write $sign(m)$ as:

$$sign\left(-\Delta S\tanh\left(\frac{x_1}{\delta}\right) + \gamma_{TI}B\right) = sign\left(-x_1 + \delta\tanh^{-1}\left(\frac{\gamma_{TI}B}{\Delta S}\right)\right), \tag{C2}$$

and for the nonchiral regime:

$$sign\left(-\Delta S\tanh\left(\frac{x_1}{\delta}\right) + \gamma_{TI}B\right) = sign(B). \tag{C3}$$

Then, doing the integration in the coordinate x_1 on the Chern-Simons term with the $sign$ functions just obtained, we arrive at the following new contributions to the effective action. For the chiral regime:

$$\Gamma_{TI}^{\text{scatt}} = i\int dtdx_2\frac{\delta\gamma_{TI}BE}{2\pi v_F}\sin\phi, \tag{C4}$$

where we did an expansion up to first order in $\gamma_{TI}B/(\Delta S)$. Of course this expansion is justified if $\gamma_{TI}B \ll \Delta S$, and this way we can write $\Delta S\tanh(x_1/\delta) + \gamma_{TI}B \approx \Delta S\tanh(x_1/\delta + \gamma_{TI}B/(\Delta S))$ and then linearize the function tanh, so the computation done for $B = 0$, based on this linearization, qualitatively holds for $B \neq 0$ in the chiral regime.

On the other hand, for the nonchiral regime we have:

$$\Gamma_{TI}^{\text{scatt}} = iS\int dtdx_2\frac{\Delta\delta sign(B)E}{4v_F}\sin\phi. \tag{C5}$$

APPENDIX D: ELECTROMAGNETIC CURRENT CONFIGURATION IN THE CHIRAL REGIME

Let us go to the chiral regime and calculate the total 1D charge density and charge current density flowing through the wall. From the real time effective action (see main text) we have:

$$J_{0,\pm}^{1D} = \mp\frac{1}{2\pi}\frac{1}{\partial_0 \pm v_F\partial_2}E, \tag{D1}$$

$$J_{1,\pm}^{1D} = 0, \tag{D2}$$

$$J_{2,\pm}^{1D} = \frac{1}{2\pi}\frac{1}{\partial_0 \pm v_F\partial_2}(v_F E - \Delta S\sin\phi\,\dot{\phi}) + \gamma_{\text{eff}}\delta B\cos\phi\,\dot{\phi}. \tag{D3}$$

Notice that the current density in the $\hat{\mathbf{x}}_2$ direction has two contributions generated by the motion of the DW, in addition to the electromagnetic contribution which we call J^{EM}:

$$J_{0,\pm}^{EM} = \mp\frac{1}{2\pi}\frac{1}{\partial_0 \pm v_F\partial_2}E, \tag{D4}$$

$$J_{2,\pm}^{EM} = \frac{v_F}{2\pi}\frac{1}{\partial_0 \pm v_F\partial_2}E. \tag{D5}$$

Due to the anomaly of the $1+1$ theory of the Wall, the 1D current density is not conserved:

$$\partial^\mu J^{1D}_{\mu,\pm} = \mp\frac{E}{2\pi}. \tag{D6}$$

Now we are going to obtain a specific configuration for the electromagnetic current by fixing the boundary conditions. Let us first compute its general form by calculating the integral operator $1/(\partial_0 \pm v_F\partial_2)$. We compute $J^{EM}_{2\pm}$, and with the nonconservation equation of the 1D current we then obtain $J^{EM}_{0\pm}$. Skipping the explicit calculation we have:

$$J^{EM}_{0\pm} = \int_t dt'\left[\mp\frac{E}{2\pi} + \partial_2\eta_\pm(t' \mp x_2/v_F)\right] + C_\pm, \tag{D7}$$

$$J^{EM}_{2\pm} = \frac{v_F}{2\pi}\int_t dt' E + \eta_\pm(t' \mp x_2/v_F), \tag{D8}$$

where $\eta_\pm$ and $C_\pm$ are a function and a constant, respectively, to be determined by the initial and boundary conditions. We impose $J^{EM}_{2\pm}$ to be time independent and

$$J^{EM}_{2\pm}(x_2 = -L_2/2) = 0, \tag{D9}$$

so we have:

$$J^{EM}_{2,\pm} = \pm\frac{E}{2\pi}(x_2 + \frac{L_2}{2}). \tag{D10}$$

If we take an electrostatic field configuration,

$$A_0(x_2) = -Ex_2 + const., \tag{D11}$$

we can write the current as a function of the voltage between the point $x_2 = -L_2/2$ and a given point x_2 along the DW:

$$J^{EM}_{2,\pm} = \mp\frac{1}{2\pi}(A_0(x_2) - A_0(-L_2/2)). \tag{D12}$$

The averaged current along the DW then is:

$$I_\pm = \frac{1}{L_2}\int_{-\frac{L_2}{2}}^{\frac{L_2}{2}} dx_2 J^{EM}_{2,\pm} = \mp\frac{V}{4\pi}, \tag{D13}$$

with $V = A_0(L_2/2) - A_0(-L_2/2)$ being the voltage between both sides of the magnetic strip. A similar current configuration was recently used in the literature [14].

[1] S. S. P. Parkin, M. Hayashi, and L. Thomas, Science **320**, 190 (2008).
[2] L. Thomas, R. Moriya, C. Rettner, and S. S. Parkin, Science **330**, 1810 (2010).
[3] J. Shibata, G. Tatara, and H. Kohno, J. Phys. D: Appl. Phys. **44**, 384004 (2011).
[4] G. S. D. Beach, C. Nistor, C. Knutson, M. Tsoi, and J. L. Erskine, Nat. Mater. **4**, 741 (2005).
[5] G. Tatara, H. Kohno, and J. Shibata, Phys. Rep. **468**, 213 (2008).
[6] I. M. Miron, T. Moore, H. Szambolics, L. D. Buda-Prejbeanu, S. Auffret, B. Rodmacq, S Pizzini, J. Vogel, M. Bonfim, A. Schuhl, and G. Gaudin, Nat. Mater. **10**, 419 (2011).
[7] H. Onho, D. Chiba, F. Matsukura, T. Oyima, E. Abe, T. Dietl, Y. Ohno, and K. Ohtani, Nature (London) **408**, 944 (2000).
[8] A. Schellekens, A. van den Brink, J. Franken, H. Swagten, and B. Koopmans, Nat. Commun. **3**, 847 (2011).
[9] M. Katsnelson, F. Guinea, and M. A. H. Vozmediano, EPL **104**, 17001 (2013).
[10] P. Wei, F. Katmis, B. A. Assaf, H. Steinberg, P. Jarillo-Herrero, D. Heiman, and J. S. Moodera, Phys. Rev. Lett. **110**, 186807 (2013).
[11] I. Garate and M. Franz, Phys. Rev. Lett. **104**, 146802 (2010).
[12] K. Nomura and N. Nagaosa, Phys. Rev. B **82**, 161401 (2010).
[13] T. Yokoyama, J. Zang, and N. Nagaosa, Phys. Rev. B **81**, 241410 (2010).
[14] Y. Tserkovnyak and D. Loss, Phys. Rev. Lett. **108**, 187201 (2012).
[15] J. C. Slonczewski, AIP Conf. Proc. **5**, 170 (1972).
[16] C. G. Callan and J. A. Harvey, Nucl. Phys. B **250**, 427 (1985).
[17] S. Chandrasekharan, Phys. Rev. D **49**, 1980 (1994).
[18] C. Fosco and A. López, Nucl. Phys. B **538**, 685 (1999).
[19] P. Cheng, C. Song, T. Zhang, Y. Zhang, Y. Wang, J.-F. Jia, J. Wang, Y. Wang, B.-F. Zhu, X. Chen, X. Ma, K. He, L. Wang, X. Dai, Z. Fang, X. Xie, X.-L. Qi, C.-X. Liu, S.-C. Zhang, and Q.-K. Xue, Phys. Rev. Lett. **105**, 076801 (2010).
[20] A. N. Redlich, Phys. Rev. D **29**, 2366 (1984).
[21] X.-L. Qi, Y.-S. Wu, and S.-C. Zhang, Phys. Rev. B **74**, 085308 (2006).
[22] R. J. Hughes, Phys. Lett. B **148**, 215 (1984).
[23] G. Nachtwei, Physica E **4**, 79 (1999).
[24] V. Singh and M. M. Deshmukh, Phys. Rev. B **80**, 081404 (2009).
[25] S. Takagi and G. Tatara, Phys. Rev. B **54**, 9920 (1996).
[26] To compute the loop integrals we used dimensional regularization. In the expression for $\Gamma^{bs}_{||}$ the argument of the logarithm should read $\ln(\Delta^2 S^2\theta^{-1}/8\pi\mu^2)$, where μ is a fake parameter with dimensions of mass, product of dim. regularization. We fix it to the scale of the low energy physics of the problem, which is ΔS.
[27] R. Jackiw and R. Rajaraman, Phys. Rev. Lett. **54**, 1219 (1985).
[28] H. T. Ueda, A. Takeuchi, G. Tatara, and T. Yokoyama, Phys. Rev. B **85**, 115110 (2012).

Article B

Dirac electrons and domain walls: A realization in junctions of ferromagnets and topological insulators

PHYSICAL REVIEW B **92**, 085416 (2015)

Dirac electrons and domain walls: A realization in junctions of ferromagnets and topological insulators

Yago Ferreiros,[1,*] F. J. Buijnsters,[2,†] and M. I. Katsnelson[2,‡]
[1]*Instituto de Ciencia de Materiales de Madrid, CSIC, Cantoblanco, 28049 Madrid, Spain*
[2]*Institute for Molecules and Materials, Radboud University Nijmegen, Nijmegen, the Netherlands*
(Received 25 June 2015; published 13 August 2015)

We study a system of Dirac electrons with finite density of charge carriers coupled to an external electromagnetic field in two spatial dimensions, with a domain wall (DW) mass term. The interface between a thin-film ferromagnet and a three-dimensional topological insulator provides a condensed-matter realization of this model, when an out-of-plane domain wall magnetization is coupled to the topological insulator surface states. We show how, for films with very weak intrinsic in-plane anisotropies, the torque generated by the edge electronic current flowing along the DW competes with an effective in-plane anisotropy energy, induced by quantum fluctuations of the chiral electrons bound to the wall, in a mission to drive the internal angle of the DW from a Bloch configuration towards a Néel configuration. Both the edge current and the induced anisotropy contribute to stabilize the internal angle, so that for weak intrinsic in-plane anisotropies DW motion is still possible without suffering from an extremely early Walker breakdown.

DOI: 10.1103/PhysRevB.92.085416 PACS number(s): 75.78.Fg, 03.65.Vf, 85.75.−d, 73.20.−r

I. INTRODUCTION

Dirac fermions in two spatial dimensions have been the object of intense study in recent times in the condensed-matter world, especially since the experimental realization of graphene [1–3] and, more recently, the discovery of three-dimensional topological insulators (TI) [4–6], which host Dirac fermions as topologically protected surface states. On the other hand, magnetic DWs and their manipulation via applied currents and electromagnetic fields hold a prominent position in the field of spintronics, especially so since the experimental realization of the "race-track" technology [7,8].

The search of efficient ways of moving a DW at the highest possible velocities has become of capital importance. Manipulation based on the application of external magnetic fields [9–15], currents [16–22], and more recently magnons [23–29] and electric fields [30,31] has been proposed and, with the exception of magnonic manipulation, experimentally realized. There is an upper limit on the DW velocity due to the phenomenon known as Walker breakdown (WB) [9]. Above a threshold applied current or magnetic field, the internal structure of the DW, as described by its internal angle, becomes unstable. The net velocity of the DW is limited by this effect. As a consequence, the search of mechanisms that can stabilize the internal angle of the DW has become an important task [15,32]. In this regard, stabilization mediated by Dzyaloshinskii-Moriya (DM) interactions [33,34] and Rashba fields [35] has been explored and experimentally realized.

The appearance of three-dimensional TIs has focused the interest on what we could call Dirac-fermion-mediated ferromagnetism [36] and spintronics. The aspect of TIs that makes them highly valuable for spintronic applications is that the spin orientation of the surface electrons is fixed relative to their propagation direction, so that the effects of spin-orbit coupling are maximal. For this reason, some proposals [37–40] have suggested that TIs could possess more efficient spin-orbit-induced torques than other materials previously considered. Indeed, the strength of the spin-transfer torque per unit charge-current density, exerted by the TI surface states on the magnetization of an adjacent ferromagnetic permalloy thin film, has recently been measured to be greater than for any other spin-transfer source measured so far [41,42].

In this context it seems natural and promising to study TIs coupled to ferromagnets [43–50] and specifically to DWs [51–57]. If we couple a TI layer to an out-of-plane magnetized ferromagnetic thin film containing a domain wall, the DW acts as a mass for the surface electrons. It is a realization of a system of Dirac fermions with a DW mass term. The theory of this system coupled to electromagnetism was studied in a field-theoretical context in Ref. [58]. These authors showed how the $2n$-dimensional anomaly of the chiral fermions living in the DW is canceled by the anomaly due to the induced $2n+1$ topological mass term. This cancellation in three space-time dimensions has been explicitly computed for fermions coupled to an Abelian gauge field in Ref. [59], where the technical difficulties that appear when trying to obtain the effective action in the presence of a DW mass become apparent.

In this article, we obtain analytical expressions for the effective action for an external electromagnetic field of a system of Dirac fermions in two spatial dimensions, at a finite density of charge carriers and with a DW mass term. We look at a physical realization in junctions of three-dimensional TIs and ferromagnets with out-of-plane easy-axis anisotropy that host an out-of-plane DW. We show how the surface electrons of the TI induce an effective in-plane anisotropy energy, which stabilizes the DW in a Bloch configuration even in thin ferromagnetic films where in-plane intrinsic and dipolar (shape) anisotropies are relatively weak. Owing to the stabilization of the internal angle, DW motion is possible without suffering from a very early Walker breakdown.

We also show how equilibrium and nonequilibrium edge currents can be generated along the DW by applying, respectively, a gate voltage (doping with electrons/holes) or an electric field.

*yago.ferreiros@csic.es
†f.buijnsters@science.ru.nl
‡m.katsnelson@science.ru.nl

This current exerts a torque on the magnetization that drives the internal angle from the Bloch configuration towards a Néel configuration. We analytically compute the behavior of the DW internal angle as a function of the chemical potential and find it to qualitatively agree with a recent numerical calculation [57]. Furthermore, this edge current contributes to the stabilization of the internal degree of freedom of the DW in a similar way as the DM interaction. It turns out that the corresponding term in the effective action, although it is first order in the magnetization, qualitatively resembles that of an interfacial DM interaction. Here the DM interaction is tunable, with the interaction strength given by the amount of edge current flowing along the DW.

Our approach has the advantage that, since the calculation is done at the microscopic level, the origin of the physics underlying the phenomenology can be traced and well understood.

II. EFFECTIVE ACTION

In this section, we present a calculation of the effective action for the electromagnetic field coupled to a system of Dirac electrons with a DW mass. Readers interested primarily in the physics and phenomenology of ferromagnet-TI junctions may skip to Sec. III.

Let us start from the action of $3d$ Dirac fermions (in the following nd will be used for n-dimensional) coupled to an external electromagnetic field:

$$\mathcal{S} = \int d^3x\, \bar{\Psi}\big(i\, l^{\mu}_{\ \nu}\gamma^{\nu}(\partial_{\mu} - ieA_{\mu}) - m - \gamma^0\mu\big)\Psi \qquad (1)$$

with the DW mass

$$m = m_0\sigma \tanh(x_1/\delta), \qquad (2)$$

where $x_{\mu} = (x_0, x_1, x_2)$, x_0 is time, and $\sigma = \pm 1$ and δ are the topological charge and the width of the DW, respectively, we define $\bar{\Psi} = \Psi\gamma^0$, μ is the chemical potential, $l^{\mu}_{\ \nu}$ is given by

$$l^{\mu}_{\ \nu} = \begin{pmatrix} 1 & 0 & 0 \\ 0 & v & 0 \\ 0 & 0 & v \end{pmatrix} \qquad (3)$$

and the gamma matrices satisfy the anticommutation relations $\{\gamma^{\mu}, \gamma^{\nu}\} = 2\eta^{\mu\nu}$. We work with a metric with signature $(+, -, -, -)$ and with $\hbar = c = 1$. We consider the general case where the velocity v is not necessarily equal to the speed of light c.

We obtain the effective action for A_{μ} up to second order in the fields. The fermionic spectrum consists of a chiral massless state bound to the DW plus massive extended states (see Appendix A). If the DW is wide enough, massive bound states also appear. The total number of bound states is given by the largest integer less than $\lambda + 1$, with the parameter λ given by

$$\lambda = \frac{m_0\delta}{v} \qquad (4)$$

(see Appendix A). Let us consider the case where we have a DW that is so steep that the only bound state is the chiral state ($\lambda \leqslant 1$), so that we can do an enlightening separation. We can consider the system as described by two theories, one $2d$ edge theory, describing the chiral electrons localized near the DW center, and one $3d$ bulk theory describing the massive extended electrons. Each of these theories, considered in isolation, is anomalous. The $2d$ chiral edge theory, on the one hand, is well known to be chiral anomalous [60], while the anomaly in the bulk theory is a consequence of the generation [via a Chern-Simons (CS) term] of a topological mass of opposite signs on either side of the DW. However, the anomalies cancel via the Callan-Harvey mechanism [58], so that the complete theory is anomaly free.

The perturbative calculation of the effective action would in principle require computing the fermionic propagator from the exact fermionic spectrum, and then performing the integration of the fermionic degrees of freedom in the path integral. This was done to second order in A_{μ} and for $\mu = 0$ in Ref. [59] as an explicit verification of the anomaly cancellation, but these authors considered only the case $m_0 \to \infty$ and focused exclusively on those terms that contain either two-dimensional or three-dimensional antisymmetric tensors, which are the terms relevant for the anomalies. The complete analytic computation for finite m_0 and μ remains a formidable task.

To make the calculation tractable, we must introduce a number of approximations. First, we consider the adiabatic limit, assuming a constant mass in the calculations and restoring the x_1 dependence at the end. This approximation captures the bulk contribution (extended states) and is reliable as long as the energy associated with the typical length of the inhomogeneities in the mass is much smaller than the energy of the extended states ($\sim m_0$). This means that the approximation is asymptotically exact, but near the DW center it translates into the condition $v/\delta \ll m_0$ which is never fulfilled if we consider the case $\lambda \leqslant 1$. As a consequence, nonadiabatic corrections will appear near the DW. Furthermore, even if the condition is fulfilled, this approach cannot describe the contribution of the bound states. Hence, as a second approximation, we add the contribution of the chiral state, assuming $\lambda \leqslant 1$ to avoid further computations for the contribution of the massive bound states. As a third and final approximation, we compute nonadiabatic corrections to the CS term of the bulk contribution. To obtain these corrections, we impose gauge invariance and the cancellation of the anomalies in the two theories (bulk-edge correspondence).

A. Edge theory

Let us first compute the $2d$ edge effective action. From the action of Eq. (1) and the fermionic spectrum obtained in Appendix A, the classical action for the chiral mode can be written as

$$\mathcal{S}_{R,L} = \int d^3x\, \rho^2_{\lambda}(x_1)\, \psi^{(0)^*}_{R,L}(x_0, x_2)(i\partial_0 + eA_0 + \sigma v(i\partial_2 + eA_2) - \mu)\psi^{(0)}_{R,L}(x_0, x_2), \qquad (5)$$

where [see Eq. (A10)]

$$\rho_{\lambda}(x_1) = B_0(\lambda)\cosh^{\lambda+1}(x_1/\delta) \times {}_2F_1\left[\tfrac{1}{2}, \lambda + \tfrac{1}{2}, \tfrac{1}{2}; -\sinh^2(x_1/\delta)\right], \qquad (6)$$

with $B_0(\lambda)$ defined in Eq. (A15) and ${}_2F_1$ the hypergeometric function. When $\sigma = -1$ we have $\mathcal{S}_R$ and when $\sigma = 1$ we have $\mathcal{S}_L$.

Before proceeding, we partially fix the gauge. Let us set

$$A_\mu \to \theta^{(\mu)}(x_1)A_\mu(x_0,x_2), \tag{7}$$

where $\theta^{(\mu)}(x_1)$ is a given function of x_1. The remaining gauge freedom is given by

$$A_\mu \to A_\mu + \partial_\mu \omega, \tag{8}$$

with $\omega \neq \omega(x_1)$.

1. Equilibrium edge current

As a consequence of having a finite chemical potential, when integrating out the chiral fermion in Eq. (5) the tadpole terms do not vanish. This gives linear terms in the effective action and an associated equilibrium (external electromagnetic fields set to zero) chiral edge current density along the DW. The linear terms can be computed from the tadpolelike term (in imaginary time):

$$\Gamma_{\rm eq} = -ie\int d^3x\, \rho_\lambda^2(x_1)\,(iA_0 + \sigma v A_2) \times \int \frac{dq_0 dq_2}{4\pi^2}\frac{1}{q_0 + \sigma i v q_2 - i\mu}. \tag{9}$$

By multiplying and dividing by $q_0 - \sigma i v q_2 + i\mu$ the integral in momenta can be rewritten as an even plus an odd part in q_0. The integration of the odd part vanishes, while the integration over both momenta of the even part gives (going back to real time)

$$\Gamma_{\rm eq} = -\frac{e\mu}{2\pi v}\int d^3x\, \rho_\lambda^2(x_1)(A_0 + \sigma v A_2), \tag{10}$$

so that we can define the equilibrium edge current density as

$$j^a_{\rm eq} = -\frac{e\mu}{2\pi v}\rho_\lambda^2(x_1)(1,\sigma v). \tag{11}$$

Here and from now on the Greek letters refer to dimensions x_0, x_2: $a = 0,2$.

2. Chiral anomaly

The action of Eq. (5) is analogous to that of the $2d$ chiral Schwinger model, which is well known to be chiral anomalous [60], so that the gauge symmetry at the quantum level is broken. Integrating out the chiral fermionic degrees of freedom in Eq. (5) up to second order in the electromagnetic field we get (using dimensional regularization) [60]

$$\Gamma_{\rm anomaly} = \frac{1}{4\pi v}\int dx_1 dx_1' \rho_\lambda^2(x_1)\rho_\lambda^2(x_1') \times \int dx_0 dx_2\, A_a(x_0,x_1,x_2)\left(\eta^{ab} - \frac{\partial^a\partial^b}{\partial^2} - \frac{\sigma}{2\partial^2}(\epsilon^{cb}\partial^a\partial_c - \epsilon^{ad}\partial_d\partial^b)\right)A_b(x_0,x_1',x_2), \tag{12}$$

where $\partial_a = (\partial_0, v\partial_2)$, $A_a = (A_0, vA_2)$, and $\partial^2 = \eta^{ab}\partial_a\partial_b$. Note that chemical potential does not play a role here, and there are two reasons for this to happen. First for massless (nonchiral) $2d$ fermions the theory at finite charge density is indistinguishable to that at zero density. Second, the chiral anomaly is well known to be insensitive to chemical potential and temperature [61,62]. However, as we obtained in Eq. (10) finite μ plays a role at first order in A_μ for chiral $2d$ fermions. The effect is equivalent to applying a chiral chemical potential to nonchiral and massless fermions, which activates the chiral magnetic effect in $2d$ generating an equilibrium current density analogous to that of Eq. (11).

Finally, from Eq. (12) we can obtain the nonequilibrium edge current density:

$$j^a_{ne} = -\sigma\frac{e^2}{2\pi}\rho_\lambda^2(x_1)\int dx_1' \frac{\rho_\lambda^2(x_1')E_2(x_0,x_1',x_2)}{\partial_0 + \sigma v\partial_2}(1,\sigma v), \tag{13}$$

with $E_2 = \partial_0 A_2 - \partial_2 A_0$ the electric field in the x_2 direction.

B. Bulk theory

To obtain the bulk contribution we will assume a constant mass for the fermions, restoring the x_1 dependence at the end of the calculations in what basically is an adiabatic approximation, as we mentioned before. This way we have $3d$ Dirac fermions with a mass term that breaks time reversal symmetry. This system is well known to give a topological response under an external electromagnetic field in the form of a CS term [63,64].

To proceed we can always split the effective action into vacuum ($\mu = 0$) and matter ($\mu \neq 0$) contributions, so that the matter contribution is zero at zero density:

$$\Gamma_{\rm bulk} = \Gamma_0 + \Gamma_{\rm matt}, \tag{14}$$

with

$$\Gamma_{0,\rm matt} = \frac{1}{2}\int d^3x\, A_\mu \Pi^{\mu\nu}_{0,\rm matt} A_\nu, \tag{15}$$

where $A_\mu = (A_0, vA_1, vA_2)$ and where $\Pi^{\mu\nu}$ is the polarization function. Doing this separation all ultraviolet divergences appear in the vacuum part, while the matter part remains finite.

1. Vacuum contribution

To be consistent with the calculations done for the edge theory, we will use dimensional regularization to treat the ultraviolet divergences. The computation of the one-loop polarization function for $\mu = 0$ is straightforward. Separating it into it's even and odd parts

$$\Pi^{\mu\nu}_0 = \Pi^{\mu\nu}_{0,e} + \Pi^{\mu\nu}_{0,o} \tag{16}$$

and doing the computation we obtain

$$\Pi^{\mu\nu}_{0,e} = \frac{e^2|m|}{12\pi v^2}\left(\frac{\partial^2}{m^2} + \mathcal{O}\left(\frac{\partial^4}{m^4}\right)\right)\left(\eta^{\mu\nu} - \frac{\partial^\mu\partial^\nu}{\partial^2}\right), \tag{17}$$

$$\Pi^{\mu\nu}_{0,o} = -\frac{e^2\,\mathrm{sgn}(m)}{4\pi v^2}\epsilon^{\mu\rho\nu}\partial_\rho\left(1 + \mathcal{O}\left(\frac{\partial^2}{m^2}\right)\right), \tag{18}$$

with $m = m_0\sigma\tanh(x_1/\delta)$. Here $\partial_\mu = (\partial_0, v\partial_1, v\partial_2)$ and $\partial^2 = \eta^{\mu\nu}\partial_\mu\partial_\nu$. Note that we presented the results as the first terms in a derivative expansion, which will be useful later on when we treat the physical system. This expansion is justified in the low energy regime $p^2 \ll m^2$, breaking down when $m^2 \lesssim p^2$. If $p^2 \ll m_0^2$ it turns out that this breakdown occurs in the region near the DW where the adiabatic limit is no longer reliable. Hence the validity of the derivative expansion coincides with the validity of the adiabatic approximation.

Now let us look at the gauge variation of the full theory (edge plus bulk). The gauge variation of the edge theory [Eq. (12)] is

$$\delta\Gamma = \frac{\sigma e^2}{4\pi}\int d^3x\, \omega\rho_\lambda^2(x_1)E_2, \tag{19}$$

which should be canceled by the gauge variation of the CS term [Eq. (18)] so that the theory is gauge invariant. This is not the case if E_2 is a function of x_1. The reason is that, while the nature of the edge theory is totally nonadiabatic, the bulk theory has been computed in the adiabatic approximation. To cure this issue, we write the CS term as

$$\Pi^{\mu\nu}_{0,o} = -\frac{e^2\sigma F_\lambda(x_1)}{4\pi v^2}\epsilon^{\mu\rho\nu}\partial_\rho \tag{20}$$

so that the nonadiabatic term $F_\lambda(x_1)$ is fixed by imposing the anomaly cancellation. This is done in Appendix B, where the explicit form of $F_\lambda(x_1)$ can be found.

2. Matter contribution

The computation of the matter contribution is more involved. We again do the separation:

$$\Pi^{\mu\nu}_{\text{matt}} = \Pi^{\mu\nu}_{\text{matt},e} + \Pi^{\mu\nu}_{\text{matt},o}. \tag{21}$$

The even part is computed in Appendix C, where adding both vacuum and matter contributions we get

$$\Pi^{00}_e = -\theta(m^2-\mu^2)\frac{e^2|\boldsymbol{\partial}|^2}{12\pi|m|} + \theta(\mu^2-m^2)\frac{e^2(|\mu|-|m|)}{2\pi v^2}, \tag{22}$$

$$\Pi^{0i}_e = \Pi^{i0}_e = \theta(m^2-\mu^2)\frac{e^2\partial^0\partial^i}{12\pi v|m|}, \tag{23}$$

$$\Pi^{ij}_e = -\theta(m^2-\mu^2)\frac{e^2\partial^2}{12\pi v^2|m|}\left(\delta^{ij}+\frac{v^2\partial^i\partial^j}{\partial^2}\right). \tag{24}$$

Some approximations have been done to arrive at these expressions. First, we are in both the adiabatic and the low energy limits. Second, the result is obtained by adding the polarization functions computed in both the static ($p_0 \to 0$) and the long wavelength ($\mathbf{p} \to 0$) limits. As explained in Appendix C, this means that within our approximations nonlocal terms which are constant in the limit $p_0 \to 0$ and zero in the limit $\mathbf{p} \to 0$ are being approximated by the constant term in Π^{00}_e. Third, we assume that in the static limit the spatial momentum $|\mathbf{p}|$ is smaller than the Fermi momentum p_F. This is generally true at low energies, except when the Fermi energy $|\mu|$ is above but very close to the value of $|m_0|$, so that p_F is very small. In this situation some corrections which are highly nonlocal would contribute. And fourth, we neglect dynamical contributions which are nonlocal (inverse powers in the spatial momentum), which we believe will not have an appreciable effect in the description of the physical system, as we acknowledge in Appendix D 2.

To complete the bulk part of the effective action let us turn our attention to the odd part of the polarization function, this is to the matter correction to the CS term. The calculation is straightforward and we obtain (vacuum plus matter contributions)

$$\Pi^{\mu\nu}_o = -\frac{e^2}{4\pi v^2}\Big(\sigma F_\lambda(x_1)\,\theta(m^2-\mu^2) + \frac{m}{|\mu|}\theta(\mu^2-m^2)\Big)\epsilon^{\mu\rho\nu}\partial_\rho. \tag{25}$$

Note that all the nonadiabaticity is encoded in $F_\lambda(x_1)$, whereas no nonadiabatic corrections have been computed for $\mu^2 > m^2$. The reason is that corrections in this last case cannot be computed as we did for $\mu^2 < m^2$, as the anomaly cancellation cannot be invoked. The gauge noninvariance of the CS term for $\mu^2 > m^2$ cannot be canceled by the chiral anomaly, which is insensitive to the chemical potential (and temperature T) [61,62]. Furthermore, for finite μ and/or T there appear infinitely many terms in the perturbative series (in A_μ) that break gauge invariance in the presence of a boundary (or a DW mass as in our case). These terms are parity breaking (the CS is the lowest order of this terms), and in the presence of a boundary are gauge invariant for zero μ and T (the only exception to this is the CS term) and gauge noninvariant for finite μ and/or T (see [65] for a computation of the next order parity breaking term for finite T). Therefore, gauge invariance can only be restored at the nonperturbative level when all the terms in the perturbative series are summed up, in a similar way as occurs with large gauge invariance in the theory with no boundaries [66–68].

III. JUNCTION OF A FERROMAGNET AND A TOPOLOGICAL INSULATOR

Let us now look at a condensed-matter realization of the theory of Sec. II. We will take a thin film of a ferromagnet and place it on top of a three-dimensional TI. The action for the ferromagnet is (we restore $\hbar$ for the rest of the main text)

$$S_{\text{FM}} = d\int dt\,dx\,dy\left(\frac{M_s}{\gamma}\dot{\phi}(\cos\theta-1) - H_{\text{FM}}\right), \tag{26}$$

which is the sum of the Berry phase term ("kinetic energy of spin precession") plus the Hamiltonian:

$$H_{\text{FM}} = \frac{1}{2}\left[A\left(\left|\frac{\partial\mathbf{m}}{\partial x}\right|^2 + \left|\frac{\partial\mathbf{m}}{\partial y}\right|^2\right) - Km_z^2 + K_\perp m_x^2\right] \tag{27}$$

(see for example [69,70]). Here d is the film thickness, $\gamma = \mu_B g_e/\hbar$ the gyromagnetic ratio ($g_e = 2$), M_s the saturation magnetization, A the exchange constant (exchange energy per unit length), and K and $K_\perp$ the easy axis and hard axis anisotropy constants (anisotropy energy per unit volume). The magnetization unit vector is $\mathbf{m} = (\sin\theta\cos\phi, \sin\theta\sin\phi, \cos\theta)$. It relates to the total magnetization as $\mathbf{M} = \hbar\gamma\,\mathbf{m}/a^3 = M_s\,\mathbf{m}$ (where a is the lattice constant) and couples to the spin of the surface electrons of the TI insulator via an exchange interaction.

The action for the TI surface electrons, including the coupling to the magnetization, takes the standard form

$$\mathcal{S}_{\text{TI}} = \int dt\,dx\,dy\,\Psi^\dagger(i\hbar\partial_0 - H_{\text{TI}} - \mu)\Psi, \tag{28}$$

with

$$H_{\rm TI} = v_F \hat{\mathbf{z}} \cdot (i(\hbar\nabla - ie\mathbf{A}) \times \boldsymbol{\sigma}) \pm \Delta_{xy}\mathbf{m}_{xy} \cdot \boldsymbol{\sigma}_{xy} \pm \Delta_z m_z \sigma_z - eA_0, \quad (29)$$

where the surface of the TI is taken to be in the $z = 0$ plane, and where we have defined the density to be zero at half-filling. Δ_{xy} and Δ_z are the in-plane and out-of-plane exchange couplings respectively (both are definite positive); v_F is the Fermi velocity of the electrons; $\mathbf{m} = (m_x,m_y,m_z) = (\mathbf{m}_{xy},m_z)$ and $\boldsymbol{\sigma} = (\sigma_x,\sigma_y,\sigma_z) = (\boldsymbol{\sigma}_{xy},\sigma_z)$; $A_\mu = (A_0,\mathbf{A})$ and the signs $+$ and $-$ correspond to antiferromagnetic and ferromagnetic exchange couplings, respectively. $S_{\rm TI}$ can be written as Eq. (1) [with the representation for the Γ matrices given by (A2)] setting $x^\mu = (t,x,y)$, $v = v_F$, $m = \pm\Delta_z m_z$, and doing the substitution: $eA_\mu \to ea_\mu = (eA_0, eA_x \pm \Delta_{xy} m_y/v_F, eA_y \mp \Delta_{xy} m_x/v_F)$.

The Hamiltonian (27) supports a nontrivial minimum energy configuration in the form of the well known Bloch DW:

$$\theta_0 = 2\ \arctan(e^{\sigma x/\delta}), \quad \phi_0 = \pm\pi/2, \quad (30)$$

where $\delta = \sqrt{A/K}$ and $\sigma = \pm 1$ are the width and the topological charge of the DW, respectively. This is valid if $K_\perp \neq 0$, while if $K_\perp = 0$ the vacuum would be degenerate and ϕ_0 could take any value. This configuration gives the equilibrium magnetization:

$$\mathbf{m}^{(0)} = (\mathrm{sech}(x/\delta)\cos\phi_0, \mathrm{sech}(x/\delta)\sin\phi_0, \sigma\tanh(x/\delta)). \quad (31)$$

We will work with fluctuations around the equilibrium configuration: $\theta(t,x) = \theta_0(x) + \tilde{\theta}(t,x)$ and $\phi(t,x) = \phi_0 + \tilde{\phi}(t,x)$, giving the total magnetization:

$$\mathbf{m} = (\sin\theta\ \cos\phi, \sin\theta\ \sin\phi, \sigma\ \tanh(x/\delta) + \tilde{m}_z), \quad (32)$$

with $\tilde{m}_z = \cos\theta - \cos\theta_0$. Note that we have imposed the magnetization to be homogeneous in the y direction.

The gauge fixing condition given by Eq. (7) has now to be fulfilled by the effective vector potential a_μ. We fix the gauge:

$$ea_0 = -eE_x x - eE_y y, \quad (33)$$

$$ea_x = \pm\Delta_{xy} m_y(t,x)/v_F, \quad (34)$$

$$ea_y = \mp\Delta_{xy} m_x(t,x)/v_F, \quad (35)$$

with

$$m_x(t,x) = \sin(\theta_0(x) + \tilde{\theta}(t))\cos\phi(t), \quad (36)$$

$$m_y(t,x) = \sin(\theta_0(x) + \tilde{\theta}(t))\sin\phi(t), \quad (37)$$

where we have chosen an electrostatic configuration of the electromagnetic field ($E_{x,y}$ are constants). Since the x dependence of $\mathbf{m}_{xy}$ has been fixed, the fluctuations can only be functions of t. To obtain an effective action for x dependent fluctuations we have to relay on the adiabatic approximation, restoring the x dependence at the end. For the adiabatic approximation to be valid the wavelength of the spin waves l_{sw} in the x direction has to be much bigger than the typical wavelength of the surface electrons $l_{el} = \hbar v_F/\Delta_z$. Assuming the parameter $\lambda = \Delta_z\delta/(\hbar v_F)$ introduced in Eq. (4) that defines the number of existent bound surface states (see Appendix A) to be $\lambda \sim 1$, we have $l_{sw} \gg \delta$.

This way, we have "almost" a completely analogous theory for the fermionic sector to that in the previous section, but now for the effective electromagnetic field a_μ. We say almost because in addition we have an extra field $\tilde{m}_z$ with which we have to deal. Before proceeding, let us fix the values of the parameters. We set (the MI parameters are obtained from [71]) $d = 3$ nm, $M_s = 3\times10^5$ A/m, $A = 10^{-11}$ J/m, $K = 2\times10^5$ J/m^3, $v_F = 5\times10^5$ m/s, and $\Delta_z = \Delta_{xy} = 30$ meV, so that $\delta \approx 7.07$ nm and $\lambda = 0.672$. We will assume a very small perpendicular anisotropy $K_\perp$, so that it can be neglected compared to the effective anisotropy induced by the TI surface electrons (see next two paragraphs and Appendix D).

The computation of the effective action for the magnetization is done in Appendixes D and E, relaying on the calculations of Sec. II. The total action reads

$$\Gamma = S_{\rm FM} + \Gamma_{\rm TI}, \quad (38)$$

with

$$\Gamma_{\rm TI} = \int dt\,dx\,dy \left\{ \Delta_{xy}\mathbf{s}\cdot\mathbf{m}_{xy} - \frac{d\delta}{2}K_\perp^{\rm eff} \times \int dx' m_x(t,x)\rho_\lambda^2(x)\rho_\lambda^2(x')m_x(t,x') \right\} \quad (39)$$

and where the spin density $\mathbf{s}$ is

$$\mathbf{s} = \frac{\sigma\rho_\lambda^2(x)}{hv_F}(\mu - e\Delta V(y))\hat{\mathbf{x}} + \frac{e}{2hv_F}\left(\sigma F_\lambda(x)\theta\left(\Delta_z^2\tanh^2(x/\delta) - \mu^2\right) + \frac{\sigma\Delta_z\tanh(x/\delta)}{|\mu|}\theta\left(\mu^2 - \Delta_z^2\tanh^2(x/\delta)\right)\right)\mathbf{E}. \quad (40)$$

Here $\Delta V(y) = V(y) - V(-L/2)$ is the voltage between $y = -L/2$ and a given point y along the DW, with $V(y) = -E_y y$, and L and $y = \pm L/2$ the length and the end points of the wall, respectively. The effective hard axis anisotropy constant $K_\perp^{\rm eff}$ is

$$K_\perp^{\rm eff} = \frac{\Delta_{xy}^2}{d\delta h v_F} \approx 3.49\times10^3\ \mathrm{J/m^3} \quad (41)$$

and the functions $\rho_\lambda(x)$ and $F_\lambda(x)$ are given by Eqs. (6), (B4), and (B5), respectively. Remember that the parameter λ is given by [see Eq. (4)]

$$\lambda = \frac{\Delta_z\delta}{\hbar v_F}. \quad (42)$$

It is important to note also that the spin density is related to the electromagnetic current density as $\mathbf{j} = \pm ev_F\mathbf{s}\times\hat{\mathbf{z}}$.

From Eqs. (39) and (40) we see that there is a spin density that couples to the magnetization, which is related to (1) [term proportional to $\hat{\mathbf{x}}$ in Eq. (40)] the edge equilibrium and nonequilibrium currents flowing along the DW, given by Eqs. (11) and (D5), respectively, and (2) [term proportional to $\mathbf{E}$ in Eq. (40)] the topological current due to the anomalous quantum Hall effect in the bulk, coming from the Chern-Simons term (25). Besides the spin density there is a nonlocal

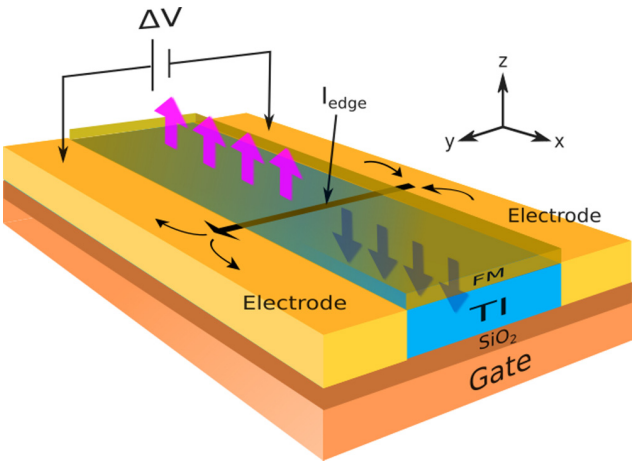

FIG. 1. (Color online) Schematics of a possible experimental setup. The ferromagnetic thin film (green) is deposited on top of the TI (blue), which itself is deposited on top of a gate. Pink and blue thick arrows represent the out-of-plane magnetization pointing up and down, respectively. A voltage ΔV is measured between the electrodes (yellow) at the flanks of the TI. The edge current I_{edge} flowing along the DW is represented by the black arrow connecting both electrodes.

contribution induced by the chiral electrons bound to the DW, which acts as a hard axis effective anisotropy energy in the direction perpendicular to the wall.

Although a interfacial DM interaction term of the form $\mathbf{m}\cdot\nabla m_z$ is not induced, as argued in Appendix E, the spin density related to the edge current generates a term that resembles it:

$$\Delta_{xy}\frac{\sigma\rho_\lambda^2(x)}{hv_F}(\mu - e\Delta V(y))\hat{\mathbf{x}}\cdot\mathbf{m}_{xy}. \tag{43}$$

For more clarity, in the special case $\lambda = 1$ we can write this as

$$\Delta_{xy}\frac{\mu - e\Delta V(y)}{2hv_F}\mathbf{m}_{xy}\cdot\nabla m_z^{(0)}, \tag{44}$$

while for different values of λ small deviations from $\nabla m_z^{(0)}$ take place. The strength of this "pseudo" DM interaction can be tuned by doping with electrons/holes and by the application of a voltage between both end points of the DW. Note, however, that this term is first order in the magnetization, while the DM interaction is second order.

In Fig. 1 we show the schematics of a possible experimental setup. A thin ferromagnetic film hosting a DW is deposited on top of a TI, which itself is deposited on top of a gate. Two electrodes are attached to the flanks of the TI such that a voltage between both edges is applied, and the gate is used to tune the chemical potential in the TI. A similar setup was realized in Ref. [72], where the TI was used as the channel of a field effect transistor.

IV. PHENOMENOLOGICAL RESULTS

Now that we have the effective action we can study the phenomenology. We will compute the chirality of the wall in it's equilibrium configuration at finite density and under applied external electric fields. We will also look at the current induced dynamics when a current is applied through the ferromagnet.

A. Equilibrium configuration of the DW

We want to look at minimum energy configurations of the total effective action given by Eqs. (38) and (39) of the type $\mathbf{m} = (\text{sech}(x/\delta)\cos\phi, \text{sech}(x/\delta)\sin\phi, \sigma\tanh(x/\delta))$. In principle ϕ will be a function of x; however, to simplify things we will assume ϕ to be constant. This will give an average equilibrium value of $\phi(x)$.

From the spin density of Eq. (40) we see that an applied electric field in the x direction will not change the average chirality of the wall, since it contributes with terms antisymmetric in x which will vanish when integrated. Contrarily, a voltage in the y direction has a nonvanishing effect on the average chirality through the (nonequilibrium) edge current that is generated [term proportional to the voltage in Eq. (40)]. This adds up to the effect of doping the system with electrons/holes, which generates a further (equilibrium) contribution to the edge current [term proportional to the chemical potential in Eq. (40)].

Then at finite density and under an applied voltage in the y direction we obtain the potential energy for the DW (after integration in x and y):

$$E(\phi) = \frac{L\Delta_{xy}C_2}{hv_F}\left(-C_1\cos\phi + \frac{\Delta_{xy}C_2}{2}\cos^2\phi\right), \tag{45}$$

with

$$C_1 = \sigma\mu - \frac{e\Delta V}{2}, \tag{46}$$

$$C_2 = -2i\frac{\mathcal{B}_{-1}(1/2+\lambda, -2\lambda)}{\mathcal{B}_{-1}(\lambda, 1-2\lambda)}, \tag{47}$$

where $\Delta V = V(L/2) - V(-L/2)$ is the voltage between both end points of the DW, $\mathcal{B}$ is the incomplete Beta function [see Eq. (A16)], and λ is given in Eq. (42). Here C_1 can take negative values, while C_2 is real and always positive and fulfills $\lim_{\lambda\to\infty} C_2 = 1$. For $|C_1| < \Delta_{xy}C_2$ the energy has a minimum at $\phi = \arccos(C_1/(\Delta_{xy}C_2))$. On the other hand, for $|C_1| \geqslant \Delta_{xy}C_2$ the minimum energy configuration is $\phi = 0$ for $C_1 > 0$ and $\phi = \pi$ for $C_1 < 0$. So at $C_1 = 0$ we have a Bloch DW ($\phi = \pm\pi/2$), and as $|C_1|$ increases ϕ is shifted until $|C_1| = \Delta_{xy}C_2$, at which point the DW stabilizes in a Néel configuration, with $\phi = 0$ for positive C_1 and $\phi = \pi$ for negative C_1 (see Fig. 2). This way the chirality of the DW can be tuned by the chemical potential (applying a gate voltage) and the electric field (appliying a voltage between both end points of the DW). Based on this mechanism, there is a way to switch between the two degenerate vacua $\phi = \pm\pi/2$ using an out-of-plane magnetic field to break the degeneracy of the vacuum. It was described in Ref. [55], where they made use of an electric field to tune the chirality through the mechanism explained above, while here we have shown that it can be done also by applying a gate voltage.

To be specific let us choose the topological charge to be $\sigma = +1$ and switch off the electric field. For the parameters introduced in Sec. III λ takes the value $\lambda = 0.672$, so that we have $C_1 = \mu$, $C_2 \approx 0.706$. For $|\mu| < 0.706\Delta_{xy}$ we get

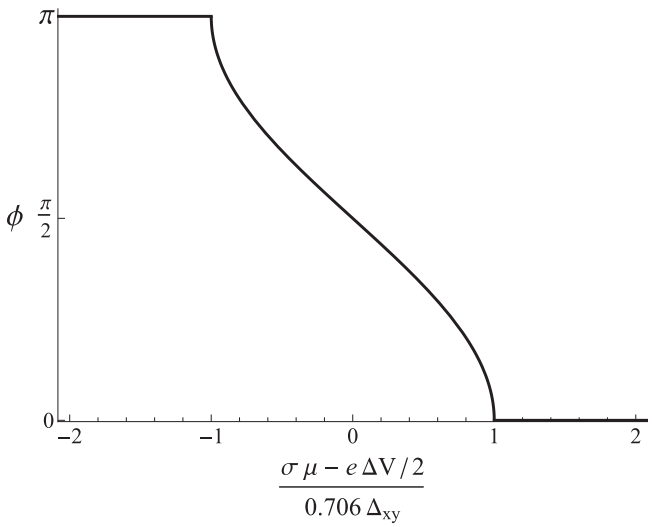

FIG. 2. Equilibrium value of the internal angle ϕ as a function of the chemical potential and the voltage, for a λ parameter value of $\lambda = 0.672$.

$\phi = \arccos(\mu/(0.706\Delta_{xy}))$, while for $|\mu| \geqslant 0.706\Delta_{xy}$ we get $\phi = 0$ for positive μ (TI doped with electrons) and $\phi = \pi$ for negative μ (TI doped with holes). This behavior qualitatively reproduces the results obtained numerically in Ref. [57]. The physical explanation lies in the competition of the torque generated by the chiral edge current on the magnetization and the effective hard axis anisotropy energy, which is also induced by the TI chiral surface electrons.

B. Current induced magnetization dynamics

We will now apply a current through the ferromagnet in the direction perpendicular to the DW. By doing so we are assuming the ferromagnet to be a metal, which would in principle pin the Fermi level so that the possibility of tuning the chemical potential of the surface states with a back gate is questionable. In such a case chemical doping of the sample could be necessary to tune the Fermi level, as was done in Refs. [41,42].

In terms of the collective coordinates $X(t)$ and $\phi(t)$, where X defines the position of the DW, we can write the total effective action as

$$\Gamma = \int dt \left(\mathcal{N}\hbar\frac{\dot{X}}{\delta}\phi + \frac{LC_2\Delta_{xy}I_{\text{edge}}}{ev_F}\cos\phi - \frac{LC_2\Delta_{xy}I^*_{\text{edge}}}{ev_F}\cos^2\phi - T_{el}\phi - F_{el}X \right), \quad (48)$$

where $\mathcal{N} = 2d\delta L/a^3$ is the number of spins in the DW and the currents I_{edge} and I^*_{edge} are

$$I_{\text{edge}} = \frac{e}{h}\left(\sigma\mu - \frac{e\Delta V}{2}\right), \quad (49)$$

$$I^*_{\text{edge}} = C_2\frac{e\Delta_{xy}}{2h} \approx 4.10 \times 10^{-7} A. \quad (50)$$

Note that $2I^*_{\text{edge}}$ is the threshold current at which the DW is completely of Néel type. Regarding T_{el} and F_{el}, they represent the spin-transfer torque and the force generated by the current on the wall, respectively [69,70]:

$$T_{el} = \frac{\hbar}{e}I_s, \quad F_{el} = \frac{\hbar}{e\delta}\beta I_s, \quad (51)$$

where $I_s = I_\uparrow - I_\downarrow$ is the applied spin current through the ferromagnet in the positive x direction, and the β term is a constant that depends on the microscopic properties of the ferromagnet. It can be quite large for perpendicular anisotropy thin films, where the force from electron reflection can be dominant [70], so following the reference we will fix it to be $\beta = 0.3$.

Now we can write the equations of motion (we include Gilbert damping):

$$e\mathcal{N}\left(\frac{\dot{X}}{\delta} - \alpha\dot{\phi}\right) = \frac{LC_2}{\hbar v_F}(I_{\text{edge}}\sin\phi - I^*_{\text{edge}}\sin 2\phi) - I_s, \quad (52)$$

$$e\mathcal{N}\left(\dot{\phi} + \alpha\frac{\dot{X}}{\delta}\right) = -\beta I_s, \quad (53)$$

where α is the Gilbert damping parameter, which we will set to be $\alpha = 0.01$. From the previous expressions we can obtain a differential equation for ϕ:

$$\dot{\phi}' = -\frac{j_s}{j^*_s} + \sin 2\phi - \frac{I_{\text{edge}}}{I^*_{\text{edge}}}\sin\phi, \quad (54)$$

where $I_s = dLj_s$, $I^*_s = dLj^*_s$, and

$$\phi' = \frac{1+\alpha^2}{\alpha a^3 C_2^2}\frac{4\hbar}{K^{\text{eff}}_\perp}\phi, \quad (55)$$

$$j^*_s = \frac{e\delta C_2^2}{2\hbar}K^{\text{eff}}_\perp\left(\frac{\beta}{\alpha} - 1\right)^{-1} \approx 3.39 \times 10^8 \text{ A/m}^2. \quad (56)$$

For vanishing edge current I_{edge} ($\mu = 0$ and $\Delta V = 0$) the DW moves with a time-averaged terminal velocity $\langle\dot{X}\rangle = -\beta\delta I_s/(e\alpha\mathcal{N})$ as long as the current flowing through the ferromagnet is smaller than the critical current I^*_s. When I_s reaches the value I^*_s however, Walker breakdown (WB) occurs and ϕ starts to change, so that the averaged terminal velocity decreases as I_s increases (see, for example [70]). Thus to obtain high velocities it is important to stay in the non WB regime, which means that one should look for the biggest possible I^*_s. We see that it's value is proportional to Δ^2_{xy}, so that the bigger the exchange coupling the higher the velocities that can be achieved. For the actual values of the parameters a velocity $\langle\dot{X}\rangle \approx 1.86$ m/s is achieved for an applied current density $j_s = j^*_s$, which is not fast for practical applications. However, if one could achieve an increase of Δ_{xy} of one order of magnitude ($\Delta_{xy} \sim 0.3$ eV) the average maximum velocity would increase by two orders of magnitude: $\langle\dot{X}\rangle \approx 186$ m/s. Although this is promising, such high values of the exchange coupling are of the order of the bulk gap of typical TIs, and are not achievable at the moment.

There is a nice way to stabilize the chirality of the DW so that WB is delayed. It was first suggested in Ref. [55], where an electric field was needed, and afterwards in Ref. [56], where it was shown that a similar effect could be achieved

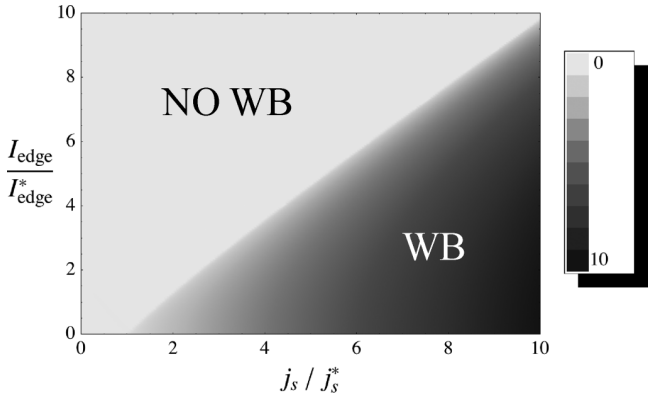

FIG. 3. Density plot of $\langle\dot{\phi}'\rangle$ in the $I_{\text{edge}}/I^*_{\text{edge}} - j_s/j_s^*$ plane. Values $\langle\dot{\phi}\rangle < 0$ (WB) occur in the dark region, while in the light region $\langle\dot{\phi}\rangle = 0$ (no WB). The frontier between the two regions gives the maximum values of j_s before WB occurs.

in equilibrium. The chirality stabilization is mediated by the edge current through the third term of the right-hand side of Eq. (54). We plot in Fig. 3 the values of j_s at which WB occurs for different values of the edge current I_{edge}. In comparison with [55,56] here it can be seen that DW stabilization can be tuned not only by applying an electric field, but also by doping the TI with electrons or holes. Depending on the competition of the equilibrium and nonequilibrium edge currents the effect can be neutralized or enhanced.

These results show that by using a TI, ferromagnets with very weak hard axis anisotropy could still be suitable for hosting DW motion without suffering from a very early WB. Furthermore by the application of an edge current, the terminal velocity can be significantly increased.

V. CONCLUSIONS

We have analytically computed an approximate effective action up to second order in the electromagnetic field, for a system of Dirac electrons in two spatial dimensions at finite density and with a DW mass term. We have presented a condensed-matter realization of this system, consisting on a ferromagnet hosting a DW (with out-of-plane magnetization domains) coupled via an exchange interaction to the TI surface electrons. There are three relevant contributions to the effective action coming from quantum fluctuations of the fermionic surface states

(i) The first one is linear in the magnetization, which couples to a spin density in the perpendicular direction to the DW. This spin density is related to the edge current of chiral electrons flowing along the DW, which itself can be seen as made of two pieces: an equilibrium current proportional to the chemical potential and a nonequilibrium current proportional to the applied voltage between both end points of the DW.

(ii) The second contribution is again linear in the magnetization, but now the spin density to which it is coupled is proportional to and has the direction of the applied electric field, and is of opposite signs to either side of the DW. It is related to the topological current generated by the anomalous quantum Hall effect in the bulk.

(iii) The last contribution is a nonlocal term quadratic in the magnetization, induced by the chiral electrons, and which acts as an effective hard axis anisotropy energy in the direction perpendicular to the DW.

The competition of the torque exerted by the edge current (first contribution) and the effective hard axis anisotropy energy (third contribution) explains the behavior of the chirality of the DW as the chemical potential and/or the voltage between both end points of the wall are modified. The stabilization of the internal angle through the induced effective hard axis anisotropy allows for the motion of the DW with velocity proportional to the applied current through the ferromagnet, especially in the case of ferromagnetic thin films with very weak in-plane anisotropy, which other ways would suffer of a very early WB. The critical current at which WB occurs is proportional to the effective anisotropy energy, which itself is quadratic in the exchange coupling, so that increasing the value of the exchange coupling would result in a significant increase of the maximum possible DW velocity.

Finally, the edge current flowing along the DW has an interesting effect on the wall dynamics. It further stabilizes the internal angle of the DW, which translates in a delay of the appearance of WB. This means the maximum DW velocity can be increased by doping the system with electrons or holes and/or applying a voltage between both end points of the DW. The two effects can be combined so that the edge current is further increased and the WB further delayed.

ACKNOWLEDGMENTS

Y.F. gratefully acknowledges A. Cortijo for valuable comments and suggestions. This research is partially supported by the Spanish MECD Grant No. FIS2011-23713 and by Foundation for Fundamental Research on Matter (FOM), which is part of the Netherlands Organisation for Scientific Research (NWO).

APPENDIX A: FERMIONIC SPECTRUM

To obtain the fermionic spectrum, we will treat the gauge field as a perturbation and think of the remaining theory [Eq. (1)] as a free theory. For the free theory, the equations of motion can be obtained from Eq. (1) for vanishing electromagnetic field:

$$\gamma^0\left(i\, l^\mu_\nu \gamma^\nu \partial_\mu - m\right)\Psi = 0. \tag{A1}$$

Let us take the following representation for the γ matrices:

$$\gamma^0 = \sigma^3, \quad \gamma^{1,2} = -i\,\sigma^{1,2} \tag{A2}$$

and write the bispinor Ψ in the basis

$$\Psi_{R,L} = e^{ip_0 x_0} e^{ip_2 x_2}\, \Phi_{R,L}(x_1)\mathbf{u}_{R,L}, \tag{A3}$$

with

$$\mathbf{u}_R = \frac{1}{\sqrt{2}}\begin{pmatrix}1\\1\end{pmatrix}, \quad \mathbf{u}_L = \frac{1}{\sqrt{2}}\begin{pmatrix}1\\-1\end{pmatrix}, \tag{A4}$$

so that $\Psi = \Psi_R + \Psi_L$. With this representation and in this basis, rewriting the first order coupled equations (A1) as

second order decoupled ones we get

$$\left(\partial_1^2+\frac{\lambda(\lambda-\sigma)}{\delta^2}\mathrm{sech}(x_1/\delta)\right)\Phi_R=\left(\frac{\lambda^2}{\delta^2}+p_2^2-\frac{p_0^2}{v^2}\right)\Phi_R, \tag{A5a}$$

$$\left(\partial_1^2+\frac{\lambda(\lambda+\sigma)}{\delta^2}\mathrm{sech}(x_1/\delta)\right)\Phi_L=\left(\frac{\lambda^2}{\delta^2}+p_2^2-\frac{p_0^2}{v^2}\right)\Phi_L, \tag{A5b}$$

with $\lambda=m_0\delta/v$. This is nothing but the Schrödinger equation in a modified Poschl-Teller potential (see, for example [73]). Let us write $p_0^2=v^2k^2+v^2p_2^2+m_0^2$, so that the eigenvalues of Eqs. (A5a) and (A5b) are $-k^2$. The general solutions of these equations are [73]

$$\begin{aligned}\Phi_R(\sigma,x_1)=\cosh^{\lambda+\frac{1-\sigma}{2}}(x_1/\delta)\Bigg\{&B(\lambda)\,{}_2F_1\\&\times\left[a+\frac{1-\sigma}{4},b+\frac{1-\sigma}{4},\frac{1}{2};-\sinh^2(x_1/\delta)\right]\\&+iC(\lambda)\sinh(x_1/\delta)\,{}_2F_1\left[a+\frac{1-\sigma}{4}+\frac{1}{2},b\right.\\&\left.+\frac{1-\sigma}{4}+\frac{1}{2},\frac{3}{2};-\sinh^2(x_1/\delta)\right]\Bigg\}\end{aligned} \tag{A6}$$

and $\Phi_L(\sigma,x_1)=\Phi_R(-\sigma,x_1)$. Here $B(\lambda)$ and $C(\lambda)$ are arbitrary constants, ${}_2F_1$ is the hypergeometric function, and the values of a and b are

$$a=\tfrac{1}{2}(\lambda+i\delta k),\quad b=\tfrac{1}{2}(\lambda-i\delta k). \tag{A7}$$

Note that the first term of the right-hand side of Eq. (A6) is even in x_1 while the second term is odd. For $k^2>0$ we have the continuum of extended states, the general solution of which is precisely given by Eq. (A6). On the other hand, for $k^2<0$ the solutions are bound to the wall, vanishing at $\pm\infty$ [73], and the energies are quantized.

Let us have a close look at the bound states. If we set $k\to ik$ we obtain the following conditions for the solutions to be normalizable (for $\sigma=-1$):

$$\begin{aligned}\Phi_R&\longrightarrow \delta k=\lambda-2n,\\ \Phi_L&\longrightarrow \delta k=\lambda-1-2n\end{aligned} \tag{A8}$$

for the even part of Eq. (A6) and

$$\begin{aligned}\Phi_R&\longrightarrow \delta k=\lambda-1-2n,\\ \Phi_L&\longrightarrow \delta k=\lambda-2-2n\end{aligned} \tag{A9}$$

for the odd part, where $n=0,1,2,\ldots$ (for $\sigma=1$ one just has to interchange the chiralities: $\Phi_{R,L}\to\Phi_{L,R}$). From these normalizability conditions and the general solution of Eq. (A6) we can obtain the bound states. For $\sigma=-1$ we have

$$n=0\begin{cases}\Phi_R^{(0)}=B_0(\lambda)\cosh^{\lambda+1}(x_1/\delta){}_2F_1\left[\frac{1}{2},\lambda+\frac{1}{2},\frac{1}{2};-\sinh^2(x_1/\delta)\right],\\ \Phi_L^{(0)}=0,\end{cases} \tag{A10}$$

$$n=1,3,5,\ldots\begin{cases}\Phi_R^{(n)}=iC_n(\lambda)\cosh^{\lambda+1}(x_1/\delta)\sinh(x_1/\delta)\,{}_2F_1\left[a_n+1,b_n+1,\frac{3}{2};-\sinh^2(x_1/\delta)\right],\\ \Phi_L^{(n)}=B_n(\lambda)\cosh^{\lambda}(x_1/\delta)\,{}_2F_1\left[a_n+\frac{1}{2},b_n+\frac{1}{2},\frac{1}{2};-\sinh^2(x_1/\delta)\right],\end{cases} \tag{A11}$$

$$n=2,4,6,\ldots\begin{cases}\Phi_R^{(n)}=B_n(\lambda)\cosh^{\lambda+1}(x_1/\delta)\,{}_2F_1\left[a_n+\frac{1}{2},b_n+\frac{1}{2},\frac{1}{2};-\sinh^2(x_1/\delta)\right],\\ \Phi_L^{(n)}=iC_n(\lambda)\cosh^{\lambda}(x_1/\delta)\sinh(x_1/\delta)\,{}_2F_1\left[a_n+1,b_n+1,\frac{3}{2};-\sinh^2(x_1/\delta)\right],\end{cases} \tag{A12}$$

with:

$$a_n=\frac{n}{2},\quad b_n=\lambda-\frac{n}{2} \tag{A13}$$

and with energies $p_0=-\sigma vp_2$ for $n=0$ and

$$p_0=\pm\sqrt{\frac{m_0^2}{\lambda^2}n(2\lambda-n)+v^2p_2^2} \tag{A14}$$

for $n\neq0$ (again, to obtain the solutions for $\sigma=1$ one just has to interchange the chiralities). There is a maximum n before k^2 is positive again: $N<\lambda$. Then we see that the number of bound states is given by the largest integer less than $\lambda+1$. Regarding the constants B_n and C_n, we impose the solutions to be normalized and obtain for the chiral state $n=0$:

$$B_0(\lambda)=\sqrt{\frac{(-1/4)^\lambda}{\delta\mathcal{B}_{-1}(\lambda,1-2\lambda)}}, \tag{A15}$$

where $\mathcal{B}_z(a,b)$ is the incomplete Beta function and can be written as

$$\mathcal{B}_z(a,b)=\int_0^z t^{a-1}(1-t)^{b-1}dt. \tag{A16}$$

Finally, we can decompose the fermionic field as follows (for $\sigma=-1$):

$$\begin{aligned}\Psi=&\sum_{n=0}^{N}\Psi_R^{(n)}(x_0,x_2)\Phi_R^{(n)}(x_1)+\sum_{n=1}^{N}\Psi_L^{(n)}(x_0,x_2)\Phi_L^{(n)}(x_1)\\&+\int dk\left(\Psi_R^{(k)}(x_0,x_2)\Phi_R^{(k)}(x_1)+\Psi_L^{(k)}(x_0,x_2)\Phi_L^{(k)}(x_1)\right),\end{aligned} \tag{A17}$$

with

$$\Psi_{R,L}^{(n,k)}(x_0,x_2)=\psi_{R,L}^{(n,k)}(x_0,x_2)\mathbf{u}_{R,L}. \tag{A18}$$

Again for $\sigma=1$ one should interchange the chiralities. The summation is over the bound states and the integral is over the continuum of extended states.

APPENDIX B: NONADIABATIC CORRECTION TO THE CS TERM

Let us write the CS term as

$$\Pi^{\mu\nu}_{0,o} = -\frac{e^2\sigma F(x_1)}{4\pi v^2}\epsilon^{\mu\rho\nu}\partial_\rho. \tag{B1}$$

To find the nonadiabatic correction $F(x_1)$ we should impose the anomaly cancellation. The gauge variation of the edge theory [Eq. (19)] has to be canceled by the gauge variation of the CS term. With this condition we get the differential equation for F:

$$\partial_1 F(x_1) = 2\rho^2_\lambda(x_1). \tag{B2}$$

There is another condition F should fulfill:

$$\lim_{x_1\to\pm\infty} F(x_1) = \pm 1, \tag{B3}$$

so that in the asymptotic limit Eq. (18) is recovered. Then F can be computed to be

$$F_\lambda(x_1) = -\delta B_0^2(\lambda)\mathrm{sgn}(x_1)\mathrm{Im}\left[\mathcal{B}_{-y^2}\left(\tfrac{1}{2}-\lambda,\tfrac{1}{2}\right)\right] \tag{B4}$$

as long as $\lambda \neq 1/2,3/2,5/2\ldots$, with $y = \cosh(x_1/\delta)$ and $\mathcal{B}$ the incomplete Beta function defined in Eq. (A16). For half integer λ we get

$$\begin{aligned}
F_{1/2}(x_1) &= 4\delta B_0^2\left(\frac{1}{2}\right)\arctan\left(\tanh\left(\frac{x_1}{2\delta}\right)\right),\\
F_{3/2}(x_1) &= \delta B_0^2\left(\frac{3}{2}\right)\left[2\arctan\left(\tanh\left(\frac{x_1}{2\delta}\right)\right)\right.\\
&\quad\left.+\,\mathrm{sech}\left(\frac{x_1}{\delta}\right)\tanh\left(\frac{x_1}{\delta}\right)\right],\\
F_{5/2}(x_1) &= \frac{\delta}{4}B_0^2\left(\frac{5}{2}\right)\left[6\arctan\left(\tanh\left(\frac{x_1}{2\delta}\right)\right)\right.\\
&\quad\left.+\,\mathrm{sech}\left(\frac{x_1}{\delta}\right)\left(3+2\,\mathrm{sech}\left(\frac{x_1}{\delta}\right)^2\right)\tanh\left(\frac{x_1}{\delta}\right)\right]\\
&\quad\vdots
\end{aligned} \tag{B5}$$

APPENDIX C: EVEN PART OF THE MATTER CONTRIBUTION IN THE BULK THEORY

The matter contribution to the polarization function in the bulk can be written as a sum of an even plus an odd part:

$$\Pi^{\mu\nu}_{\mathrm{matt}} = \Pi^{\mu\nu}_{\mathrm{matt},e} + \Pi^{\mu\nu}_{\mathrm{matt},o}. \tag{C1}$$

The even part is a symmetric second rank tensor. Assuming rotational invariance, the most general tensor of this type can be constructed as a linear combination of $\eta_{\mu\nu}$, $p_\mu p_\nu$, $u_\mu u_\nu$, and $p_\mu u_\nu + p_\nu u_\mu$, where $u_\mu = (1,0,0)$ defines the rest frame of the system (see, for example [74]). Imposing transversality $[p_\mu\Pi^{\mu\nu}_{\mathrm{matt},e}(p) = 0]$ we obtain the general form for the even contribution:

$$\Pi^{\mu\nu}_{\mathrm{matt},e}(p) = G_1\left(\eta^{\mu\nu} - \frac{p^\mu p^\nu}{p^2}\right) + (G_1+G_2)P^{\mu\nu}_\perp, \tag{C2}$$

with $P^{00}_\perp = P^{0i}_\perp = P^{i0}_\perp$ and

$$P^{ij}_\perp = \delta^{ij} - \frac{p^i p^j}{|\mathbf{p}|^2} \tag{C3}$$

and where G_1 and G_2 are scalar functions of p^0 and $|\mathbf{p}|$. In the vacuum there is no preferred rest frame, so u_μ can not appear. In that case, the even part of the polarization function must be proportional to $\eta^{\mu\nu} - p^\mu p^\nu/p^2$ which implies $G_1 = -G_2$.

To simplify the computation we will treat the static limit ($p^0 = 0$) and long wave limit ($\mathbf{p} = 0$) separately. In the static limit we have

$$\begin{aligned}
&\Pi^{00}_{\mathrm{matt},e} = G_1(p^0=0), \quad \Pi^{0i}_{\mathrm{matt},e} = \Pi^{i0}_{\mathrm{matt},e} = 0,\\
&\Pi^{ij}_{\mathrm{matt},e} = G_2(p^0=0)\left(\delta^{ij} - \frac{p^i p^j}{|\mathbf{p}|^2}\right).
\end{aligned} \tag{C4}$$

The calculation of G_1 and G_2 has been done in the context of massive graphene [75]. The only difference with the present case is that in graphene there is a multiplicative factor of 4 that counts the two valleys and the spin degeneracy. We should note that computations for graphene are done with cutoff regularization, which actually breaks gauge invariance. However, the matter part is finite and independent of the regularization, so results [75] can directly be imported as long as the degeneracy is set to 1. In the static limit we have

$$\begin{aligned}
G_1(p^0=0) &= \frac{e^2\,\theta(|\mu|-|m|)}{v^2}\left[-\frac{|m|}{4\pi} + \frac{|\mu|}{2\pi} - \frac{|\mu|}{4\pi}\sqrt{1-\frac{4\,p_F^2}{v^2|\mathbf{p}|^2}}\,\theta(|\mathbf{p}|-2p_F)\right.\\
&\quad\left.-\,\frac{v^2|\mathbf{p}|^2-4m^2}{8\pi\,v|\mathbf{p}|}\left(\arccos\left(\frac{2|m|}{\sqrt{v^2|\mathbf{p}|^2+4m^2}}\right) - \arccos\left(\frac{2|\mu|}{\sqrt{v^2|\mathbf{p}|^2+4m^2}}\right)\theta(|\mathbf{p}|-2p_F)\right)\right],
\end{aligned} \tag{C5}$$

$$\begin{aligned}
G_2(p^0=0) &= \frac{e^2\,\theta(|\mu|-|m|)}{v^2}\left[\frac{|m|}{4\pi} - \frac{|\mu|}{4\pi}\sqrt{1-\frac{4\,p_F^2}{v^2|\mathbf{p}|^2}}\,\theta(|\mathbf{p}|-2p_F)\right.\\
&\quad\left.+\,\frac{v^2|\mathbf{p}|^2-4m^2}{8\pi\,v|\mathbf{p}|}\left(\arccos\left(\frac{2|m|}{\sqrt{v^2|\mathbf{p}|^2+4m^2}}\right) - \arccos\left(\frac{2|\mu|}{\sqrt{v^2|\mathbf{p}|^2+4m^2}}\right)\theta(|\mathbf{p}|-2p_F)\right)\right],
\end{aligned} \tag{C6}$$

where the Fermi momentum is defined as $vp_F = \sqrt{\mu^2-m^2}$. In configuration space, restoring the x_1 dependence of m we have $vp_F = \sqrt{\mu^2 - m_0^2\tanh(x_1/\delta)^2}$. When $|\mu| > m_0$ we are safe to do $\theta(|\mathbf{p}|-2p_F) = 0$ for the description of the low

energy theory as long as $|\mu|$ does not get too close to m_0. On the other hand, when $|\mu| < m_0$ we will always have a region in space where p_F is small. However, this region is localized near the DW where the adiabaticity is lost. This means that within the adiabatic approximation we are safe to do $\theta(|\mathbf{p}| - 2p_F) = 0$ for any value of μ except when $|\mu| \sim m_0$, in which case corrections proportional to $\theta(|\mathbf{p}| - 2p_F)$ would be needed.

Then, supposing $|\mu|$ is below or sufficiently above m_0, we can forget about the terms proportional to $\theta(|\mathbf{p}| - 2p_F)$ and do a derivative expansion to get

$$G_1(p^0 = 0) = \theta(|\mu| - |m|) \times e^2\left(\frac{|\mu| - |m|}{2\pi v^2} - \frac{|\mathbf{p}|^2}{12\pi|m|} + \mathcal{O}\left(\frac{|\mathbf{p}|^4}{|m|^3}\right)\right), \tag{C7}$$

$$G_2(p^0 = 0) = \theta(|\mu| - |m|)\left(\frac{e^2|\mathbf{p}|^2}{12\pi|m|} + \mathcal{O}\left(\frac{|\mathbf{p}|^4}{|m|^3}\right)\right). \tag{C8}$$

These terms are finite in the limit $\mathbf{p} \to 0$.

At the same time, in the long wavelength limit we have

$$\Pi^{00}_{\mathrm{matt},e} = 0, \quad \Pi^{ij}_{\mathrm{matt},e} = G_2(\mathbf{p} = 0)\delta^{ij}, \qquad \Pi^{0i}_{\mathrm{matt},e} = \Pi^{i0}_{\mathrm{matt},e} = G_1(\mathbf{p} = 0)\frac{vp^i}{p^0}. \tag{C9}$$

Note that we maintain a linear dependence in p^i as we impose spatial homogeneity in the electric and magnetic fields. Now we search for terms linear and quadratic in p^0 in $G_{1,2}$ which are finite in the limit $\mathbf{p} \to 0$, so that we go up to second order in a derivative expansion. With this procedure we get rid of nonlocal terms (negative powers in $\mathbf{p}$). From [75] we obtain, in the low energy regime $p_0^2 \ll m^2$,

$$G_1(\mathbf{p} = 0) = \theta(|\mu| - |m|) \times \left(\frac{e^2 p_0^2}{12\pi v^2|m|} + \mathcal{O}\left(\frac{p_0^4}{|m|^3}\right) + n.l.t.\right), \tag{C10}$$

$$G_2(\mathbf{p} = 0) = -\theta(|\mu| - |m|) \times \left(\frac{e^2 p_0^2}{12\pi v^2|m|} + \mathcal{O}\left(\frac{p_0^4}{|m|^3}\right) + n.l.t.\right), \tag{C11}$$

where $n.l.t.$ are nonlocal terms.

Adding the vacuum and matter contributions (in both static and long wavelength limits) just obtained and neglecting the nonlocal terms in Eqs. (C10) and (C11) we arrive at the following expression for the even part of the polarization function (in configuration space):

$$\Pi^{00}_e = -\theta(|m| - |\mu|)\frac{e^2|\boldsymbol{\partial}|^2}{12\pi|m|} + \theta(|\mu| - |m|)\frac{e^2(|\mu| - |m|)}{2\pi v^2}, \tag{C12}$$

$$\Pi^{0i}_e = \Pi^{i0}_e = \theta(|m| - |\mu|)\frac{e^2\partial^0\partial^i}{12\pi v|m|}, \tag{C13}$$

$$\Pi^{ij}_e = -\theta(|m| - |\mu|)\frac{e^2\partial^2}{12\pi v^2|m|}\left(\delta^{ij} + \frac{v^2\partial^i\partial^j}{\partial^2}\right). \tag{C14}$$

Let us note that if we do $p_0 \to 0$ in the expressions for the long wavelength limit, the polarization function obtained does not coincide with the one we get if we do $\mathbf{p} \to 0$ in the expressions for the static limit. This is due to the nonlocality of the matter part. Withing our approximations, the commutator of the limits $p_0 \to 0$ and $\mathbf{p} \to 0$ gives precisely the constant term of $G_1(p^0 = 0)$, which contributes to Π^{00}_e in the static limit. This means that when adding the static plus the long wavelength contributions, nonlocal terms which are constant in the limit $p_0 \to 0$ and zero in the limit $\mathbf{p} \to 0$ are being approximated by a constant term.

APPENDIX D: ACTION FOR THE IN-PLANE MAGNETIZATION

To obtain the action for the in-plane magnetization we can directly import results from Sec. II. The only place where a bit of care is needed is in the computation of the action for the chiral edge theory, as the sign of the chiral anomaly depends on the sign of the mass. For clarity we will obtain the first order and second order terms (in the magnetization) separately.

1. First order terms

From Eqs. (10), (12), (24), and (25) we obtain

$$\Gamma^{(1)} = \int dt\, dx\, dy\, \Delta_{xy}\mathbf{s}\cdot\mathbf{m}_{xy}, \tag{D1}$$

where the spin density $\mathbf{s}$ is (restoring $\hbar$)

$$\mathbf{s} = \frac{\rho_\lambda^2(x)}{h}\left(\frac{\sigma\mu}{v_F} \pm \frac{e}{\partial_0 \pm \sigma v_F\partial_y}E_y\right)\hat{\mathbf{x}} + \frac{e}{2hv_F}\left(\sigma F_\lambda(x)\theta\left(\Delta_z^2\tanh^2(x/\delta) - \mu^2\right) + \frac{\sigma\Delta_z\tanh(x/\delta)}{|\mu|}\theta\left(\mu^2 - \Delta_z^2\tanh^2(x/\delta)\right)\right)\mathbf{E}. \tag{D2}$$

It is related to the electromagnetic current density as $\mathbf{j} = \pm ev_F\mathbf{s}\times\hat{\mathbf{z}}$. To evaluate the nonequilibrium term, which is nonlocal (the one with inverse derivatives), we will assume the electromagnetic current to be time independent. We get [55]

$$\pm\frac{1}{\partial_0 \pm \sigma v_F\partial_y}E_y = -\frac{\sigma}{v_F}V(y), \tag{D3}$$

with $V(y) = -E_y y + \text{const}$. We will further set the voltage to zero at $y = -L/2$, where L is the length and $y = \pm L/2$ are the end points of the DW. We finally have

$$\pm\frac{1}{\partial_0 \pm \sigma v_F\partial_y}E_y = -\frac{\sigma}{v_F}\Delta V(y), \tag{D4}$$

where $\Delta V(y) = V(y) - V(-L/2)$ is the voltage between the end point $y = -L/2$ and a given point y along the wall. The nonequilibrium edge current density along the DW then reads

$$j^a_{ne} = \pm\frac{e^2\Delta V(y)}{hv_F}\rho_\lambda^2(x)(1,\sigma v_F). \tag{D5}$$

For more clarity let us take the spatial component and compute the average $\langle j^y_{ne}\rangle$:

$$\langle j^y_{ne}\rangle = \frac{1}{L}\int_{-\frac{L}{2}}^{\frac{L}{2}} dy\, j^y_{ne} = \pm\sigma\frac{e^2}{2h}|\rho_\lambda(x)|^2\Delta V, \tag{D6}$$

where here $\Delta V = V(L/2) - V(-L/2)$ is the voltage between both end points of the DW. A similar current configuration has been used recently in the literature [52,55].

Finally we can write the spin density as

$$\mathbf{s} = \frac{\sigma\rho_\lambda^2(x)}{hv_F}(\mu - e\Delta V(y))\hat{\mathbf{x}} + \frac{e}{2hv_F}\left(\sigma F_\lambda(x)\theta\left(\Delta_z^2\tanh^2(x/\delta) - \mu^2\right) + \frac{\sigma\Delta_z\tanh(x/\delta)}{|\mu|}\theta\left(\mu^2 - \Delta_z^2\tanh^2(x/\delta)\right)\right)\mathbf{E}. \tag{D7}$$

2. Second order terms

The quadratic terms in the magnetization can be obtained from Eqs. (12), (24), and (25). Expressions (24) (taken in the static limit) and (25) give corrections to the exchange energy and the Berry phase term, respectively. Their contribution to the second order terms of the effective action is

$$\Gamma^{(2)}_{\text{bulk}} = -d\int dt\,dx\,dy\Big\{A^{\text{eff}}\theta\left(\mu^2 - \Delta_z^2\tanh^2(x/\delta)\right)((\partial_x m_x)^2 + (\partial_y m_y)^2) \mp \frac{M_s^{\text{eff}}}{\gamma}\Big(\sigma F_\lambda(x_1)\theta\left(\Delta_z^2\tanh^2(x/\delta) - \mu^2\right)$$
$$+ \frac{\sigma\Delta_z\tanh(x/\delta)}{|\mu|}\theta\left(\mu^2 - \Delta_z^2\tanh^2(x/\delta)\right)\Big)(m_y\partial_t m_x - m_x\partial_t m_y)\Big\}, \tag{D8}$$

with

$$A^{\text{eff}} = \frac{\Delta_{xy}^2}{12\pi\Delta_z d}, \quad M_s^{\text{eff}} = \frac{\Delta_{xy}^2\gamma}{2hdv_F^2}. \tag{D9}$$

The values of the effective exchange constant and saturation magnetization are $A^{\text{eff}} \approx 4.24\times10^{-14}$ J/m and $M_s^{\text{eff}} \approx 4.3$ A/m, which is much smaller than the values of the ferromagnet A and M_s, so that the contribution $\Gamma^{(2)}_{\text{bulk}}$ can be neglected. Besides the exchange energy and saturation magnetization renormalization, Eq. (24) gives also an extra dynamical contribution, but is second order in time derivatives, and hence higher order in the derivative expansion than the CS contribution and can be neglected. There would also be further nonlocal dynamical corrections at finite density, which are highly nontrivial to compute and which should be again of no importance for the physics compared to the Berry phase term of the ferromagnet.

Regarding the second order contribution coming from the edge theory [Eq. (12)] we can write

$$\Gamma^{(2)}_{\text{anomaly}} = -\frac{\Delta_{xy}^2}{2hv_F}\int dt\,dt'dx\,dx'dy\,dy'\rho_\lambda^2(x)\rho_\lambda^2(x')m_x(t,x,y)(-i\partial_t)G(t-t',y-y')m_x(t',x',y'), \tag{D10}$$

where we defined the Green function G as

$$G(t-t',y-y') = \int\frac{d^2q}{4\pi^2}\frac{e^{iq_0(t-t')}e^{iq_y(y-y')}}{q_0 \mp \sigma v_F q_y} = \frac{i}{2}\text{sgn}(t-t')\delta(\pm\sigma v_F(t-t') + y - y'). \tag{D11}$$

Doing the derivative of the Green function we get

$$\Gamma^{(2)}_{\text{anomaly}} = -\frac{\Delta_{xy}^2}{2hv_F}\int dt\,dx\,dx'dy\,\rho_\lambda^2(x)\rho_\lambda^2(x')\Big(m_x(t,x,y)m_x(t,x',y)$$
$$+\frac{1}{2}\int dt'dy'm_x(t,x,y)\text{sgn}(t-t')\partial_t\delta(\pm\sigma v_F(t-t') + y - y')m_x(t',x',y')\Big). \tag{D12}$$

Taking into account that the magnetization does not depend on the y coordinate, the second term of the right-hand side of Eq. (D12) can be simplified to

$$\pm\sigma\frac{\Delta_{xy}^2}{4hv_F}\int dt\,dx\,dx'dy\,\rho_\lambda^2(x)\rho_\lambda^2(x')m_x(t,x)(m_x(t\mp L/v_F,x') + m_x(t\pm L/v_F,x') - 2m_x(t,x')), \tag{D13}$$

where L is the DW length, and L/v_F is the typical time that an electron takes to travel the whole length of the wall. Making use of the translation operator we can write

$$m_x(t\pm L/v_F,x) = e^{\pm\frac{L}{v_F}\partial_t}m_x(t,x)\left(1 \pm \frac{L}{v_F}\partial_t + \frac{L^2}{2v_F^2}\partial_t^2 + \mathcal{O}\left(\frac{L^3}{v_F^3}\partial_t^3\right)\right)m_x(t,x), \tag{D14}$$

so that we have

$$\pm\sigma\frac{\Delta_{xy}^2}{4hv_F}\frac{L^2}{v_F^2}\int dt\,dx\,dx'dy\,|\rho_\lambda(x)|^2|\rho_\lambda(x')|^2\,m_x(t,x)\partial_t^2 m_x(t,x')+\mathcal{O}\left(\frac{L^3}{v_F^3}\partial_t^3\right). \tag{D15}$$

This is second and higher order in derivatives and so can be neglected, and we finally get

$$\Gamma^{(2)}_{\text{anomaly}}=-\frac{d\delta}{2}K_\perp^{\text{eff}}\int dt\,dx\,dx'dy\,\rho_\lambda^2(x)\rho_\lambda^2(x')\times m_x(t,x)m_x(t,x'), \tag{D16}$$

where the effective hard axis anisotropy constant is

$$K_\perp^{\text{eff}}=\frac{\Delta_{xy}^2}{d\delta\,hv_F}\approx 3.49\times 10^3\ \text{J/m}^3. \tag{D17}$$

Assuming a ferromagnetic thin film with a weak in-plane anisotropy, the whole contribution to the hard axis anisotropy can be assumed to come from $K_\perp^{\text{eff}}$.

APPENDIX E: ACTION FOR THE OUT-OF-PLANE MAGNETIZATION

Let us now compute the contributions linear and quadratic in $\tilde{m}_z$. We integrate out the fermions in Eq. (28) with magnetization given by Eq. (32), which includes fluctuations around the equilibrium configuration [Eq. (31)]. We work in the adiabatic approximation taking the mass $m=\pm\sigma\Delta_z\tanh(x/\delta)$ as a constant and at the end restoring the x dependence. Picking only the terms linear and quadratic in $\tilde{m}_z$ we have, in imaginary time,

$$\Gamma_z=-\frac{1}{2v_F^2}\int\frac{d^3p\,d^3q}{(2\pi)^6}((q_0-i\mu)^2+\mathcal{E}^2(\mathbf{q}))^{-1}\times((q_0+p_0-i\mu)^2+\mathcal{E}^2(\mathbf{q}+v_F\mathbf{p}))^{-1}(A+B+C), \tag{E1}$$

where $\mathcal{E}(\mathbf{q})=\sqrt{|\mathbf{q}|^2+m^2}$ and

$$A=-\Delta_z^2\text{Tr}[(i(\vec{\not{q}}+\not{p})-m)(i\vec{\not{q}}-m)]\tilde{m}_z(p)\tilde{m}_z(-p), \tag{E2}$$

$$B=i\Delta_z\text{Tr}[(i(\vec{\not{q}}+\not{p})-m)\not{a}(p)(i\vec{\not{q}}-m)]\tilde{m}_z(-p), \tag{E3}$$

$$C=i\Delta_z\text{Tr}[(i(\vec{\not{q}}+\not{p})-m)(i\vec{\not{q}}-m)\not{a}(-p)]\tilde{m}_z(p). \tag{E4}$$

We defined $\bar{q}^\mu=(q^0-i\mu,\mathbf{q})$, $p^\mu=(p^0,v_F\mathbf{p})$, and $\not{s}=\gamma^\mu s^\nu\delta_{\mu\nu}$, since we are working in Euclidean space-time. It can be seen that at $\mu=0$ the calculation gives no dynamical terms first order in time derivatives, so in this limit dynamical contributions can be neglected. At finite μ we will take the static limit, assuming any dynamical contribution arising from finite density effects can again be neglected compared to the Berry phase term of the ferromagnet. Hence doing $p_0=0$ and performing the traces we get

$$A=\Delta_z^2\left(2\bar{q}_0^2+2|\mathbf{q}|^2-2m^2+\bar{q}_i p_j\delta^{ij}\right)\tilde{m}_z(p)\tilde{m}_z(-p), \tag{E5}$$

$$B=2\Delta_z(\epsilon^{0\alpha\beta}\bar{q}_0 p_\alpha a_\beta(p)+\epsilon^{0\alpha\beta}\bar{q}_\alpha p_\beta a_0(p)+2m\bar{q}_\alpha a_\beta(p)\delta^{\alpha\beta}+m\,\mathbf{p}\cdot\mathbf{a}(p))\tilde{m}_z(-p), \tag{E6}$$

$$C=-2\Delta_z(\epsilon^{0\alpha\beta}\bar{q}_0 p_\alpha a_\beta(-p)+\epsilon^{0\alpha\beta}\bar{q}_\alpha p_\beta a_0(-p)-2m\bar{q}_\alpha a_\beta(-p)\delta^{\alpha\beta}-m\,\mathbf{p}\cdot\mathbf{a}(-p))\tilde{m}_z(p). \tag{E7}$$

The first term of B and C has the form of a DM interaction $\mathbf{m}_{xy}\cdot\mathbf{p}\,\tilde{m}_z$, while the second term would give a coupling to the electric field.

We go up only to linear order in the external momentum, so we expand the denominator of Eq. (E1) to first order in $\mathbf{p}$ and pick only up to linear terms in the resulting expression. Then performing the integrals in the internal momentum and using dimensional regularization for the divergent integrals present in the vacuum contribution we get (still in imaginary time)

$$\Gamma_z=\frac{\Delta_z}{16\pi v_F}\int\frac{d^3p}{(2\pi)^3}\frac{m(\mu^2-m^2)}{|\mu|^3}\times\theta(\mu^2-m^2)\,\mathbf{p}\cdot(\mathbf{a}(p)\tilde{m}_z(-p)+\mathbf{a}(-p)\tilde{m}_z(p))+\frac{\Delta_z^2}{8\pi v_F^2}\int\frac{d^3p}{(2\pi)^3}\left(4|m|\theta(m^2-\mu^2)+\left(|m|+|\mu|+\frac{2m^2}{|\mu|}\right)\theta(\mu^2-m^2)\right)\tilde{m}_z(p)\tilde{m}_z(-p). \tag{E8}$$

The first integral of Eq. (E8) above is antisymmetric in $\mathbf{p}$ and vanishes up to a total derivative. The second one gives the final nonzero result. We see that the terms mixing a_μ with $\tilde{m}_z$ vanish, which means that there is no coupling of the out-of-plane magnetization with the electric field to this order and that there is not effective DM interaction. The reason these terms vanish resides in the following vanishing integral:

$$\int_{-\infty}^{\infty}\frac{q_0}{2\pi}((q_0-i\mu)^2+\mathcal{E}^2(\mathbf{q}))^{-2}(q_0-i\mu)=0. \tag{E9}$$

Going back to real time and configuration space, and doing the substitution $m=\pm\sigma\Delta_z\tanh(x/\delta)$, we get (restoring $\hbar$)

$$\Gamma_z=-\frac{dK^{\text{eff}}}{2}\times\int dt\,dx\,dy\left(4|\tanh(x/\delta)|\theta\left(\Delta_z^2\tanh^2(x/\delta)-\mu^2\right)+\left(\frac{|\mu|}{\Delta_z}+|\tanh(x/\delta)|+\frac{2\Delta_z\tanh^2(x/\delta)}{|\mu|}\right)\times\theta\left(\mu^2-\Delta_z^2\tanh^2(x/\delta)\right)\right)\tilde{m}_z^2, \tag{E10}$$

which gives just a renormalization of the easy axis anisotropy energy with

$$K^{\text{eff}}=\frac{\pi\Delta_z^3}{v_F^2 dh^2}\approx 1.05\times 10^3\ \text{J/m}^3. \tag{E11}$$

This is much smaller than the easy axis anisotropy constant of the ferromagnet, so this term can be neglected.

[1] K. S. Novoselov, A. K. Geim, S. V. Morozov, D. Jiang, Y. Zhang, S. V. Dubonos, I. V. Grigorieva, and A. A. Firsov, Science **306**, 666 (2004).

[2] A. H. Castro Neto, F. Guinea, N. M. R. Peres, K. S. Novoselov, and A. K. Geim, Rev. Mod. Phys. **81**, 109 (2009).

[3] M. I. Katsnelson, *Graphene. Carbon in two dimensions* (Cambridge University Press, New York, 2012).

[4] L. Fu, C. L. Kane, and E. J. Mele, Phys. Rev. Lett. **98**, 106803 (2007).

[5] M. Z. Hasan and C. L. Kane, Rev. Mod. Phys. **82**, 3045 (2010).

[6] X.-L. Qi and S.-C. Zhang, Rev. Mod. Phys. **83**, 1057 (2011).

[7] S. S. P. Parkin, M. Hayashi, and L. Thomas, Science **320**, 190 (2008).

[8] L. Thomas, R. Moriya, C. Rettner, and S. S. Parkin, Science **330**, 1810 (2010).

[9] N. L. Schryer and L. R. Walker, J. Appl. Phys. **45**, 5406 (1974).

[10] T. Ono, H. Miyajima, K. Shigeto, K. Mibu, N. Hosoito, and T. Shinjo, Science **284**, 468 (1999).

[11] D. Atkinson, D. A. Allwood, G. Xiong, M. D. Cooke, C. C. Faulkner, and R. P. Cowburn, Nat. Mater. **2**, 85 (2003).

[12] Y. Nakatani, N. Hayashi, T. Ono, and H. Miyajima, IEEE Trans. Magn. **37**, 2129 (2001).

[13] A. Thiaville, J. M. García, and J. Miltat, J. Magn. Magn. Mater. **242-245**, 1061 (2002).

[14] Y. Nakatani, A. Thiaville, and J. Miltat, Nat. Mater. **2**, 521 (2003).

[15] G. S. D. Beach, C. Nistor, C. Knutson, M. Tsoi, and J. L. Erskine, Nat. Mater. **4**, 741 (2005).

[16] L. Berger, J. Appl. Phys. **55**, 1954 (1984).

[17] P. P. Freitas and L. Berger, J. Appl. Phys. **57**, 1266 (1985).

[18] C. Hung and L. Berger, J. Appl. Phys. **63**, 4276 (1988).

[19] L. Gan, S. Chung, K. Aschenbach, M. Dreyer, and R. Gomez, IEEE Trans. Magn. **36**, 3047 (2000).

[20] H. Koo, C. Krafft, and R. D. Gomez, Appl. Phys. Lett. **81**, 862 (2002).

[21] A. Yamaguchi, T. Ono, S. Nasu, K. Miyake, K. Mibu, and T. Shinjo, Phys. Rev. Lett. **92**, 077205 (2004).

[22] J. Grollier, P. Boulenc, V. Cros, A. Hamzić, A. Vaurès, A. Fert, and G. Faini, Appl. Phys. Lett. **83**, 509 (2003).

[23] P. Yan, X. S. Wang, and X. R. Wang, Phys. Rev. Lett. **107**, 177207 (2011).

[24] J.-S. Kim, M. Stärk, M. Kläui, J. Yoon, C.-Y. You, L. Lopez-Diaz, and E. Martinez, Phys. Rev. B **85**, 174428 (2012).

[25] X.-g. Wang, G.-h. Guo, Y.-z. Nie, G.-f. Zhang, and Z.-x. Li, Phys. Rev. B **86**, 054445 (2012).

[26] X.-g. Wang, G.-h. Guo, G.-f. Zhang, Y.-z. Nie, and Q.-l. Xia, Appl. Phys. Lett. **102**, 132401 (2013).

[27] H. Hata, T. Taniguchi, H.-W. Lee, T. Moriyama, and T. Ono, Appl. Phys. Express **7**, 033001 (2014).

[28] A. Manchon, P. B. Ndiaye, J.-H. Moon, H.-W. Lee, and K.-J. Lee, Phys. Rev. B **90**, 224403 (2014).

[29] W. Wang, M. Albert, M. Beg, M.-A. Bisotti, D. Chernyshenko, D. Cortés-Ortuño, I. Hawke, and H. Fangohr, Phys. Rev. Lett. **114**, 087203 (2015).

[30] H. Onho, D. Chiba, F. Matsukura, T. Oyima, E. Abe, T. Dietl, Y. Ohno, and K. Ohtani, Nature (London) **408**, 944 (2000).

[31] A. Schellekens, A. van den Brink, J. Franken, H. Swagten, and B. Koopmans, Nat. Commun. **3**, 847 (2011).

[32] A. Brataas, Nat. Nanotechnol. **8**, 485 (2013).

[33] A. Thiaville, S. Rohart, É. Jué, V. Cros, and A. Fert, EPL (Europhys. Lett.) **100**, 57002 (2012).

[34] S. Emori, U. Bauer, S.-M. Ahn, E. Martinez, and G. S. D. Beach, Nat. Mater. **12**, 611 (2013).

[35] I. M. Miron, T. Moore, H. Szambolics, L. D. Buda-Prejbeanu, S. Auffret, B. Rodmacq, S. Piazzini, J. Vogel, M. Bomfim, A. Schuhl *et al.*, Nat. Mater. **10**, 419 (2011).

[36] J. G. Checkelsky, J. Ye, Y. Onose, Y. Iwasa, and Y. Tokura, Nat. Phys. **8**, 729 (2012).

[37] A. A. Burkov and D. G. Hawthorn, Phys. Rev. Lett. **105**, 066802 (2010).

[38] D. Culcer, E. H. Hwang, T. D. Stanescu, and S. Das Sarma, Phys. Rev. B **82**, 155457 (2010).

[39] D. Pesin and A. H. MacDonald, Nat. Mater. **11**, 409 (2012).

[40] M. H. Fischer, A. Vaezi, A. Manchon, and E.-A. Kim, arXiv:1305.1328.

[41] Y. Fan, P. Upadhyaya, X. Kou, M. Lang, S. Takei, Z. Wang, J. Tang, L. He, L.-T. Chang, M. Montazeri *et al.*, Nat. Mater. **13**, 699 (2014).

[42] A. R. Mellnik, J. S. Lee, A. Richardella, J. L. Grab, P. J. Mintun, M. H. Fischer, A. Vaezi, A. Manchon, E. A. Kim, N. Samarth *et al.*, Nature (London) **511**, 449 (2014).

[43] T. Yokoyama, Y. Tanaka, and N. Nagaosa, Phys. Rev. B **81**, 121401 (2010).

[44] T. Yokoyama, J. Zang, and N. Nagaosa, Phys. Rev. B **81**, 241410 (2010).

[45] I. Garate and M. Franz, Phys. Rev. Lett. **104**, 146802 (2010).

[46] T. Yokoyama, Phys. Rev. B **84**, 113407 (2011).

[47] H. T. Ueda, A. Takeuchi, G. Tatara, and T. Yokoyama, Phys. Rev. B **85**, 115110 (2012).

[48] F. S. Nogueira and I. Eremin, Phys. Rev. Lett. **109**, 237203 (2012).

[49] F. S. Nogueira and I. Eremin, Phys. Rev. B **90**, 014431 (2014).

[50] Y. Tserkovnyak, D. A. Pesin, and D. Loss, Phys. Rev. B **91**, 041121 (2015).

[51] K. Nomura and N. Nagaosa, Phys. Rev. B **82**, 161401 (2010).

[52] Y. Tserkovnyak and D. Loss, Phys. Rev. Lett. **108**, 187201 (2012).

[53] C. Wickles and W. Belzig, Phys. Rev. B **86**, 035151 (2012).

[54] R. Hammer and W. Pötz, Phys. Rev. B **88**, 235119 (2013).

[55] Y. Ferreiros and A. Cortijo, Phys. Rev. B **89**, 024413 (2014).

[56] J. Linder, Phys. Rev. B **90**, 041412 (2014).

[57] R. Wakatsuki, M. Ezawa, and N. Nagaosa, arXiv:1412.7910.

[58] C. G. Callan and J. A. Harvey, Nucl. Phys. B **250**, 427 (1985).

[59] S. Chandrasekharan, Phys. Rev. D **49**, 1980 (1994).

[60] R. Jackiw and R. Rajaraman, Phys. Rev. Lett. **54**, 1219 (1985).

[61] H. Itoyama and A. Mueller, Nucl. Phys. B **218**, 349 (1983).

[62] A. Das and A. Karev, Phys. Rev. D **36**, 623 (1987).

[63] A. J. Niemi and G. W. Semenoff, Phys. Rev. Lett. **51**, 2077 (1983).

[64] A. N. Redlich, Phys. Rev. D **29**, 2366 (1984).

[65] F. T. Brandt, A. Das, and J. Frenkel, Phys. Rev. D **62**, 085012 (2000).

[66] G. Dunne, K. Lee, and C. Lu, Phys. Rev. Lett. **78**, 3434 (1997).

[67] S. Deser, L. Griguolo, and D. Seminara, Phys. Rev. Lett. **79**, 1976 (1997).
[68] F. T. Brandt, A. Das, J. Frenkel, S. Pereira, and J. C. Taylor, Phys. Rev. D **64**, 065018 (2001).
[69] G. Tatara, H. Kohno, and J. Shibata, Phys. Rep. **468**, 213 (2008).
[70] J. Shibata, G. Tatara, and H. Kohno, J. Phys. D: Appl. Phys. **44**, 384004 (2011).
[71] E. Martinez, L. Lopez-Diaz, O. Alejos, and L. Torres, J. Appl. Phys. **106**, 043914 (2009).
[72] F. Xiu, L. He, Y. Wang, L. Cheng, L.-T. Chang, M. Lang, G. Huang, X. Kou, Y. Zhou, X. Jiang *et al.*, Nat. Nanotechnol. **6**, 216 (2011).
[73] S. Flügge, *Practical Quantum Mechanics* (Springer, Germany, 1998).
[74] J. I. Kapusta and C. Gale, *Finite-Temperature Field Theory: Principles and Applications* (Cambridge University Press, USA, 2006).
[75] A. Scholz and J. Schliemann, Phys. Rev. B **83**, 235409 (2011).

Article C

Visco elasticity in 2D materials

Visco elasticity in 2D materials

2016 2D Mater. 3 011002

(http://iopscience.iop.org/2053-1583/3/1/011002)

2D Materials

LETTER

Visco elasticity in 2D materials

Alberto Cortijo[1], **Yago Ferreirós**[1], **Karl Landsteiner**[2] **and María A H Vozmediano**[1]

[1] Instituto de Ciencia de Materiales de Madrid, CSIC, Cantoblanco; E-28049 Madrid, Spain
[2] Instituto de Física Teórica UAM/CSIC, Nicolás Cabrera 13-15, Cantoblanco, E-28049 Madrid, Spain

E-mail: vozmediano@icmm.csic.es

Keywords: elastic gauge fields, Hall viscosity, dirac matter

RECEIVED
15 October 2015

REVISED
8 December 2015

ACCEPTED FOR PUBLICATION
12 December 2015

PUBLISHED
7 January 2016

Abstract

The combination of Dirac physics and elasticity has been explored at length in graphene where the so-called 'elastic gauge fields' have given rise to an entire new field of research and applications: straintronics. The fact that these elastic fields couple to fermions as the electromagnetic field, implies that many electromagnetic responses will have elastic counterparts not yet explored. In this work we will first show that the presence of elastic gauge fields is the rule rather than the exception in most of the topologically non-trivial materials in two- and three-dimensions. We will show that, associated to the physics of the anomalies, and as a counterpart of the Hall conductivity, elastic two-dimension materials will have a Hall viscosity with a coefficient orders of magnitude bigger than the previously studied response. The magnitude and generality of the new effect will greatly improve the chances for the experimental observation of this topological response.

1. Introduction

New two-dimensional (2D) materials of scientific and technological interest are being synthesized in the 'post-graphene' era [1]. The 2D nature has important implications on the electronics and, singularly, on the morphological and elastic properties. As happens in graphene, new and fascinating behavior emerges from the interplay between lattice and electronics degrees of freedom [1–3]. Also singular in 2D are the topological properties associated with breaking of time reversal symmetry (quantum Hall effect (QHE) and anomalous QHE) or other discrete symmetries (spin or valley HE, etc). In the 2D family of materials, special interest is put on the 'Dirac materials' [4], a generic name for electronic systems whose low energy excitations are described by a Dirac Hamiltonian, graphene being the paradigmatic example. Those who have the Fermi points located at non-equivalent points of the Brillouin zone will support elastic gauge fields similar to those found in graphene [5].

In this work we will show that in 2D materials supporting elastic gauge fields, the presence of Hall conductivity automatically implies a new type of Hall viscosity orders of magnitude bigger than the standard one. We will first introduce the Hall viscosity (section 2), then show the mechanism at work in graphene (section 3) and later extend it to other 2D materials and to layered compounds (section 4).

2. The Hall viscosity

In elasticity theory Hooke's law tells us that in an elastic solid the stress tensor T_{ij} is proportional to the strain tensor $u_{ij} = (\partial_i u_j + \partial_j u_i)/2$ as $T_{ij} = \lambda_{ijlr} u_{lr}$ through a four-rank tensor λ_{ijlr}. If the system is viscoelastic the stress tensor is also proportional to the *time derivative* of u_{ij}:

$$T_{ij} = \eta_{ijlr} \dot{u}_{lr}, \tag{1}$$

through another four-rank tensor η_{ijlr}. In general, this viscosity tensor possesses both symmetric and antisymmetric components under the permutation of pairs of indices. While the symmetric part is generally associated to dissipation and vanishes at zero temperature, the antisymmetric part arises when time reversal symmetry is broken [6]. As usually happens with transport coefficients like the gyrotropic term of the permittivity in dielectrics, the antisymmetric part of the coefficients that are odd under time inversion are dissipation-less and they are not constrained to vanish at zero temperature. In 2D, isotropy and the aforementioned antisymmetry in permutations of pairs of indices allow for only one independent element

of the antisymmetric part of the tensor η_{ijlr}: $\eta_{ijlr} = \frac{\eta^{\mathrm{H}}}{2}(\delta_{il}\epsilon_{jr} + \delta_{ir}\epsilon_{jl} + \delta_{jl}\epsilon_{ir} + \delta_{jr}\epsilon_{il})$, where ϵ_{ij} is the Levi–Civita tensor in 2D.

The first context where this antisymmetric, dissipation-less coefficient was described was the QHC (this is why this coefficient is called Hall viscosity) [6]. Being non-dissipative and appearing in quantum Hall systems, it is not strange that the Hall viscosity could be associated to a certain Berry phase endowed with a topological meaning. In the case of the Hall conductivity, the off diagonal part of the conductivity tensor σ_{xy} is related to a non-zero Berry phase associated to the evolution of the phase of the wave function in the Brillouin zone [7]. In the case of the Hall viscosity, the parameter space is the space of the displacements of the atoms in the continuum limit, $\boldsymbol{u}(\boldsymbol{r})$. Since these displacements are considered adiabatic with respect to the electronic motion, one can consider a cyclic evolution of the wave function in this particular parameter space and define an associated Berry curvature of the wave function Φ_a at some energy level ε_a: $\Omega^{(a)}_{ijlr} = \mathrm{i}\langle\partial_{u_{ij}}\Phi_a|\partial_{u_{lr}}\Phi_a\rangle$.

Also the Hall viscosity can be computed from a Kubo formula [8] in terms of the stress–stress correlation function $\eta_{ijlr} = \int \mathrm{d}t\mathrm{e}^{\mathrm{i}0^+t}\langle[T_{ij}(t),\, T_{lr}(0)]\rangle$ with the stress tensor defined as the variation of the Hamiltonian with the strain tensor $T_{ij} = \frac{\delta H}{\delta u_{ij}}$. After some mathematical manipulations, a part of this Kubo formula appears to be proportional to the Berry curvature Ω_{ijlr} defined above [6].

Besides, as it happens in all transport coefficients in electronic systems, the Hall viscosity appears in the effective action of elasticity after integrating out the fermionic degrees of freedom. The effective energy functional for elastic displacements (phonons after quantizing) for a system in two spatial dimensions consists of two terms, the standard elastic terms (possibly renormalized by the effect of electrons) and the Hall viscosity term (neglecting microscopic sources of dissipation):

$$\mathcal{U} = \frac{1}{2}\int \mathrm{d}^2\boldsymbol{r}\,[\lambda_{ijlr}\partial_i u_j \partial_l u_r + \eta^H_{ijlr}\partial_i u_j \partial_l \dot{u}_r]. \qquad (2)$$

Today there is a consensus about the meaning and the origin of the Hall viscosity. The quantum Hall state is a topologically ordered state so it is natural to extend the search to other topologically non-trivial quantum systems. Much work has been done in this direction and Hall viscosities have been found in many topologically non-trivial condensed matter phases apart from the quantum Hall phase [6], like the fractional quantum Hall phase [9, 10], chiral superfluids [9, 11] and superconductors [12], Chern insulators in presence of torsion in 2D [13–15] and, more recently, in three-dimensions [15, 16] as well. The question at this point is how to define the coupling between electrons and the elastic displacements u_i or better, to the strain tensor u_{ij} and where to seek for it.

As we will discuss in detail later, the way how the elasticity couples to the low energy degrees of freedom (electrons or phase fluctuations in the case of superfluids or superconductors) is crucial to determine if a topologically non-trivial phase displays Hall viscosity. Most of the studies available in the literature are based on a continuum formulation of the system and the elastic degrees of freedom. The philosophy is that, since elastic deformations can be viewed as geometric deformations in the medium hosting the system, the excitations feel a distorted or curved space where to propagate. We can thus define an effective metric tensor related to elastic distortions and postulate that our system now develops its dynamics in a curved space. The general formalism of field theories in curved spaces and linear responses does the job [17]. Although powerful, this approach has some limitations in the scope of systems that can be treated. For instance, in the metric formalism (in absence of torsion), some non-trivial topological phases with non-zero Hall conductivity have zero Hall viscosity. This is the case of Chern insulators in 2D and Weyl semimetals in three-dimensions. On the other hand, only a small fraction of the literature devoted to the Hall viscosity in electronic systems treats the problem from the more conventional perspective in solid state physics through general electron–phonon couplings [16, 18]. The goal in these approaches is to define an effective electron-metric coupling by taking the continuum limit from a lattice formulation, thus reaching similar success and suffering from the same limitations as in the former case.

The present work offers a different alternative. We will show how the electron–phonon coupling in a class of electronic systems with an underlying lattice not only gives rise to a metric formulation in the continuum, but as we know from graphene, emergent vector fields arise in such effective description coupling to the electrons in a very similar way as the electromagnetic gauge field. These vector couplings between electrons and elastic deformations offer new results and enlarge the kind of systems where the Hall viscosity can in principle be measured.

3. Hall viscosity from Hall conductivity in graphene

In this section we will show that anomalous Hall conductivity implies anomalous Hall viscosity in graphene. We will later extend the discussion to other Weyl materials.

The low energy action around one of the two Fermi points of graphene coupled to a U(1) electromagnetic background field is

$$S = \int \mathrm{d}^3x\bar{\psi}\left(\mathrm{i}\gamma^0\partial_0 - \mathrm{i}v_F\gamma^i\partial_i + \frac{ev_F}{c}\gamma^i A_i\right)\psi. \quad (3)$$

A way to break time reversal invariance suggested by Haldane is to add complex next-to-nearest neighbor hopping terms in the tight-binding on the honeycomb lattice [19]. In the continuum limit, these complex hoppings lead to a mass term with opposite sign at each Fermi point. After integrating out fermions it is easy to find the Chern–Simons term as a part of the effective electromagnetic action:

$$S_{\mathrm{CS}} = \frac{e^2}{\pi c}\mathrm{sign}(m)\int \mathrm{d}^3x\epsilon^{ijk}A_i\partial_j A_k, \quad (4)$$

after considering all the degeneracies (and in units of $\hbar = 1$). Coupling the effective action (4) to a source J^iA_i allows to derive an anomalous QHE:

$$J^i \equiv \frac{\delta S}{\delta A_i} = \frac{2e^2}{\pi c}\mathrm{sign}(m)\,\epsilon^{ijk}\partial_j A_k. \quad (5)$$

A very interesting aspect of graphene shared by many other 2D materials is the tight connection between lattice structure and electronic excitations. Within the simplest tight binding-elasticity approach, lattice deformations couple to the Dirac fermion as elastic U(1) vector fields that depend linearly on the strain tensor u_{ij} as [5, 20, 21]

$$A_1^{\mathrm{el}} = \frac{\beta}{a}(u_{11} - u_{22}),$$
$$A_2^{\mathrm{el}} = -\frac{2\beta}{a}u_{12}, \quad (6)$$

where β is the dimensionless Grüneisen parameter estimated to be of order two in graphene, and a is the lattice constant. Since lattice deformations do not break time reversal symmetry, the elastic vector field couples with opposite signs to the two Dirac points and behaves as an axial vector field when both Fermi points are considered. Notice that, in the derivation of the Chern–Simons term (4) for a vector field coupled to the fermionic current, the sign of the coupling appears twice, hence the coefficient is the same in the two valleys despite the oposite coupling of the elastic gauge field. We will deduce the contribution of a single valley and multiply the final result by the degeneracy.

If we consider this elastic axial vector coupling to electrons instead of the electromagnetic field we have

$$S_g = \int \mathrm{d}^3x\bar{\psi}(\mathrm{i}\gamma^0\partial_0 - \mathrm{i}v_F\gamma^i\partial_i + v_F\gamma^i A_i^{\mathrm{el}})\psi + m\bar{\psi}\psi. \quad (7)$$

It is obvious that the same line of arguments as before will give rise to a Chern–Simons action like (4) in terms of the elastic instead of the electromagnetic field. In particular we will get

$$S_{\mathrm{CS}} = \frac{2}{\pi}\mathrm{sign}(m)\int \mathrm{d}^3x(A_1^{\mathrm{el}}\dot{A}_2^{\mathrm{el}} - A_2^{\mathrm{el}}\dot{A}_1^{\mathrm{el}}). \quad (8)$$

Substituting from equation (6) we get in the Chern–Simons action a term of the form

$$S_{\mathrm{CS}}[u] = \frac{4\beta^2}{\pi a^2}\mathrm{sign}(m)\int \mathrm{d}^3x[u_{22}\dot{u}_{12} - u_{11}\dot{u}_{12} + u_{12}\dot{u}_{11} - u_{12}\dot{u}_{22}]. \quad (9)$$

To this effective action we can now couple a source term for elastic deformations $S_u = u_{ij}T^{ij}$ and compute the averaged value of the 11 component of the stress tensor

$$\langle T_{11}\rangle \equiv \frac{\delta S}{\delta u_{11}} = \frac{8\beta^2}{\pi a^2}\mathrm{sign}(m)\,\dot{u}_{12}, \quad (10)$$

obtaining a Hall viscosity

$$\eta^{\mathrm{H}} = \frac{8\beta^2}{\pi a^2}\mathrm{sign}(m). \quad (11)$$

The coefficient is determined by the parity anomaly in (2 + 1)-dimensions, and the characteristic length associated to the viscosity is given by the lattice spacing a. This new response is a genuine viscoelastic response: Elastic gauge fields inducing a Hall viscosity.

The Hall viscosity described here is an intrinsic property of the Haldane model of graphene in the same sense as the quantum anomalous Hall effect (QAHE) of the original proposal [19]. It has been argued [22] that the intrinsic Hall viscosity in the topological phase of the Haldane model is $\eta_{\mathrm{H}} = \hbar\rho/4$, where ρ is the electronic density. When the Fermi level lies within the gap, the standard Hall viscosity is zero in the Haldane model.

A technical remark is in order here. In the case of having non-uniform strain, an effective space dependent mass term appears in equation (7). Since the CS term only depends on the sign of the mass, our result will remain valid as long as the strain-dependent mass does not change its sign, or the value of the mass remains much smaller than the bandwidth and an effective description in terms of the massive Dirac Hamiltonian around each Dirac point is valid in the continuum.

Although the Haldane model has been realised experimentally in optical lattices [23] it seems challenging to generate it in graphene. However, the QAHE in graphene by magnetic proximity effect has been measured in graphene [24], making it a suitable platform to potentially measure effects induced by the presence of the Hall viscosity.

The same reasoning as done in the Haldane model can be applied to real graphene in a perpendicular magnetic field breaking time reversal symmetry. The Hall conductivity in graphene is [25, 26] $\sigma_{\mathrm{H}} = 4e^2(n + 1/2)/\pi$, $n = 0, 1, \ldots$. By the same argument as before in the quantum limit where only the lowest Landau level is filled ($n = 0$), there is a contribution to the Hall viscosity coming from the elastic vector fields:

$$\eta_{\mathrm{H}} \sim \frac{2\beta^2}{a^2}. \quad (12)$$

In the presence of a magnetic field this is not the only contribution to the Hall viscosity. Now other terms coupling the elasticity to the Dirac fermions

come into play [27]. In particular the following term

$$H = \frac{\mathrm{i}}{2}\beta u_{ij}(\psi^{+}\sigma_i\partial_j\psi + \partial_j\psi^{+}\sigma_i\psi), \tag{13}$$

gives a contribution to the Hall viscosity that has been computed to be [6, 22]

$$\eta_{\mathrm{H}}^{(B)} = 4\beta^2[|n|(|n|+1)/4 + 1/8]eB/2\pi. \tag{14}$$

In the quantum limit ($n=0$) we thus have $\eta_{\mathrm{H}}^{(B)} \sim \beta^2/l_B^2$, where l_B is the magnetic length. This result might seem a little bit puzzling at a first glance. We have stressed that in the absence of torsional couplings and magnetic fields, the Haldane model has no Hall viscosity unless one considers the elastic gauge fields while now a second contribution from (13) appears. The reason is that the coupling in (13) is a derivative coupling. When one consider both terms (7) and (13) and find the effective theory for elasticity, the term coming from (13) has more than one space-time derivatives and it does not contribute to the Hall viscosity. When a magnetic field is taken into account, the partial derivative ∂_j transforms into a covariant derivative $\partial_j + \mathrm{i}eA_j$ (with $\vec{B} = \nabla \times \vec{A}$) and the magnetic length $l_B = \sqrt{c/eB}$ permeates through the calculations allowing for the result (14). Taking graphene as an example, the ratio between the two contributions is

$$\frac{\eta_{\mathrm{H}}}{\eta_{\mathrm{H}}^{(B)}} \sim \frac{l_B^2}{a^2} \sim \frac{10^4}{B}, \tag{15}$$

where a is the lattice constant and B is the magnitude of the magnetic field in Tesla. For a magnetic field of 10 T, the contribution from the elastic gauge fields is three orders of magnitude larger than the one coming from (13). It means that if the Hall viscosity is measured in graphene under quantizing magnetic fields, probably it is the component discussed in the present work the one that will be measured.

4. Generality of the effect

The novel effect described in graphene is based on two main ingredients: the existence of elastic gauge fields and the non-trivial topology of the electronic bands of the system. This last ingredient is what allows to write down a Chern–Simons effective action in 2D given in equation (4) which is the key issue of the approach. The non trivial topology can arise directly as a Berry phase associated to the Bloch bands of the crystal as in the Haldane model [19], or from the topology of a general 2D electron gas in a perpendicular magnetic field through the Hofstadter model [7, 28]. In all cases the Hall conductivity is associated to the topological Chern–Simons action depicted in equation (4). As we have demonstrated, a Hall conductivity and elastic gauge fields immediately implies the new Hall viscosity. We will now discuss the generality of the presence of elastic gauge fields in real systems and give some concrete examples.

Although first derived in a tight binding formulation on the lattice, the generation of elastic gauge fields in the low energy effective Hamiltonian of electron systems, is a very general phenomenon. It also arises in a general construction of low energy effective actions based on a symmetry analysis as described in [29–31]. The general conditions for a 2D lattice to support elastic gauge fields have been discussed in [29]. The two essential ingredients are: the presence of (at least) two electronic degrees of freedom per unit cell (this can arise from lattice (graphene), orbital (MoS_2) or by other mechanisms). Lack of inversion symmetry in the little group leaving a Fermi point invariant, ensures that the Fermi points sit at non-equivalent high symmetry points of the Brillouin zone. It is easy to see that the same structure giving rise to the Dirac Hamiltonian causes the minimal coupling to the vector fields associated to lattice deformations implying that the phenomenon can be generalized to other crystals in two and three-dimensions. As it is clear from the analyses in [29, 31] the symmetry group of the lattice dictates the precise form of the elastic vector fields.

Figure 1 shows the lattice and band structure of two representative examples of the so-called Dirac materials in two spatial dimensions. Graphene in the left has a planar honeycomb lattice structure and its Fermi energy is made of two Dirac cones. In the right hand side we represent the transition metal dichalcogenide MoS_2. It is a semiconductor with bands that admit a low energy effective description in terms of two species of massive Dirac fermions.

Single-layer and multilayer transition metal dichalcogenides MX_2 (M= Mo, W and X= S, Se) [1] do support elastic gauge fields [32]. Although having a noticeable band gap and a complicated orbital structure, MoS_2 and the related compounds based on the honeycomb lattice, support at low energy, the same elastic gauge fields as graphene given in equation (6) [33]. These are also found in bilayer graphene [34] which has a quadratic dispersion and a Hall conductivity two times that of graphene. They will also occur in rombohedral multilayer graphene where the effective low energy model of the n layer compound has a Lifschitz dispersion relation $\omega \sim k^n$. Our mechanism for Hall viscosity will directly apply in these 2D (or effectively 2D) compounds. The magnitude of the effect will also be similar to that found in graphene since the parameter β/a has the same order of magnitude [35].

In these multilayer systems formed by a family of isolated metallic 2D lattice planes indexed by a primitive reciprocal lattice vector G, the 3D Hall conductivity is [36]

$$\sigma_{\mathrm{H}}^{ab} = \frac{1}{2\pi}\sigma_{\mathrm{H}}^{2D}\epsilon^{abc}G_c. \tag{16}$$

Any 2D system having a QHE will exhibit, when stacked to form a 3D material, a 3DQHE if the interplane coupling is sufficiently weak, as it is the case of

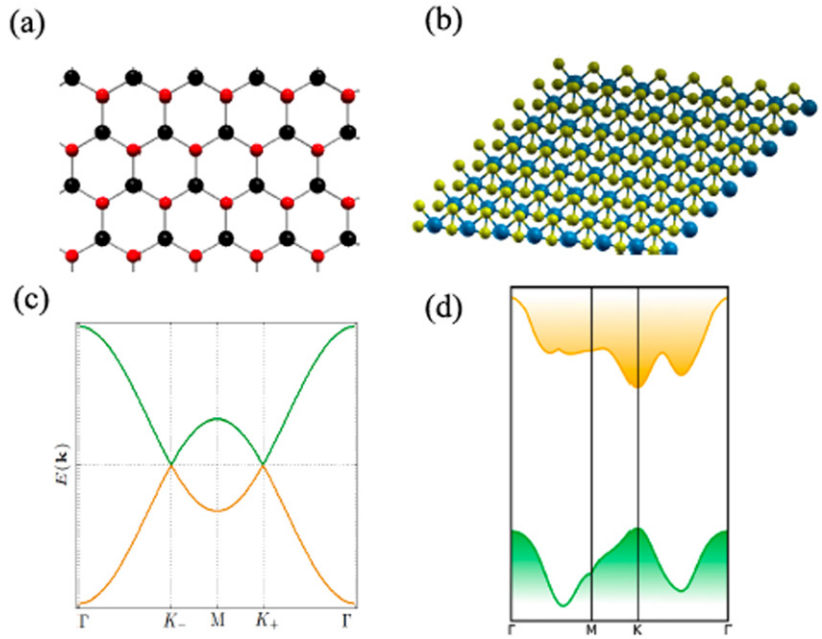

Figure 1. Two-dimensional Dirac materials. The most representative example of the so-called Dirac materials in two spatial dimensions is graphene. In graphene, carbon atoms are arranged in a honeycomb lattice, (a). The highest occupied and the lowest empty bands touch at the corners of the Brillouin zone and the low energy band dispersion is well described by two species of massless Dirac fermions, (c). MoS_2 is the representative of the family of transition metal dichalcogenides, (b). MoS_2 is a semiconductor with bands that admit a low energy effective description in terms of two species of massive Dirac fermions (d).

the so called Van der Waals (VdW) systems. In this way, when the 2D constituents support elastic gauge fields, a 3D Hall viscosity will arise. The obvious example in this class is graphite whose 3D Hall conductivity has been described in [37]. In a homogeneous magnetic field perpendicular to the layers and when the Fermi level is in the 3D gap, the Hall conductance is found to be (in units of the quantum of conductance) $\sigma_{xy} = 2\dfrac{(2n+1)}{c_0}$, where c_0 is the c-axis coupling constant of graphite estimated to be $c_0 = 6.74$ Å. The corresponding 3D Hall viscosity will have an in-plane component

$$\eta^{\mathrm{H}}_{1112} = 2\frac{(2n+1)\beta^2}{\pi a^2 c_0}, \tag{17}$$

where $a = 2.456$ Å is the in-plane lattice constant of graphene. Nowadays the family of VdW materials constitutes an intense area of research so we cannot limit ourselves to consider graphite or transition metal dichalcogenides. Hexagonal boron nitride is another VdW system where these effects are potentially observable and even bulk black phosphorus that has recently been proposed to have Weyl nodes under pressure [38], we expect it to display elastic vector fields in its elastic response.

5. Discussion and future

In the present work we have identified a new mechanism to generate a Hall viscosity and a large number of new materials and systems that will display such effect. As it can be understood from the previous general discussion [16, 18], it is natural to measure changes in the phonon structure due to the presence of η^H. In-plane phonon dispersion measurements can be performed by x-ray scattering [39], Brillouin scattering [40], and electron energy loss spectroscopy [41], all already done in the case of graphene and VdW materials. Also, since now we are open to three-dimensional electronic systems, three-dimensional probes like neutron scattering can in principle be used. In order to get some numbers we can take graphene as the paradigmatic example. Using standard values [42] for the Lamé coefficients $\lambda = 2$ eV Å^{-2} and $\mu = 10$ eV Å^{-2} a characteristic frequency associated to the Hall viscosity can be defined, $\omega_{\mathrm{H}} = \dfrac{\pi a^2 \mu}{\beta^2 \hbar} \simeq 95$ eV, which is a rather large frequency scale compared with typical in-plane acoustic phonon frequencies (∼hundreds of meV). It intuitively means that the changes in the acoustic phonons will be hard to observe within current experimental resolutions at least in 2D. In spite of that, we believe that increasing the number of systems that display a Hall viscosity through elastic gauge fields, it is a matter of time to find an experimental probe that could detect and measure η^{H}.

We end up summarizing the main findings of this work and their physical implications:

- The elastic gauge fields encoding the interaction of the electronic properties with lattice deformations of crystals are a very general phenomenon. First described in graphene, they have also been obtained

in the low energy effective models of other 2D systems as MoS_2. The necessary condition for their presence is that the singular points in the dispersion relation sit at non-equivalent points of the Brillouin zone.

- In any compound supporting elastic gauge fields Hall conductivity implies Hall viscosity. The contribution to the Hall viscosity from elastic gauge fields is several orders of magnitude bigger than that coming from phonons or metric deformations.

Several aspects of the viscoelastic response of lattice topological crystals have been recently analyzed in [16]. Our new contribution to the Hall viscosity, although not explicitly discussed, could certainly be worked out as a part of their general analysis. What we emphasize here is the analogy of the elastic gauge fields with the standard electromagnetic partners which makes the connection with the anomaly related topological aspects very transparent.

Acknowledgments

We thank Carlos Hoyos for enlightening discussions on the Hall viscosity and Juan Mañes for comments on the elastic gauge fields. Special thanks go also to José Silva-Guillén for help with the figures. This research was supported in part by the Spanish MECD grants FIS2011-23713, PIB2010BZ-00512, the European Union structural funds and the Comunidad de Madrid MAD2D-CM Program (S2013/MIT-3007), by the National Science Foundation under Grant No. NSF PHY11-25915, and by the European Union Seventh Framework Programme under grant agreement no. 604391 Graphene Flagship, FPA2012-32828 and by the Centro de Excelencia Severo Ochoa Programme under grant SEV-2012-0249.

References

[1] Roldán R, Castellanos-Gomez A, Cappelluti E and Guinea F 2015 Strain engineering in semiconducting two-dimensional crystals *J. Phys. Condens. Matter* **27** 313201
[2] Plechinger G *et al* 2015 Control of biaxial strain in single-layer molybdenite using local thermal expansion of the substrate *2D Mater.* **2** 015006
[3] Castellanos-Gomez A, Singh V, van der Zant H S J and Steele G A 2015 Mechanics of freely-suspended ultrathin layered materials *Ann. Phys., Lpz.* **527** 27–44
[4] Goerbig M and Montambaux G 2014 Dirac fermions in condensed matter and beyond arXiv:1410.4098
[5] Vozmediano M A H, Katsnelson M I and Guinea F 2010 Gauge fields in graphene *Phys. Rep.* **493** 109
[6] Avron J E, Seiler R and Zograf P G 1995 Viscosity of quantum hall fluids *Phys. Rev. Lett.* **75** 697
[7] Thouless D J, Kohmoto M, Nightingale M P and den Nijs M 1982 Quantized hall conductance in a two-dimensional periodic potential *Phys. Rev. Lett.* **49** 405–8
[8] Bradlyn B, Goldstein M and Read N 2012 Kubo formulas for viscosity: Hall viscosity, ward identities, and the relation with conductivity *Phys. Rev.* B **86** 245309
[9] Read N 2009 Non-abelian adiabatic statistics and hall viscosity in quantum hall states and $p_x + ip_y$ paired superfluids *Phys. Rev.* B **79** 045308
[10] Gromov A, Cho G Y, You Y, Abanov A G and Fradkin E 2015 Framing anomaly in the effective theory of the fractional quantum hall effect *Phys. Rev. Lett.* **114** 016805
[11] Hoyos C, Moroz S and Son D T 2014 Effective theory of chiral two-dimensional superfluids *Phys. Rev.* B **89** 174507
[12] Shitade A and Kimura T 2014 Bulk angular momentum and hall viscosity in chiral superconductors *Phys. Rev.* B **90** 134510
[13] Hughes T L, Leigh R G and Fradkin E 2013 Torsional response and dissipationless viscosity in topological insulators *Phys. Rev. Lett.* **107** 075502
[14] Hughes T L, Leigh R G and Parrikar O 2013 Torsional anomalies, Hall viscosity, and bulk-boundary correspondence in topological states *Phys. Rev.* D **88** 025040
[15] Sun L and Wan S 2014 Chiral viscoelastic response in Weyl semimetals *Eur. Phys. Lett.* **108** 37007
[16] Shapourian H, Hughes T L and Ryu S 2015 The viscoelastic response of topological tight-binding models in 2d and 3d arXiv:1505.03868
[17] Hoyos C 2014 Hall viscosity, topological states and effective theories *Int. J. Mod. Phys.* B **28** 1430007
[18] Barkeshli M, Chung S B and Qi X 2012 Dissipationless phonon hall viscosity *Phys. Rev.* B **85** 245107
[19] Haldane F D M 1988 Model for a quantum hall effect without landau levels: condensed-matter realization of the parity anomaly *Phys. Rev. Lett.* **61** 2015–8
[20] Kane C L and Mele E J 1997 Size, shape, and low energy electronic structure of carbon nanotubes *Phys. Rev. Lett.* **78** 1932–5
[21] Suzuura H and Ando T 2002 Phonons and electron–phonon scattering in carbon nanotubes *Phys. Rev.* B **65** 235412
[22] Kimura T 2010 Hall and spin Hall viscosity in topological insulators arXiv:1004.2688
[23] Jotzu G *et al* 2014 Experimental realization of the topological haldane model with ultracold fermions *Nature* **515** 237
[24] Qiao Z *et al* 2014 Quantum anomalous hall effect in graphene proximity coupled to an antiferromagnetic insulator *Phys. Rev. Lett.* **112** 116404
[25] Jackiw R 1984 Fractional charge and zero modes for planar systems in a magnetic field *Phys. Rev.* D **29** 2375–7
[26] Gusynin V P and Sharapov S G 2005 Unconventional integer quantum hall effect in graphene *Phys. Rev. Lett.* **95** 146801
[27] Mañes J L, de Juan F, Sturla M and Vozmediano M A H 2013 Generalized effective Hamiltonian for graphene under nonuniform strain *Phys. Rev.* B **88** 155405
[28] Hofstadter D R 1976 Energy levels and wave functions of bloch electrons in rational and irrational magnetic fields *Phys. Rev.* B **14** 2239–49
[29] Mañes J L 2007 Symmetry-based approach to electron–phonon interactions in graphene *Phys. Rev.* B **76** 045430
[30] de Juan F, Sturla M and Vozmediano M A H 2012 Space dependent fermi velocity in strained graphene *Phys. Rev. Lett.* **108** 227205
[31] de Juan F, Mañes J L and Vozmediano M A H 2013 Gauge fields from strain in graphene *Phys. Rev.* B **87** 165131
[32] Rostami H, Roldán R, Cappelluti E, Asgari R and Guinea F 2015 Theory of strain in single-layer transition metal dichalcogenides *Phys. Rev.* B **92** 195402
[33] Cazalilla M A, Ochoa H and Guinea F 2014 Quantum spin hall effect in two-dimensional crystals of transition-metal dichalcogenides *Phys. Rev. Lett.* **113** 077201
[34] Mariani E, Pearce A J and von Oppen F 2012 Fictitious gauge fields in bilayer graphene *Phys. Rev.* B **86** 165448
[35] Girifalko L A 2000 *Statistical Mechanics of Solids* (Oxford: Oxford University Press)
[36] Halperin B I 1987 Possible states for a three-dimensional electron gas in a strong magnetic field *Japan. J. Appl. Phys. Suppl.* **26** 1913
[37] Bernevig B A, Hughes T L, Raghu S and Arovas D P 2007 Theory of the three-dimensional quantum hall effect in graphite *Phys. Rev. Lett.* **99** 146804

[38] Fei R, Tran V and Yang L 2015 Topologically protected dirac cones in compressed bulk black phosphorus *Phys. Rev.* B **91** 195319
[39] Mohr M *et al* 2007 Phonon dispersion of graphite by inelastic x-ray scattering *Phys. Rev.* B **76** 035439
[40] Wang Z, Lim H, Ng S, Zyilmaz B and Kuok M 2008 Brillouin scattering study of low-frequency bulk acoustic phonons in multilayer graphene *Carbon* **46** 2133–6
[41] Generalov A and Dedkov Y 2012 Eels study of the epitaxial graphene/ni(111) and graphene/au/ni(111) systems *Carbon* **50** 183–91
[42] Zakharchenko K V, Katsnelson M I and Fasolino A 2009 Finite temperature lattice properties of graphene beyond the quasiharmonic approximation *Phys. Rev. Lett.* **102** 046808

Article D

Elastic Gauge Fields in Weyl Semimetals

Elastic Gauge Fields in Weyl Semimetals

Alberto Cortijo,[1] Yago Ferreirós,[1] Karl Landsteiner,[2] and María A. H. Vozmediano[1]
[1]*Instituto de Ciencia de Materiales de Madrid, CSIC, Cantoblanco, 28049 Madrid, Spain*
[2]*Instituto de Física Teórica UAM/CSIC, Nicolás Cabrera 13-15, Cantoblanco, 28049 Madrid, Spain*
(Received 30 July 2015; revised manuscript received 4 September 2015; published 20 October 2015)

We show that, as happens in graphene, elastic deformations couple to the electronic degrees of freedom as pseudogauge fields in Weyl semimetals. We derive the form of the elastic gauge fields in a tight-binding model hosting Weyl nodes and see that this vector electron-phonon coupling is chiral, providing an example of axial gauge fields in three dimensions. As an example of the new response functions that arise associated with these elastic gauge fields, we derive a nonzero phonon Hall viscosity for the neutral system at zero temperature. The axial nature of the fields provides a test of the chiral anomaly in high energy with three axial vector couplings.

DOI: 10.1103/PhysRevLett.115.177202 PACS numbers: 75.30.Ds, 62.20.D-, 73.43.-f

Introduction.—The occurrence of Weyl fermions (massless Dirac fermions of definite chirality) in condensed matter has always come with unexpected phenomena and new physics. Although having a long tradition [1], the best examples so far have arisen in one spacial dimension (Luttinger liquids) [2] or in two (graphene [3] and the surface of three-dimensional topological insulators [4]). Charged massless fermions are particularly interesting in three dimensions: they do not have counterparts in particle physics and they experience the chiral anomaly [5–9] and its related physical responses.

The Dirac equation comes from the existence of band crossings, "Fermi points" in the dispersion relation, and the subsequent low energy expansion around them. Coming from a lattice, these Weyl fermions must always arise in pairs of opposite chirality—or helicity—according to the Nielsen-Ninomiya theorem [7]. Dirac semimetals [10] have the crossing points at the γ point of the Brillouin zone and the contribution from the two opposite chiralities cancel the anomaly related responses. The importance of the so-called Weyl semimetals (WSMs) is that, as happens in graphene, the two chiral partners sit at nonequivalent points in momentum space and the physics of anomalies is present in full glory. This is why the recent experimental discovery of WSMs [11–15] is attracting so much excitement [16].

WSMs have been named "the 3D graphene." One of the most exotic and fruitful aspects of graphene has arisen from the demonstration that elastic lattice deformations couple to its electronic excitations in the form of fictitious gauge fields [17]. This fact, first deduced in a tight-binding model [18], was soon recognized to arise from very general symmetry considerations [19,20]. The experimental observation of the predicted Landau levels associated with the elastic magnetic fields [21,22] has given rise to a whole new field of research called "straintronics."

In what follows we will show the presence of elastic gauge fields in WSMs. We first make a microscopic derivation starting from a tight-binding description [18] and taking the continuum limit around the Weyl points. As a physical consequence, we will show the presence of an anomalous phonon Hall viscosity in the WSMs with time reversal symmetry $\mathcal{T}$ broken. Similar to the Hall conductivity, the Hall viscosity can be used to classify topologically nontrivial states of matter [23–28]. We will see that the elastic gauge fields provide a new mechanism for generating the Hall viscosity not previously studied in the literature. Because of the chiral nature of the coupling between Weyl fermions and elastic degrees of freedom, this new coupling provides an example of axial vector-fermion interaction with no analogue in high energy physics, and paves the way for studying the consequences of such couplings in a more general context.

Elastic gauge fields in a model for WSMs.—To illustrate how emergent vector fields associated with elasticity appear in a WSM phase we can consider the following simple model of s- and p-like electrons hopping in a cubic lattice and chirally coupled to an on-site constant vector field $\boldsymbol{b}$ [29,30]:

$$H_0 = \sum_{i,j} c_i^+ (it\alpha_j - r\hat{\beta}) c_{i+j} + (m+3r)\sum_i c_i^+ \hat{\beta} c_i + \sum_{i,l} b_l c_i^+ \alpha_l \gamma_5 c_i + \text{H.c.}, \quad (1)$$

where i labels the position $\mathbf{R}_i$ and j labels the six next nearest neighbors $\mathbf{a}_j$ of length a in the cubic lattice. The matrices α_i and $\hat{\beta}$ are the standard Dirac matrices. In the unstrained situation we will set all the hopping terms t equal for simplicity. The parameters t, r, and m represent, in a tight-binding description, the hopping matrix elements between s and p states, hopping between the same kind of states, and the difference of on-site energies between s and p states, respectively. The vector field $\boldsymbol{b}$ breaks $\mathcal{T}$ as well as the cubic lattice symmetry and thus the SO(3) rotational

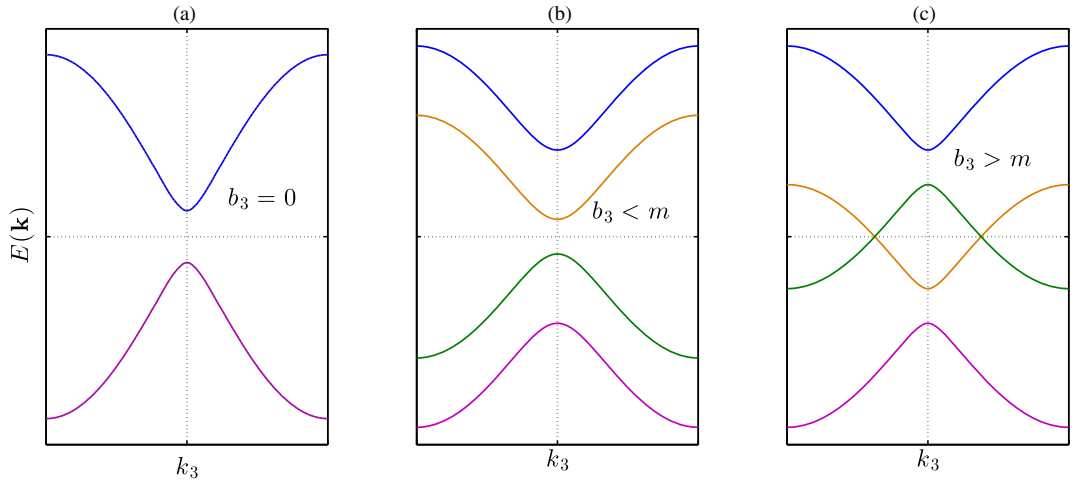

FIG. 1 (color online). Evolution of the band structure of the model given in Eq. (1) as a function of the parameter b. For $b_3 = 0$ the spectrum consists of two pairs of degenerate bands due to time reversal symmetry (a). When $0 < b_3 < m$ the band degeneracy breaks down and a high energy sector differentiates from a low energy sector, but the system is still gap full (b). When $b_3 > m$, the low energy bands cross each other at two definite points in the Brillouin zone. At sufficiently low energies, the system consists of two pairs of Weyl fermions with opposite chirality (c).

symmetry in the continuum description. Without loss of generality, we will choose the vector field $\boldsymbol{b}$ to point along the OZ direction. The model of Eq. (1) with $b_3 = 0$ is the standard model to exemplify the transition from a trivial to a topological insulating phase as a function of the parameters m and r. The region $0 > m > -2r$ corresponds to a topological insulating phase and the long wavelength limit around the Γ point ($\boldsymbol{k} = 0$) corresponds to an isotropic massive Dirac system. As can be seen in Fig. 1 the WSM phase appears when $b_3 > m$. The spectrum of the Hamiltonian in Eq. (1) consists of two bands crossing at two Fermi points in the BZ and two bands at higher and lower energies [Fig. 1(c)]. Let us choose the following representation for the Dirac matrices: $\alpha_1 = \tau_0\sigma_1$, $\alpha_2 = \tau_0\sigma_2$, $\alpha_3 = \tau_1\sigma_3$, $\hat{\beta} = \tau_3\sigma_3$, $\gamma_5 = \tau_1\sigma_0$, so $\alpha_3\gamma_5 = \tau_0\sigma_3$. Fourier transforming Eq. (1) we obtain

$$\mathcal{H}_0(\boldsymbol{k}) = \begin{pmatrix} t\sum_s \sigma_s \sin(k_s a) + [b_3 + m(\boldsymbol{k})]\sigma_3 & t\sin(k_3 a)\sigma_3 \\ t\sin(k_3 a)\sigma_3 & t\sum_s \sigma_s \sin(k_s a) + [b_3 - m(\boldsymbol{k})]\sigma_3 \end{pmatrix} \tag{2}$$

with $s = (1, 2)$, and $m(\boldsymbol{k}) = m + 3r - r\sum_j \cos(k_j a)$. The four-component wave function can be written in two-component blocks $(\phi_{\boldsymbol{k}}, \psi_{\boldsymbol{k}})$. For energies $E \ll m + b_3$ we can write $\phi_{\boldsymbol{k}} \simeq -[vk_3/(m + b_3)]\psi_{\boldsymbol{k}}$. Projecting out the high energy sector represented by $\phi_{\boldsymbol{k}}$ and expanding around the $\boldsymbol{k} = 0$ point, we find the following effective two-band model in the continuum ($v = ta$):

$$H_{\text{eff}} = \sum_{\boldsymbol{k}} \psi^{+}_{\boldsymbol{k}} \left(v\boldsymbol{\sigma}_\perp \cdot \boldsymbol{k}_\perp + \frac{1}{m + b_3}(b_3^2 - m^2 - v^2 k_3^2)\sigma_3 \right) \psi_{\boldsymbol{k}}. \tag{3}$$

The existence of Weyl points $\boldsymbol{\lambda}$ is met when for $k_1 = k_2 = 0$, the equation $b_3^2 - m^2 - v^2 k_3^2 = 0$ has real solutions. In this case, the two Weyl points are located at $\boldsymbol{\lambda}_\pm = (0, 0, \pm\sqrt{[(b_3^2 - m^2)/v^2]})$. Expanding now around these two points $\boldsymbol{k} \simeq \boldsymbol{\lambda}_\pm + \delta\boldsymbol{k}$, the low energy effective Hamiltonian takes the form of two massless three-dimensional Dirac fermions $\psi_\pm$ separated by the vector $\boldsymbol{\lambda}_+ - \boldsymbol{\lambda}_-$ in momentum space

$$H_W = \sum_{\delta\boldsymbol{k}} \psi^{+}_{\pm,\delta\boldsymbol{k}} (v\boldsymbol{\sigma} \cdot \delta\boldsymbol{k}_\perp \mp v_3 \delta k_3 \sigma_3) \psi_{\pm,\delta\boldsymbol{k}} \tag{4}$$

with $v_3 = 2v\sqrt{[(b_3 - m)/(b_3 + m)]}$.

Now we will apply strain to the original tight-binding Hamiltonian and find the modifications it induces in the low energy Hamiltonian (4). The strain tensor u_{ij} enters in the tight-binding approach through the change of the hopping parameters t when the lattice is distorted. In the model of Eq. (1), there are two types of corrections to t. One, similar to that arising in graphene [17], is due to the change in the bond length. It is isotropic and exists for all orbitals:

$$r \to r_j \simeq r(1-\beta u_{jj}), \tag{5}$$

where β is the Grüneisen parameter of the model. The second contribution affects the hopping between different orbitals and is associated with a rotation with respect to the reference frames of neighboring atoms as described in Ref. [30]. Following this reference, the changes for t_j are

$$t\alpha_j \to t(1-\beta u_{jj})\alpha_j + t\beta \sum_{j'\neq j} u_{jj'}\alpha_{j'}. \tag{6}$$

Inserting these modifications in the original Hamiltonian (1), we can define the strained Hamiltonian as the sum of the original Hamiltonian H_0 and the strain dependent part $H[u_{ij}]$. Projecting out the high energy sector and expanding around the two nodal points $\boldsymbol{\lambda}_\pm$, the strain dependent Hamiltonian part takes the form

$$\begin{aligned} H^W_{\text{eff}}[u]_\pm = {} & \pm\beta\sqrt{b_3^2-m^2}\sum_{\boldsymbol{k},s=1,2} u_{3s}\psi^+_{\pm,\boldsymbol{k}}\sigma_s\psi_{\pm,\boldsymbol{k}} \\ & + \beta\sum_{\boldsymbol{k}}\left(2(b_3-m)u_{33} - r\sum_j u_{jj}\right)\psi^+_{\pm,\boldsymbol{k}}\sigma_3\psi_{\pm,\boldsymbol{k}}. \end{aligned} \tag{7}$$

We have found that, around the two nodal points, strain couples to the low energy electronic sector as a vector field:

$$\begin{aligned} A^{\text{el}}_1 &= \beta\sqrt{b_3^2-m^2}u_{31}, \\ A^{\text{el}}_2 &= \beta\sqrt{b_3^2-m^2}u_{32}, \\ A^{\text{el}}_3 &= 2\beta(b_3-m)u_{33} - \beta r\sum_j u_{jj}. \end{aligned} \tag{8}$$

This is the first main result of this Letter.

The low energy effective action in the continuum limit around the Weyl nodes ($\boldsymbol{\lambda}_\pm$) is thus given by

$$H_W = \sum_{\delta\boldsymbol{k}} \psi^+_{\pm,\delta\boldsymbol{k}}(\boldsymbol{\sigma}(v\delta\boldsymbol{k}_\perp \pm \boldsymbol{A}^{\text{el}}_\perp) \mp (v_3\delta k_3 \pm A^{\text{el}}_3)\sigma_3)\psi_{\pm,\delta\boldsymbol{k}}. \tag{9}$$

Similarly to what happens in graphene or other two-dimensional systems, strain couples to electrons as a chiral vector field; i.e., it couples with opposite signs to the electronic excitations around the two Weyl nodes. The specific form of Eq. (8) is due to the choice of the vector $\mathbf{b}$ pointing along the OZ axis.

Hall viscosity.—As a physical consequence of the presence of the elastic gauge fields, we will next show that WSMs have an intrinsic Hall viscosity. In viscoelastic systems the viscosity tensor is defined as the transport coefficient relating the stress tensor τ_{ij} and the time derivative of the strain tensor u_{rs}, $\tau_{ij} = \eta_{ijrs}\dot{u}_{rs}$. The antisymmetric part of η_{ijrs} is a dissipationless coefficient allowed only when $\mathcal{T}$ is broken. In three dimensions rotational symmetry must also be broken to get a non-vanishing Hall viscosity. For axially symmetric systems with broken $\mathcal{T}$ there are two independent components of the Hall viscosity tensor that can be chosen: η_{3231} and η_{1112} [23]. The Hall viscosity was first defined as an intrinsic property of the quantum fluid. When a topologically nontrivial electronic fluid is coupled to the crystal environment it will induce a Hall viscosity term in the elastic free energy of phonons [31]. The electronic contribution to the field theory for the elastic degrees of freedom can be obtained by integrating out the electronic fields in Eq. (9). The effective action will contain the following term (in units of $\hbar = 1$):

$$\begin{aligned} \Gamma_H[u] &= \frac{1}{48\pi^2}\int d^4x \epsilon^{\mu\nu\rho\sigma}\lambda_\mu A^{\text{el}}_\nu \partial_\rho A^{\text{el}}_\sigma \\ &= \frac{\beta^2}{48\pi^2 a^3}\left(\frac{b_3^2-m^2}{t^2}\right)^{(3/2)}\int d^4x(u_{31}\dot{u}_{32} - u_{32}\dot{u}_{31}). \end{aligned} \tag{10}$$

From this expression, we can easily read the coefficient $\eta_H = \eta_{3231}$ of the Hall viscosity coming from the presence of the elastic gauge fields:

$$\eta_H = \frac{\beta^2}{24\pi^2}\frac{1}{a^3}\left(\frac{b_3^2-m^2}{t^2}\right)^{(3/2)}. \tag{11}$$

This is the second main result of this Letter: in the simple model considered, both $\mathcal{T}$ and rotational invariance are broken by the presence of the constant vector $\boldsymbol{b}$ giving rise to a Hall viscosity through the elastic vector fields. This response is rooted in the topological nature of the material and is universal in the sense that it is directly related to the Hall conductivity. For a general 3D Weyl semimetal breaking time reversal symmetry, the anomalous Hall effect is characterized by a momentum space vector called the Chern vector. In our model, this is the vector λ_μ separating the two Weyl nodes in momentum space. The anomalous Hall conductivity is given by the expression $\sigma_{ij} = (e^2/2\pi c)\epsilon_{ijk}\lambda_k$, coming from a 3D Chern-Simons term of the form

$$S_{\text{CS}} \sim \nu_H \int d^4x \lambda_i \epsilon^{ijkl} A_j \partial_k A_l, \tag{12}$$

where ν_H is the 3D Hall conductivity. It is easy to recognize the first term of Eq. (10) as the Chern-Simons term associated with the elastic gauge fields. As a rule, what we have shown is that any Hall system supporting elastic gauge fields will automatically present a Hall viscosity response.

Discussion.—As a proof of concept, we have shown that WSMs couple to elasticity through chiral vector fields by using a minimal tight-binding lattice model. This fact is not

tied to the breakdown of time reversal symmetry, although we have used a model where the Weyl points appear by breaking $\mathcal{T}$ (a system with broken time reversal symmetry has been reported in Ref. [15]). A necessary condition (albeit it might not be sufficient) for having such elastic gauge fields (technically, to have a vector representation of the elastic degrees of freedom at the Weyl point) is to have the Weyl points sitting at nonequivalent points of the Brillouin zone (which excludes the Γ point) [19]. The presence of Weyl points is compatible with $\mathcal{T}$ if the pair of Weyl nodes are related by inversion symmetry $\mathcal{I}$ [32]. This implies that these elastic gauge fields will appear in most of the $\mathcal{T}$-invariant systems displaying Weyl nodes, implying the generality of this phenomenon.

As a direct consequence of this chiral vector coupling between elasticity and the electronic degrees of freedom, a new type of Hall viscosity arises in WSMs. In three dimensions the Hall viscosity has been discussed in the literature associated with two instances only: the topological insulator phase with $\mathcal{T}$ broken and a WSM system in the presence of torsion [30,33]. The elastic gauge fields coupled to a topologically nontrivial system defines a third mechanism that will act on topologically nontrivial crystals supporting elastic vector fields.

Several aspects of the viscoelastic response of lattice topological crystals have been recently analyzed in Ref. [30]. Our new contribution to the Hall viscosity, although not explicitly discussed, could certainly have been worked out as a part of the authors' general analysis. The examples chosen there having the Weyl nodes at the γ point prevented them from finding the elastic gauge fields. The coupling giving rise to the Hall viscosity in that reference is linear in momentum and corresponds to the standard phonon viscosity found in the hydrodynamic approach [24]. In contrast, the elastic gauge field term described in our work couples directly to the fermionic current and is of lowest order in a derivative expansion.

Another important aspect of the present analysis arises in the connection of the new term with the chiral anomaly. As we discussed, the elastic vector fields are chiral in the sense that they couple with opposite signs to the two chiralities. Moreover, the field λ_μ is also an axial field, which implies that the coefficient in Eq. (10) is associated with the triangular graph with three axial vertices (AAA). This triangular graph has an additional symmetry factor of $1/3$ compared to the usual one (one axial and two vector vertices AVV). We would like to emphasize that this gives rise to the exciting possibility to test the AAA anomaly in a condensed matter context. In contrast it is generally believed that this type of anomaly does not lead to physical consequences in high energy physics [34].

The existence of elastic gauge fields in WSMs extends the field of straintronics to three-dimensional materials and paves the path for the study of a plethora of emergent phenomena. Notice that Weyl points are not an exclusive property of the dispersion relation of electronic systems. They have also been described in three-dimensional photonic systems [35,36], which allows us to envisage the extension of straintronics to photonic media by controlling the Weyl nodes with deformations through these elastic gauge fields.

We thank Carlos Hoyos for enlightening discussions on the Hall viscosity and Juan Mañes for comments on the elastic gauge fields. Special thanks go also to José Silva-Guillén for help with the figures. This research was supported in part by Spanish MECD Grants No. FIS2011-23713 and No. PIB2010BZ-00512, by the European Union structural funds and the Comunidad de Madrid MAD2D-CM Program (S2013/MIT-3007), by the National Science Foundation under Grant No. NSF PHY11-25915, and by the European Union Seventh Framework Programme under Grant Agreement No. 604391 Graphene Flagship, FPA2012-32828, and by the Centro de Excelencia Severo Ochoa Programme under Grant No. SEV-2012-0249.

[1] G. E. Volovik, *The Universe in a Helium Droplet* (Clarendon Press, Oxford, 2003).
[2] T. Giamarchi, *Quantum Physics in One Dimension* (University Press, Oxford, 2004).
[3] A. H. Castro Neto, F. Guinea, N. M. R. Peres, K. S. Novoselov, and A. K. Geim, The electronic properties of graphene, Rev. Mod. Phys. **81**, 109 (2009).
[4] X. Qi and S. Zhang, Topological insulators and superconductors, Rev. Mod. Phys. **83**, 1057 (2011).
[5] S. L. Adler, Axial-vector vertex in spinor electrodynamics, Phys. Rev. **177**, 2426 (1969).
[6] J. S. Bell and R. Jackiw, A pcac puzzle: $\pi_0 \to \gamma\gamma$ in the σ model, Nuovo Cimento A **60**, 47 (1969).
[7] H. B. Nielsen and M. Ninomiya, Absence of neutrinos on a lattice: (i). Proof by homotopy theory, Nucl. Phys. **185B**, 20 (1981).
[8] A. G. Grushin, Consequences of a condensed matter realization of Lorentz-violating QED in Weyl semi-metals, Phys. Rev. D **86**, 045001 (2012).
[9] P. Goswami and S. Tewari, Axionic field theory of $(3+1)$-dimensional Weyl semimetals, Phys. Rev. B **88**, 245107 (2013).
[10] Z. K. Liu *et al.*, A stable three-dimensional topological Dirac semimetal cd_3as_2, Nat. Mater. **13**, 677 (2014).
[11] S.-M. Huang *et al.*, A Weyl fermion semimetal with surface Fermi arcs in the transition metal monopnictide TaAs class, Nat. Commun. **6**, 7373 (2015).
[12] S.-Y. Xu *et al.*, Discovery of a Weyl fermion semimetal and topological Fermi arcs, Science **349**, 613 (2015).
[13] S.-Y. Xu *et al.*, Discovery of a Weyl fermion state with Fermi arcs in niobium arsenide, Nat. Phys., **11**, 748 (2015).
[14] S. M. Huang *et al.*, A new type of Weyl semimetal with quadratic double Weyl fermions in Sr Si2, arXiv:1502.05868.

[15] S. Borisenko *et al.*, Time-reversal symmetry breaking Weyl state in Yb Mn Bi_2, arXiv:1507.04847.
[16] H. Johnston, Weyl fermions are spotted at long last, Phys. World (2015).
[17] M. A. H. Vozmediano, M. I. Katsnelson, and F. Guinea, Gauge fields in graphene, Phys. Rep. **496**, 109 (2010).
[18] H. Suzuura and T. Ando, Phonons and electron-phonon scattering in carbon nanotubes, Phys. Rev. B **65**, 235412 (2002).
[19] J. L. Mañes, Symmetry-based approach to electron-phonon interactions in graphene, Phys. Rev. B **76**, 045430 (2007).
[20] J. L. Mañes, F. de Juan, M. Sturla, and M. A. H. Vozmediano, Generalized effective Hamiltonian for graphene under nonuniform strain, Phys. Rev. B **88**, 155405 (2013).
[21] F. Guinea, M. I. Katsnelson, and A. G. Geim, Energy gaps, topological insulator state and zero-field quantum Hall effect in graphene by engineering, Nat. Phys. **6**, 30 (2010).
[22] N. Levy, S. A. Burke, K. L. Meaker, M. Panlasigui, A. Zettl, F. Guinea, A. H. C. Neto, and M. F. Crommie, Strain-induced pseudomagnetic fields greater than 300 tesla in graphene nanobubbles, Science **329**, 544 (2010).
[23] J. E. Avron, R. Seiler, and P. G. Zograf, Viscosity of Quantum Hall fluids, Phys. Rev. Lett. **75**, 697 (1995).
[24] I. V. Tokatly and G. Vignale, Lorentz shear modulus of a two-dimensional electron gas at high magnetic field, Phys. Rev. B **76**, 161305 (2007).
[25] N. Read, Non-Abelian adiabatic statistics and Hall viscosity in quantum Hall states and $p_x + ip_y$ paired superfluids, Phys. Rev. B **79**, 045308 (2009).
[26] T. L. Hughes, R. G. Leigh, and E. Fradkin, Torsional Response and Dissipationless Viscosity in Topological Insulators, Phys. Rev. Lett. **107**, 075502 (2011).
[27] B. Bradlyn, M. Goldstein, and N. Read, Kubo formulas for viscosity: Hall viscosity, ward identities, and the relation with conductivity, Phys. Rev. B **86**, 245309 (2012).
[28] C. Hoyos and D. T. Son, Hall Viscosity and Electromagnetic Response, Phys. Rev. Lett. **108**, 066805 (2012).
[29] M. M. Vazifeh and M. Franz, Electromagnetic Response of Weyl Semimetals, Phys. Rev. Lett. **111**, 027201 (2013).
[30] H. Shapourian, T. L. Hughes, and S. Ryu, The viscoelastic response of topological tight-binding models in 2d and 3d, arXiv:1505.03868.
[31] M. Barkeshli, S. B. Chung, and X. L. Qi, Dissipationless phonon Hall viscosity, Phys. Rev. B **85**, 245107 (2012).
[32] J. L. Mañes, Existence of bulk chiral fermions and crystal symmetry, Phys. Rev. B **85**, 155118 (2012).
[33] L. Sun and S. Wan, Chiral viscoelastic response in Weyl semimetals, Eur. Phys. Lett. **108**, 37007 (2014).
[34] M. D. Schwartz, *Quantum Field Theory and the Standard Model* (Cambridge University Press, Cambridge, England, 2013).
[35] L. Lu, L. Fu, J. D. Joannopoulos, and M. Soljacic, Weyl points and line nodes in gyroid photonic crystals, Nat. Photonics **7**, 294 (2013).
[36] L. Lu, Z. Wang, D. Ye, L. Ran, L. Fu, J. D. Joannopoulos, and M. Soljačić, Experimental observation of Weyl points, Science **349**, 622 (2015).

Article E

Unconventional electromagnetic mode in neutral Weyl semimetals

PHYSICAL REVIEW B **93**, 195154 (2016)

Unconventional electromagnetic mode in neutral Weyl semimetals

Yago Ferreiros* and Alberto Cortijo†
Instituto de Ciencia de Materiales de Madrid, CSIC, Cantoblanco, 28049 Madrid, Spain
(Received 4 August 2015; revised manuscript received 4 May 2016; published 25 May 2016)

We study light propagation in a neutral Weyl semimetal with the Fermi level lying at the Weyl nodes in the weak self-interacting regime. The nontrivial topology induces a screening effect in one of the two transverse gauge fields, for which we find two branches of attenuated collective excitations. In addition to the known topologically gapped photon mode, a different massless and slightly damped excitation appears. Strikingly, at low energies, this excitation has a linear dispersion and it propagates with the same velocity as the electrons, while at energies well above the electron-hole continuum threshold it behaves as a massive attenuated photon with velocity similar to the speed of light in the material. There is a crossover at a certain momentum in the direction perpendicular to the separation of the Weyl nodes above which this gapless mode enters into an overdamped regime. Regarding the unscreened gauge field, we show that it is also attenuated, which is a nontopological property shared by Dirac semimetals as well.

DOI: 10.1103/PhysRevB.93.195154

I. INTRODUCTION

Weyl semimetals (WSMs) are three-dimensional topological electronic systems whose low-energy band structure is described by pairs of Weyl fermions separated in momentum space. They were first proposed to occur in a class of iridate materials [1], but it was only recently that they were experimentally realized [2–6]. The topological properties of WSMs are encoded in a Chern-Simons (CS) term that stems from the axial anomaly. The anomaly is responsible for a plethora of phenomena such as the axial magnetic effect [7–9], chiral separation effect [10], chiral magnetic waves [11], and, more recently, a new mechanism for the phonon Hall viscosity [12].

The experimental evidence of the WSM phase is based on angle-resolved photoemission spectroscopy (ARPES) and transport experiments [2,3], and on optical conductivity experiments [6] (optical measurements have been done in Dirac semimetals as well [13,14]). The CS term induces birefringence [15,16] and circular dichroism [17]. It has been also proposed that chiral electromagnetic waves exist and propagate along domain walls in magnetic WSMs [18]. The interaction of light with magnons in WSMs has been addressed in Ref. [19], while plasmons in Weyl metals have also been studied [20–22]. More recently, a new type of helicon mode under applied magnetic fields has been proposed [23] at finite doping. Here, we address the problem of light propagation in a WSM at the neutrality point (i.e., the Fermi level lies at the Weyl nodes) by computing the poles of the full photon propagator. A similar approach was done for quantum electrodynamics (QED) under an external magnetic field [24]. For the case of the solid-state-realized WSM there are two key aspects that are central: (1) Nontrivial topology is present even in the absence of an external magnetic field and (2) contrary to QED, there are two velocity scales in WSMs: the Fermi velocity of the electrons and the velocity of light in the material. We will see how these two features combine so that different collective excitation behavior is realized. We will resort to a random phase approximation (RPA) treatment of the problem. This implies that we will effectively consider non-self-interacting Weyl fermions interacting with an external electromagnetic field. The validity of a RPA treatment has been extensively studied in the literature for two-dimensional (2D) Dirac materials [25] and more recently in the general case of interacting three-dimensional (3D) Dirac systems [26,27]. Following these references, some of the results presented here might be extended to the self-interacting case under particular conditions ($1/N$ expansions and so on).

The rest of the paper is structured as follows. In Sec. II we describe the model for WSM that we use and set notations. In Sec. III, we give the necessary details for the computation of the polarization function and explain it. In Sec. IV, we compute the spectrum of the electromagnetic collective modes through the spectral function, and describe the most salient features observed. In Sec. V, we discuss the results and mention some future lines to follow from this work.

II. THE MODEL

Our starting point is the low-energy action of a WSM coupled to an electromagnetic field,

$$S = \int d^4x \overline{\Psi}\Big[i\gamma^0(\partial_0 + ieA_0) - iv\gamma^i\left(\partial_i + \frac{ie}{c}A_i\right) + b_i\gamma^i\gamma^5\Big]\Psi, \tag{1}$$

where v is the Fermi velocity and c is the speed of light in the corresponding material. This action describes two Weyl fermions separated in momentum space by a vector $2\boldsymbol{b}/v$ so that time-reversal symmetry is broken. Without loss of generality, we will fix $\boldsymbol{b} = b\hat{x}_3$. Quantum corrections to (1) are well known to generate a nonzero odd part of the polarization function of the photon in the form of a CS term [28–32]. The coefficient accompanying the CS term is ill defined, as it depends on the routing of internal momenta in the loop integrals as well as on the regularization method. In a solid-state realization of a WSM this coefficient can be fixed

*yago.ferreiros@csic.es
†alberto.cortijo@csic.es

by means of the bulk-boundary correspondence relating the theory in the bulk with the Fermi arcs at the edges [33,34]. Another way is by considering the 3D band structure of a WSM as a set of independent 2D band structures, each of them with a well-defined Chern number [16,35,36].

In addition to the action for the fermionic sector (1), the action for the electromagnetic field is

$$S = \int d^4x \frac{1}{2}\left(\epsilon |\boldsymbol{E}|^2 - \frac{|\boldsymbol{B}|^2}{\mu}\right), \tag{2}$$

where $\epsilon = \epsilon_0\epsilon_r$ and $\mu = \mu_0\mu_r$ are the dielectric permittivity and magnetic permeability of the material, respectively. The electric and magnetic fields are related to the gauge field A_μ as

$$E_i = \frac{1}{c}\partial_0 A_i - \partial_i A_0, \quad B_i = \frac{1}{c}\epsilon_{ijk}\partial^j A^k. \tag{3}$$

III. POLARIZATION FUNCTION

In what follows, we will obtain the 1-loop order polarization function in terms of A_μ. The computation has been performed and deeply examined by several authors, both the parity-even [37–40] and parity-odd [28–32] parts of the polarization function. We can write it as

$$\Pi^{\mu\nu} = \Pi_0^{\mu\nu} + \Pi_b^{\mu\nu}, \tag{4}$$

where $\Pi_0^{\mu\nu}$ is the contribution at zero order in b, and $\Pi_b^{\mu\nu}$ is the first-order correction. In Ref. [37] it was shown that the polarization function is analytic in b, and the correction to the even part is second order in b, which breaks gauge invariance and gives a mass to the photon. Imposing gauge invariance by using a regularization which preserves it, as dimensional or Pauli-Villars regularizations, one obtains a zero correction [37,40]. Regarding the odd part, it is known to be linear in b [29,32] and no corrections appear beyond the first order. Hence, Eq. (4) is exact, i.e., there are no higher-order corrections in b.

The computation of $\Pi_0^{\mu\nu}$ is standard. Using dimensional regularization and in the minimal subtraction renormalization scheme,

$$\Pi_0^{\mu\nu} = \frac{e^2}{4\pi v^3}\left(\frac{v}{c}\right)^{2-\delta_{\mu 0}-\delta_{\nu 0}} \Pi\left(p^2/\mu_0^2\right)\left(p^2\eta^{\mu\nu} - p^\mu p^\nu\right), \tag{5}$$

$$\Pi\left(p^2/\mu_0^2\right) = \frac{1}{9\pi}\left[3\log\left(-p^2/\mu_0^2\right) - 5\right], \tag{6}$$

where the four-momentum is $p_\mu = (\omega, v\boldsymbol{p})$, and where the space components of $\Pi_0^{\mu\nu}$ have a relative weight v/c with respect to the time components, as can be read from Eq. (1). From now on we will redefine $\boldsymbol{p}$ as $v\boldsymbol{p} \to \boldsymbol{p}$ so that $p^2 = \omega^2 - |\boldsymbol{p}|^2$. The parameter μ_0 is an energy scale that appears in the process of dimensional regularization (see, for example, Ref. [41]). The appearance of this parameter reflects the formal absence of any characteristic scale in the linear electronic spectrum. It could be fixed by either the experiment or by invoking a standard renormalization program (here we are dealing with a modification of standard quantum electrodynamics that is well known to be renormalizable) or related to the lattice cutoff of the underlying band structure by considering a full lattice model of the Weyl semimetal, keeping in mind that there are several materials with very different lattice structures proposed to be Weyl semimetals. For typical values of lattice spacings of the order of angstroms, μ_0 can be estimated to be $\mu_0 \sim 10$ eV, however, the reader should keep in mind that the low-energy/long-wavelength aspects of the results presented here do not depend on the particular value of μ_0 as long as all the frequencies and momenta involved in the problem are presented in a *dimensionless* fashion (that is, divided by μ_0) no matter which regularization scheme is used.

Note that the function $\Pi(p^2/\mu_0^2)$ in Eq. (6) has a constant imaginary part for $p^2 > 0$ which defines the electron-hole continuum threshold. A normal procedure would be to take the local limit $\omega/|\boldsymbol{p}| \gg 1$ in $\Pi_0^{\mu\nu}$. As we know for graphene, at the neutrality point and zero temperature no well-defined plasmon mode exists within the random phase approximation (RPA). However, it was shown that a plasmon pole appears beyond RPA when the momentum dependence in the polarization tensor is maintained [42], which highlights the importance of not considering the local limit in some circumstances. Here, we will limit ourselves to the RPA approximation but we will keep the momentum dependence, and we will see that staying away from the local limit is crucial for capturing the physics near the electron-hole continuum threshold.

$\Pi_b^{\mu\nu}$ is precisely the CS term. We invoke the boundary-bulk correspondence to fix its value [33,34]. On the $A_0 = 0$ gauge, $\Pi_b^{\mu\nu}$ has only one independent component:

$$\Pi_b^{12} = -\Pi_b^{21} = i\frac{e^2 b}{2\pi^2 c^2 v}\omega. \tag{7}$$

The presence of this nondiagonal term in the polarization tensor induces gyrotropy in the WSM, so that left- and right-handed polarized light propagates at different speeds [15–17].

Since we are working under the free electron approximation, Eq. (7) is exact. In an interacting theory, Π_b^{12} acquires dynamically generated corrections (see Ref. [43] for an explicit discussion when interactions at constant external magnetic field and finite densities are considered, or Ref. [44] for corrections in the strong coupling regime).

IV. COLLECTIVE MODES

The inverse full photon propagator can be written as

$$(\Delta^{\mu\nu})^{-1} = \left(\Delta_{\text{free}}^{\mu\nu}\right)^{-1} - \Pi_0^{\mu\nu} - \Pi_b^{\mu\nu}, \tag{8}$$

where the inverse free propagator can be obtained from Eqs. (2) and (3). To obtain the collective excitations we look for the poles of the full propagator. The equation $\det[(\Delta^{\mu\nu})^{-1}] = 0$ on the $A_0 = 0$ gauge reads

$$\begin{aligned}&\left[1 - g\Pi\left(p^2/\mu_0^2\right)\right]\omega^2\left[1 - g\Pi\left(p^2/\mu_0^2\right)\right]\\ &\times\left[\omega^2 - \beta\Gamma\left(p^2/\mu_0^2\right)|\boldsymbol{p}|^2\right]\Bigg[\left[1 - g\Pi\left(p^2/\mu_0^2\right)\right]\\ &\times\left[\omega^2 - \beta\Gamma\left(p^2/\mu_0^2\right)|\boldsymbol{p}|^2\right] - J\left(\frac{\omega^2}{\mu_0^2}, \frac{|\boldsymbol{p}_\perp|^2}{\mu_0^2}, \frac{p_3^2}{\mu_0^2}\right)\Bigg] = 0,\end{aligned} \tag{9}$$

where $|\boldsymbol{p}_\perp|^2 = p_1^2 + p_2^2$ represents the momentum in the plane perpendicular to $\boldsymbol{b}$, $g = e^2/(4\pi v\epsilon_0\epsilon_r)$ is the fine structure

constant, $\beta = c^2/v^2$ gives the squared ratio between the speed of light and the Fermi velocity, and

$$\Gamma\left(p^2/\mu_0^2\right) = \frac{1 - \frac{g}{\beta}\Pi\left(p^2/\mu_0^2\right)}{1 - g\Pi\left(p^2/\mu_0^2\right)}, \tag{10}$$

$$J(x,y,z) = \frac{4g^2}{\pi^2}\frac{b^2}{1 - g\Pi(x-y-z)} \times \frac{x - \beta\Gamma(x-y-z)y}{x - \beta\Gamma(x-y-z)(y+z)}. \tag{11}$$

We will take the Fermi velocity of the WSM similar to that of graphene ($v = 10^6$ m/s) and assume a coupling constant $g = 1$, which is reached with a relative permittivity of the material of $\epsilon_r \approx 2.3$. The speed of light of the WSM is given by $c = c_{\text{vacuum}}/\sqrt{\epsilon_r}$ (assuming a relative permeability $\mu_r = 1$) and the value of the squared ratio between the speed of light and the Fermi velocity is $\beta \approx 3.9 \times 10^4$. Since we are not taking into account interactions between Weyl electrons, a value of the effective coupling $g = 1$ is not problematic, and this precise value has been chosen for convenience. In realistic solid-state WSM, however, it is not expected to have these values for v_F and/or larger values of ϵ_r, resulting effectively in a smaller value of g.

There is a zero mode $\omega^2 = 0$ corresponding to the unphysical longitudinal gauge field, arising from the residual gauge freedom, as $A_0 = 0$ does not completely fix the gauge. For the remaining part, there are two physical transverse gauge fields. The dispersion relation of the unscreened field can be obtained from

$$\left[1 - g\Pi\left(p^2/\mu_0^2\right)\right]\left[\omega^2 - \beta\Gamma\left(p^2/\mu_0^2\right)|\boldsymbol{p}|^2\right] = 0. \tag{12}$$

Instead of directly solving the equation, we will define a spectral function for this field:

$$\rho = -2\,\mathrm{Im}\left[\frac{\mu_0^2}{\left[1 - g\Pi\left(p^2/\mu_0^2\right)\right]\left[\omega^2 - \beta\Gamma\left(p^2/\mu_0^2\right)|\boldsymbol{p}|^2\right]}\right]. \tag{13}$$

The spectral function is plotted in Fig. 1(a). We see that there is a peak with finite width, which corresponds to a damped mode, so that the delta function corresponding to a free photon is replaced in a WSM by an attenuated excitation. Hence our first finding is that light is attenuated when propagating through a WSM. This behavior is rooted to the existence of two different velocity scales: The value of the Fermi velocity is much smaller than the speed of light. This mismatch is encoded in the function Γ appearing in Eq. (12), which fulfills $\lim_{\beta\to 1}\Gamma = 1$. This means that in the limit where the value of the Fermi velocity matches the value of the speed of light in the material, we have a nonattenuated free photon traveling at the speed of light with dispersion relation $\omega = |\boldsymbol{p}|$. Although the gapless nature of WSMs means that there is no gap to overcome for electron-hole pair creation, we just showed that this is not enough for light attenuation, and that damping is generated for a system of gapless electrons only when there exist two nonequal competing velocity scales. This happens also in Dirac semimetals since this property is not related to the CS term.

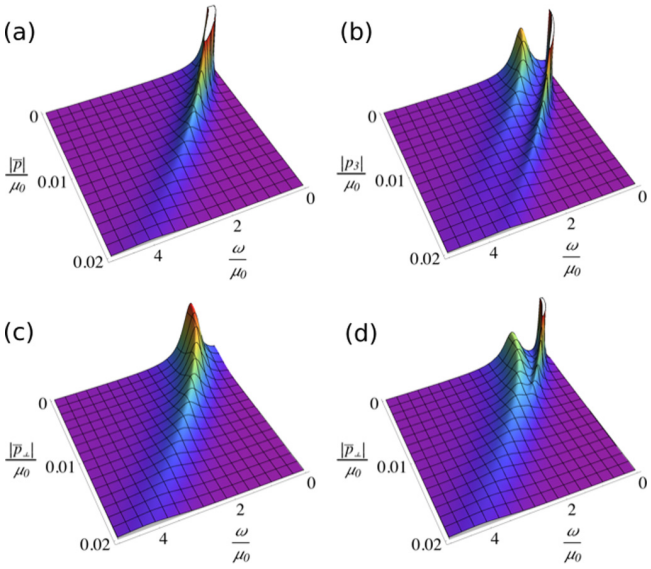

FIG. 1. (a) Spectral function ρ for the unscreened gauge field as a function of the frequency ω and momentum $|\boldsymbol{p}|$ in units of μ_0. (b) Spectral function ρ for the screened gauge field as a function of ω and $|p_3|$ in units of μ_0, for zero transverse momentum $|\boldsymbol{p}_\perp| = 0$. (c), (d) Spectral function ρ for the screened gauge field as a function of the frequency ω and the transverse momentum $|\boldsymbol{p}_\perp|$ in units of μ_0, for (c) $|p_3| = 0$ and (d) $|p_3|/\mu_0 = 3 \times 10^{-3}$. All plots for the screened gauge field are presented for $b^2/\mu_0^2 = 3$.

The nontrivial topology of the WSM phase shows up inducing a screening in the other transverse gauge field. The dispersion relation can be obtained from the second line of Eq. (9). Instead of solving the equation, we will again introduce a spectral function for this field:

$$\rho = -2\,\mathrm{Im}\left[\mu_0^2\left\{\left[1 - g\Pi\left(p^2/\mu_0^2\right)\right]\left[\omega^2 - \beta\Gamma\left(p^2/\mu_0^2\right)|\boldsymbol{p}|^2\right] - J\left(\frac{\omega^2}{\mu_0^2}, \frac{|\boldsymbol{p}_\perp|^2}{\mu_0^2}, \frac{p_3^2}{\mu_0^2}\right)\right\}^{-1}\right]. \tag{14}$$

In the following analysis we will consider two separate cases: $\boldsymbol{p}_\perp = 0$ and $\boldsymbol{p}_\perp \neq 0$.

(i) $\boldsymbol{p}_\perp = 0$. In Fig. 1(b) the spectral function is plotted as a function of ω and the momentum $|p_3|$ in the direction of $\boldsymbol{b}$. Two branches of attenuated collective excitations coexist, one of them clearly gapped. The gapped nature of the screened field is expected in WSMs, as the CS term acts as a topological mass for the photon [15]. However, we see that the second branch corresponds to a different excitation which seems to be gapless and considerably less attenuated than its gapped companion. In fact, at a certain large momentum p_3 there is a crossover where the gapped excitation enters into an overdamped regime, as can be seen from the absence of a well-defined peak in Fig. 1(b). To highlight the behavior of this gapless excitation at low frequencies near the electron-hole continuum threshold $\omega = |\boldsymbol{p}|$, we plot in Fig. 2(a) the spectral function as a function of the frequency in a logarithmic scale, for different values of p_3. We see that there is a low-energy crossover also for the excitation from an underdamped to an overdamped regime as the wavelength increases. Overdamping appears for

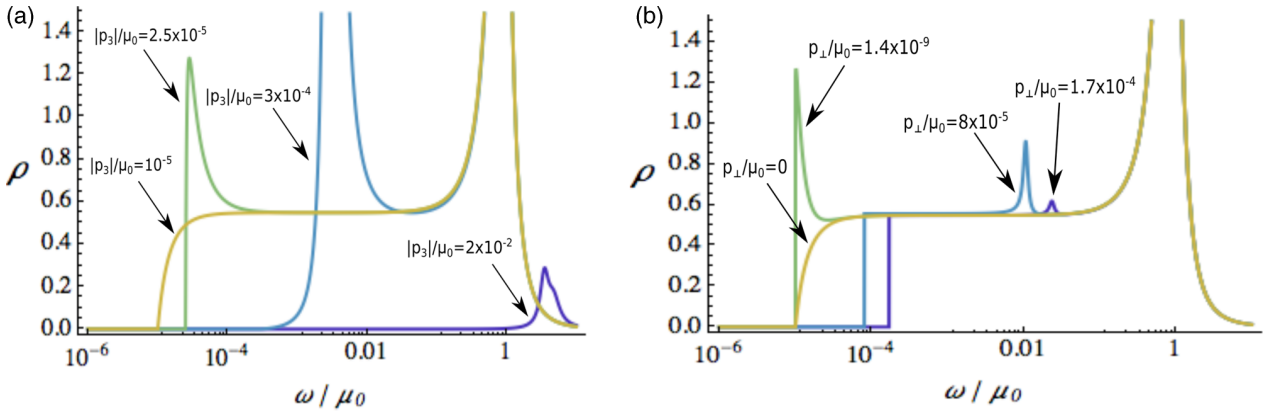

FIG. 2. Both plots are presented for a value $b^2/\mu_0^2 = 3$ and in a logarithmic scale for the horizontal axis. (a) Spectral function ρ for the screened gauge field as a function of the frequency ω in units of μ_0 for $\boldsymbol{p}_\perp = 0$ and different values of $|p_3|$. (b) Spectral function ρ for the screened gauge field as a function of the frequency ω in units of μ_0 for $p_3 = 0$ and different values of $|\boldsymbol{p}_\perp|$.

frequencies near the electron-hole continuum threshold. This suggests a gapless nature of this excitation with a dispersion relation $\omega \sim |\boldsymbol{p}|$ at low energies. We see also that by increasing the momentum p_3, the gapless branch deviates from the linear dispersion behavior and approaches the gapped one. From Fig. 1(b) it is clear that the gapless branch starts to behave as a massive excitation for large enough momentum p_3.

(ii) $\boldsymbol{p}_\perp \neq 0$. Figures 1(c) and 1(d) show the spectral function as a function of ω and $|\boldsymbol{p}_\perp|$ for the values $p_3 = 0$ and $|p_3|/\mu_0 = 3 \times 10^{-3}$, respectively. It can be seen that increasing the perpendicular momentum produces a merging of the two branches into a single peak. This is a result of a second, high-energy crossover for the gapless excitation which again becomes overdamped, but now at big enough $\boldsymbol{p}_\perp$. For energies near the electron-hole continuum threshold, we can see in Fig. 2(b) that small fluctuations in $\boldsymbol{p}_\perp$ drive the gapless excitation across the low-energy crossover from the overdamped to the underdamped regime, so in a realistic situation when the propagation is not perfectly aligned with the $\boldsymbol{b}$ direction, the gapless branch behaves as a well-defined attenuated excitation at low energies.

It is important to note that the behavior near the electron-hole continuum would have not been captured in the local limit $\omega/|\boldsymbol{p}| \gg 1$ of the polarization function. In particular, the low-energy crossover into the overdamped regime of the massless branch would have not been captured without considering the full momentum dependence.

V. DISCUSSION AND CONCLUSIONS

We have studied light propagation in a neutral WSM where the Fermi level lies at the Weyl nodes. In this situation there are two degrees of freedom corresponding to two transverse gauge fields, while the plasmon longitudinal mode that appears at the finite chemical potential is absent. Besides the generation of a plasmon mode, the presence of a plasma frequency would also induce a gap to both transverse gauge fields, however, at the neutrality point there is only one gapped mode, whose mass is a consequence of the nontrivial topology.

Our first finding is that light is attenuated when propagating through both Weyl and Dirac semimetals. In the case of WSMs, nontrivial topology shows up as a screening effect in one of the two transverse gauge fields, for which we find two branches of attenuated collective excitations. In addition to the known topologically gapped photon mode, a massless attenuated excitation appears, which is our second and most important finding. This splitting of a transverse field into two branches was obtained before for QED in the presence of an external magnetic field [24], where the cyclotron frequency defines the mass threshold for the electron-hole continuum. In the case of a WSM there is no mass threshold as nontrivial topology is present in the absence of magnetic fields. Furthermore, for the case of the solid-state-realized WSM, the Fermi velocity of the electrons is much smaller than the speed of light, which translates into a completely different collective behavior of the two branches.

In particular, we find that in a realistic situation of light collimated along the direction of $\boldsymbol{b}$ but with small deviations in the perpendicular direction, the massless branch shows up as a well-defined and damped peak in the spectral function. At low energies its dispersion relation is given by $\omega \simeq v|\boldsymbol{p}|$, which defines an excitation traveling coherently with the electrons at the Fermi velocity. At the other limit of the spectrum ($\omega \gg v|\boldsymbol{p}|$) the gapless branch behaves as a massive damped photon with velocity close to the speed of light. In the situation where light propagation is not aligned with $\boldsymbol{b}$ and the momentum in the transverse direction is large enough, a crossover exists and the massless branch enters into an overdamped regime, corresponding to a peak with divergent width in the spectral function.

This optical excitation could provide a clean signature for WSMs. It could be detected in experiments as an additional resonance on the transmission coefficient of light. There are also indirect proofs, such as electron energy-loss spectroscopy (EELS) or subluminal Cherenkov radiation spectroscopy [45] stemming from the small phase velocity of this excitation. In addition, due to the matching of the propagation velocity of this mode with the Fermi velocity of the electrons, a counterintuitive enhancement of the effective dressed electron-photon interaction is expected. This is qualitatively different from the effect of the Coulomb interaction enhancement due to the renormalization of the Fermi velocity that appears,

for instance, in graphene [46]. It should be noted that, although their effect is negligible on the bulk propagation of light, the one-dimensional (1D) Fermi arc chiral states at the edges of a WSM would give additional resonances as surface electromagnetic modes. However, the polarization tensor of 1D chiral electrons has already been computed in the literature [47,48] and therefore the Fermi arc contribution can be distinguished from bulk propagation.

ACKNOWLEDGMENTS

We thank M. A. H. Vozmediano for enlightening discussions and encouragement. This research is partially supported by the Spanish MECD Grant No. FIS2011-23713, the European Union structural funds and the Comunidad de Madrid MAD2D-CM Program (S2013/MIT-3007), and by the European Union Seventh Framework Programme under Grant Agreement No. 604391 Graphene Flagship.

[1] X. Wan, A. M. Turner, A. Vishwanath, and S. Y. Savrasov, Phys. Rev. B **83**, 205101 (2011).
[2] S.-Y. Xu, I. Belopolski, N. Alidoust, M. Neupane, G. Bian, C. Zhang, R. Sankar, G. Chang, Z. Yuan, C.-C. Lee *et al.*, Science **349**, 613 (2015).
[3] B. Q. Lv, H. M. Weng, B. B. Fu, X. P. Wang, H. Miao, J. Ma, P. Richard, X. C. Huang, L. X. Zhao, G. F. Chen *et al.*, Phys. Rev. X **5**, 031013 (2015).
[4] J. Y. Liu, J. Hu, D. Graf, S. M. A. Radmanesh, D. J. Adams, Y. L. Zhu, G. F. Chen, X. Liu, J. Wei, I. Chiorescu *et al.*, arXiv:1507.07978.
[5] C. Shekhar, F. Arnold, S.-C. Wu, Y. Sun, M. Schmidt, N. Kumar, A. G. Grushin, J. H. Bardarson, R. Donizeth dos Reis, M. Naumann *et al.*, Nat. Commun. **7**, 11615 (2016).
[6] B. Xu, Y. M. Dai, L. X. Zhao, K. Wang, R. Yang, W. Zhang, J. Y. Liu, H. Xiao, G. F. Chen, A. J. Taylor *et al.*, Phys. Rev. B **93**, 121110 (2016).
[7] K. Fukushima, D. E. Kharzeev, and H. J. Warringa, Phys. Rev. D **78**, 074033 (2008).
[8] A. A. Zyuzin and A. A. Burkov, Phys. Rev. B **86**, 115133 (2012).
[9] M. N. Chernodub, A. Cortijo, A. G. Grushin, K. Landsteiner, and M. A. H. Vozmediano, Phys. Rev. B **89**, 081407 (2014).
[10] D. T. Son and A. R. Zhitnitsky, Phys. Rev. D **70**, 074018 (2004).
[11] D. E. Kharzeev and H.-U. Yee, Phys. Rev. D **83**, 085007 (2011).
[12] A. Cortijo, Y. Ferreirós, K. Landsteiner, and M. A. H. Vozmediano, Phys. Rev. Lett. **115**, 177202 (2015).
[13] J. Xiong, S. Kushwaha, J. Krizan, T. Liang, R. J. Cava, and N. P. Ong, arXiv:1502.06266.
[14] C. Zhang, E. Zhang, Y. Liu, Z.-G. Chen, S. Liang, J. Cao, X. Yuan, L. Tang, Q. Li, T. Gu *et al.*, arXiv:1504.07698.
[15] S. M. Carroll, G. B. Field, and R. Jackiw, Phys. Rev. D **41**, 1231 (1990).
[16] A. G. Grushin, Phys. Rev. D **86**, 045001 (2012).
[17] P. Hosur and X.-L. Qi, Phys. Rev. B **91**, 081106 (2015).
[18] A. A. Zyuzin and V. A. Zyuzin, Phys. Rev. B **92**, 115310 (2015).
[19] J. A. Hutasoit, J. Zang, R. Roiban, and C.-X. Liu, Phys. Rev. B **90**, 134409 (2014).
[20] L.-V. Min and S.-C. Zhang, Int. J. Mod. Phys. B **27**, 1350177 (2013).
[21] I. Panfilov, A. A. Burkov, and D. A. Pesin, Phys. Rev. B **89**, 245103 (2014).
[22] J. Zhou, H.-R. Chang, and D. Xiao, Phys. Rev. B **91**, 035114 (2015).
[23] F. M. D. Pellegrino, M. I. Katsnelson, and M. Polini, Phys. Rev. B **92**, 201407 (2015).
[24] K. Fukushima, Phys. Rev. D **83**, 111501 (2011).
[25] V. N. Kotov, B. Uchoa, V. M. Pereira, F. Guinea, and A. H. Castro Neto, Rev. Mod. Phys. **84**, 1067 (2012).
[26] J. Hofmann, E. Barnes, and S. Das Sarma, Phys. Rev. B **92**, 045104 (2015).
[27] R. E. Throckmorton, J. Hofmann, E. Barnes, and S. Das Sarma, Phys. Rev. B **92**, 115101 (2015).
[28] R. Jackiw and V. A. Kostelecký, Phys. Rev. Lett. **82**, 3572 (1999).
[29] M. Pérez-Victoria, Phys. Rev. Lett. **83**, 2518 (1999).
[30] J.-M. Chung and P. Oh, Phys. Rev. D **60**, 067702 (1999).
[31] A. A. Andrianov, P. Giacconi, and R. Soldati, J. High Energy Phys. 02 (2002) 030.
[32] J.-M. Chung, Phys. Rev. D **60**, 127901 (1999).
[33] P. Goswami and S. Tewari, Phys. Rev. B **88**, 245107 (2013).
[34] S. T. Ramamurthy and T. L. Hughes, Phys. Rev. B **92**, 085105 (2015).
[35] A. A. Burkov and L. Balents, Phys. Rev. Lett. **107**, 127205 (2011).
[36] K.-Y. Yang, Y.-M. Lu, and Y. Ran, Phys. Rev. B **84**, 075129 (2011).
[37] B. Altschul, Phys. Rev. D **69**, 125009 (2004).
[38] B. Altschul, Phys. Rev. D **73**, 036005 (2006).
[39] G. Bonneau, L. Costa, and J. Tomazelli, Int. J. Theor. Phys. **47**, 1764 (2008).
[40] B. Altschul, Phys. Rev. D **70**, 101701 (2004).
[41] M. Srednicki, *Quantum Field Theory* (Cambridge University Press, Cambridge, U.K., 2007).
[42] S. Gangadharaiah, A. M. Farid, and E. G. Mishchenko, Phys. Rev. Lett. **100**, 166802 (2008).
[43] E. V. Gorbar, V. A. Miransky, and I. A. Shovkovy, Phys. Rev. B **88**, 165105 (2013).
[44] P. V. Buividovich, M. Puhr, and S. N. Valgushev, Phys. Rev. B **92**, 205122 (2015).
[45] T. E. Stevens, J. K. Wahlstrand, J. Kuhl, and R. Merlin, Science **291**, 627 (2001).
[46] J. Gonzalez, F. Guinea, and M. Vozmediano, Nucl. Phys. B **424**, 595 (1994).
[47] R. Jackiw and R. Rajaraman, Phys. Rev. Lett. **54**, 1219 (1985).
[48] Y. Ferreiros and A. Cortijo, Phys. Rev. B **89**, 024413 (2014).

Article F

Large conduction band and Fermi velocity spin splitting due to Coulomb interactions in single-layer MoS_2

PHYSICAL REVIEW B **90**, 195426 (2014)

Large conduction band and Fermi velocity spin splitting due to Coulomb interactions in single-layer MoS_2

Yago Ferreiros* and Alberto Cortijo†
Instituto de Ciencia de Materiales de Madrid, CSIC, Cantoblanco, 28049 Madrid, Spain
(Received 19 March 2014; revised manuscript received 13 October 2014; published 19 November 2014)

We study the effect of Coulomb interactions on the low-energy band structure of single-layer transition metal dichalcogenide semiconductors using an effective low-energy model. We show how a large conduction band spin splitting and a spin dependent Fermi velocity are generated in MoS_2, as a consequence of the difference between the gaps of the two spin projections induced by the spin-orbit interaction. The conduction band and Fermi velocity spin splitting found are in agreement with the optical absorption energies of the excitonic peaks A, B measured in the experiments.

DOI: 10.1103/PhysRevB.90.195426 PACS number(s): 73.22.−f, 31.70.−f, 78.67.−n

I. INTRODUCTION

In the post-graphene era [1], the search for new low-dimensional materials has placed the transition metal dichalcogenides (TMDCs) in a prominent situation. Known for decades, these materials share attracting features common to graphene: They are layered materials with strong covalent bonding within layer and weak Van der Waals interlayer forces, perhaps the most known member being molybdenum disulphide (MoS_2) [2]. A subset of the large family of TMDCs are semiconductors, with sizable direct gaps ranging from one to several eV around the K and K' points of the Brillouin zone (BZ) [3]. The presence of a gap in the band structure of these systems is a feature that distinguishes them from graphene and makes these materials highly valuable for electronic and optoelectronic applications.

Apart from their potential applicability in electronics, TMDCs monolayers are also an attractive arena of research in the field of spintronics. The transition metals forming the TMDCs display a rather large intra-atomic spin-orbit interaction. Together with the absence of inversion symmetry of the crystalline structure of TMDCs monolayers, this induces a spin splitting between the two (otherwise degenerate) spin projections in the band structure [3]. Due to time reversal symmetry requirements, this spin splitting is opposite in both valleys, and consequently it allows for controlling valley population employing circularly polarized light [4].

The orbital nature of the electronic states around the K, K' points indicates that the effect of the spin-orbit interaction is quite different for the conduction band (formed predominantly by the $d_{3z^2-r^2}$ orbital, with $m_l = 0$) and the valence band (mostly made of a linear combination of the $d_{x^2-y^2}$ and d_{xy} orbitals, with $m_l = \pm 2$). Such a particular atomic band population implies that the splitting of the valence band is first order in the spin-orbit interaction, while the splitting of the conduction band is second order in the mentioned orbitals and a very small contribution of first order processes of higher energy orbitals [5,6]. According to several density functional theory (DFT) calculations [3,6,7], this favors a weak spin splitting in the conduction band, of the order of a few meV, and a considerably larger splitting in the valence band, of the order of hundreds of meV. On the experimental side, characterization of the low-energy band structure of TMDC semiconductors is still incomplete. The most common procedure to determine the parameters entering in the band structure description, that are later employed in other methods (e.g., in tight binding calculations [8,9]), consists of contrasting experimental data obtained by optical means with theoretical results obtained by solving the GW-corrected Kohn-Sham equations in its several variations with different degrees of success [10].

Here we follow an alternative route: We will use a self consistent GW treatment of the Coulomb interaction together with the effective Hamiltonian around the K, K' points, using experimental data and physically motivated considerations to determine the band structure parameters of the system. We will find, for MoS_2, that a self consistent treatment of the many-body problem based on an unscreened Coulomb interaction, together with an effective low-energy model for the electrons around the K and K' points, gives much larger values for the conduction spin splitting λ_c than the ones reported by *ab initio* calculations, and, importantly, these values are fully consistent with the experimental values reported for the excitonic spectrum.

Our results are pertinent since recently a realization of the quantum spin hall (QSH) phase has been proposed using TMDCs as a viable platform [11]. In this proposal the system has to be doped with holes in order to take into account the large value of the spin splitting in the valence band. However, doping with holes turns out to be much more difficult than doping with electrons from an experimental perspective. Our findings suggest that it is possible to realize such phase also doping with electrons since our results for λ_c are considerably larger than those previously reported in the literature.

The paper is organized as follows: In Sec. II we describe the effective continuum model that captures the essential low-energy physics of TMDCs together with the Coulomb interaction. In Sec. III we define the elements for the self-consistent treatment of the Schwinger-Dyson equation and the quantum corrections to be obtained. In Sec. IV we give a physical description of the conditions that we will employ to reduce the number of free parameters to just two: the coupling constant and the momentum cutoff, putting special emphasis on which conditions come from experimental measurements

*yago.ferreiros@csic.es
†alberto.cortijo@csic.es

and which ones have to be fixed by some other physical insight. In Sec. V we discuss the most salient qualitative features of the solutions obtained, finishing with Sec. VI, where we give a brief account of the results obtained.

II. THE MODEL

We start from the following low-energy bare Hamiltonian density for single-layer TMDC semiconductors close to the K, K' points [3]:

$$\mathcal{H}_0 = \psi^+\left((\tau\sigma_x p_x + \sigma_y p_y)V_\tau^0 + \frac{\Delta^0}{2}\sigma_z s_0\right)\psi + \psi^+\left(\frac{\lambda_c^0}{2}\tau(\sigma_0+\sigma_z)s_z + \frac{\lambda_v^0}{2}\tau(\sigma_0-\sigma_z)s_z\right)\psi, \quad (1)$$

where $(s_0 \equiv \mathbf{1}, s_{x,y,z})$ and $(\sigma_0 \equiv \mathbf{1}, \sigma_{x,y,z})$ are the Pauli and identity matrices for the spin and the sublattice degrees of freedom, respectively, $2\lambda_c^0$ ($2\lambda_v^0$) is the conduction (valence) band splitting, $\tau = \pm 1$ is the valley index, and the matrix V_τ^0 is

$$V_{+1}^0 = \begin{pmatrix} v_+^0 & 0 \\ 0 & v_-^0 \end{pmatrix}; \quad V_{-1}^0 = \begin{pmatrix} v_-^0 & 0 \\ 0 & v_+^0 \end{pmatrix}, \quad (2)$$

with $v_\pm^0$ the Fermi velocities for spin up/down $(+/-)$ electrons. The superscript 0 is the notation used for the bare parameters. Although the Fermi velocities for both spins are assumed to be equal in the absence of interactions (since the hopping parameters should be insensitive to spin), we define the bare Fermi velocity for each spin separately, because as we will see, quantum corrections renormalize each velocity differently. Also we neglect terms of second order in momentum in a $\mathbf{k}\cdot\mathbf{p}$ scheme [9] that are not relevant in the discussion in the next sections. Coulomb interaction will be modeled by a coupling to an auxiliary scalar field φ [12]:

$$\mathcal{H}_{\text{int}} = e\psi^\dagger\psi\varphi + \epsilon\varphi|\vec{\nabla}|\varphi, \quad (3)$$

where ϵ is the dielectric permitivity (we use units $\hbar = 1$ at the intermediate stages, restoring standard units at the end of the calculations).

III. SCHWINGER-DYSON EQUATIONS

To self-consistently find the effects of the interaction on the low-energy band structure we shall make use of the Schwinger-Dyson equation for the electron propagator [13–15]:

$$\Sigma_\tau(p) = e^2\int\frac{d^3q}{(2\pi)^3}D(q)G_\tau(p-q), \quad (4)$$

where $D(q)^{-1} = \epsilon|\vec{q}| + \Pi(q)$ is the (inverse of the) dynamically screened Coulomb interaction (with $\Pi(q)$ the dressed polarization function) and $G_\tau(p)^{-1} = G_0^{-1}(p) + \Sigma_\tau(p)$ is the (inverse of the) full fermion propagator. The form of the self-energy $\Sigma_\tau(p)$ can be parametrized in terms of corrections to the bare parameters defined in Eq. (1):

$$\Sigma_\tau(p) = -(\tau\sigma_x p_x + \sigma_y p_y)\delta V_\tau - \frac{\delta\Delta}{2}\sigma_z s_0 - \frac{\delta\lambda_c}{2}\tau(\sigma_0+\sigma_z)s_z - \frac{\delta\lambda_v}{2}\tau(\sigma_0-\sigma_z)s_z. \quad (5)$$

The renormalized parameters are defined as the sum of the bare parameters plus the quantum corrections:

$$\Delta = \Delta^0 + \delta\Delta, \quad \lambda_{c,v} = \lambda_{c,v}^0 + \delta\lambda_{c,v}, \quad v_\pm = v_\pm^0 + \delta v_\pm. \quad (6)$$

Only terms up to order one in momentum have been taken into account in the definition of the self-energy, being consistent with the low-energy expansion of the effective Hamiltonian (1), which is also first order. Note also that in Eq. (4) we could have chosen a different run of momentum $D(p-q)G_\tau(q)$, as both runs are consistent with momentum conservation, and both give the same final result.

The computation of $\Pi(q)$ to leading order in a $1/N$ expansion, where N is the number of fermion flavors ($N = 2$ in our case, one for each valley), is a standard calculation and the result reads [15,16]:

$$\Pi(q) = \frac{e^2}{4\pi}|\vec{q}|^2\sum_{s=\pm}\left[\frac{2m_s}{q_s^2} + \frac{q_s^2 - 4m_s^2}{q_s^3}\arctan\left(\frac{q_s}{2m_s}\right)\right], \quad (7)$$

where $s = \pm$ denotes the spin degrees of freedom, $q_s^2 = q_0^2 + v_s^2|\vec{q}|^2$, $m_+ = (\Delta + \lambda_c - \lambda_v)/2$, and $m_- = (\Delta - \lambda_c + \lambda_v)/2$.

In what follows we will work with only one of the two valleys, $\tau = +1$, since it can be easily seen that the equations obtained for one valley are equivalent to those obtained for the other valley just by changing the sign of the spin splitting. The next step is to compute

$$e^2\int\frac{d^3q}{(2\pi)^3}D(q)G_{+1}(p-q) \equiv \begin{pmatrix} I_+(p) & 0 \\ 0 & I_-(p)\end{pmatrix}, \quad (8)$$

with

$$I_s(p) = -I_s^z\sigma_z - v_s I_s(\sigma_x p_x + \sigma_y p_y) + \mathcal{O}(p^2). \quad (9)$$

Performing the integral in Eq. (8) we obtain (see Appendix A for details on the computation of the fermionic self-energy):

$$I_s^z = \frac{3m_r}{4}\ln\left(1 + \frac{2g_s m_s}{3m_r}\right) + \frac{g_s m_s}{2+\pi g_r}\ln\left(\frac{\Lambda v_s}{m_s}\right), \quad (10a)$$

$$I_s = \frac{3m_r}{4m_s}\ln\left(1 + \frac{2g_s m_s}{3m_r}\right) + \frac{g_s}{4+2\pi g_r}\ln\left(\frac{\Lambda v_s}{m_s}\right), \quad (10b)$$

where Λ is a momentum cutoff and we have defined:

$$g_s = e^2/(4\pi\epsilon v_s); \quad g_r = e^2/(4\pi\epsilon v_r), \quad m_r = \frac{2\,m_+m_-}{m_+ + m_-}; \quad v_r = \frac{2\,v_+v_-}{v_+ + v_-}. \quad (11)$$

In terms of the quantities $I_s^z(p)$, and $I_s(p)$, the Schwinger-Dyson equations are written as

$$\Sigma(p) = \begin{pmatrix} I_+(p) & 0 \\ 0 & I_-(p)\end{pmatrix}. \quad (12)$$

Equation (12) is a set of four equations for the diagonal elements (two for each spin), from which only three are linearly independent, and four equations for the off-diagonal elements, from which only two (one for each spin) are linearly independent. Thus we have five linearly independent equations for five variables:

$$\frac{\delta\Delta}{2} + s\delta\lambda_c = I_s^z, \quad \frac{\delta\Delta}{2} - \delta\lambda_v = I_+^z, \quad \delta v_s = v_s I_s. \quad (13)$$

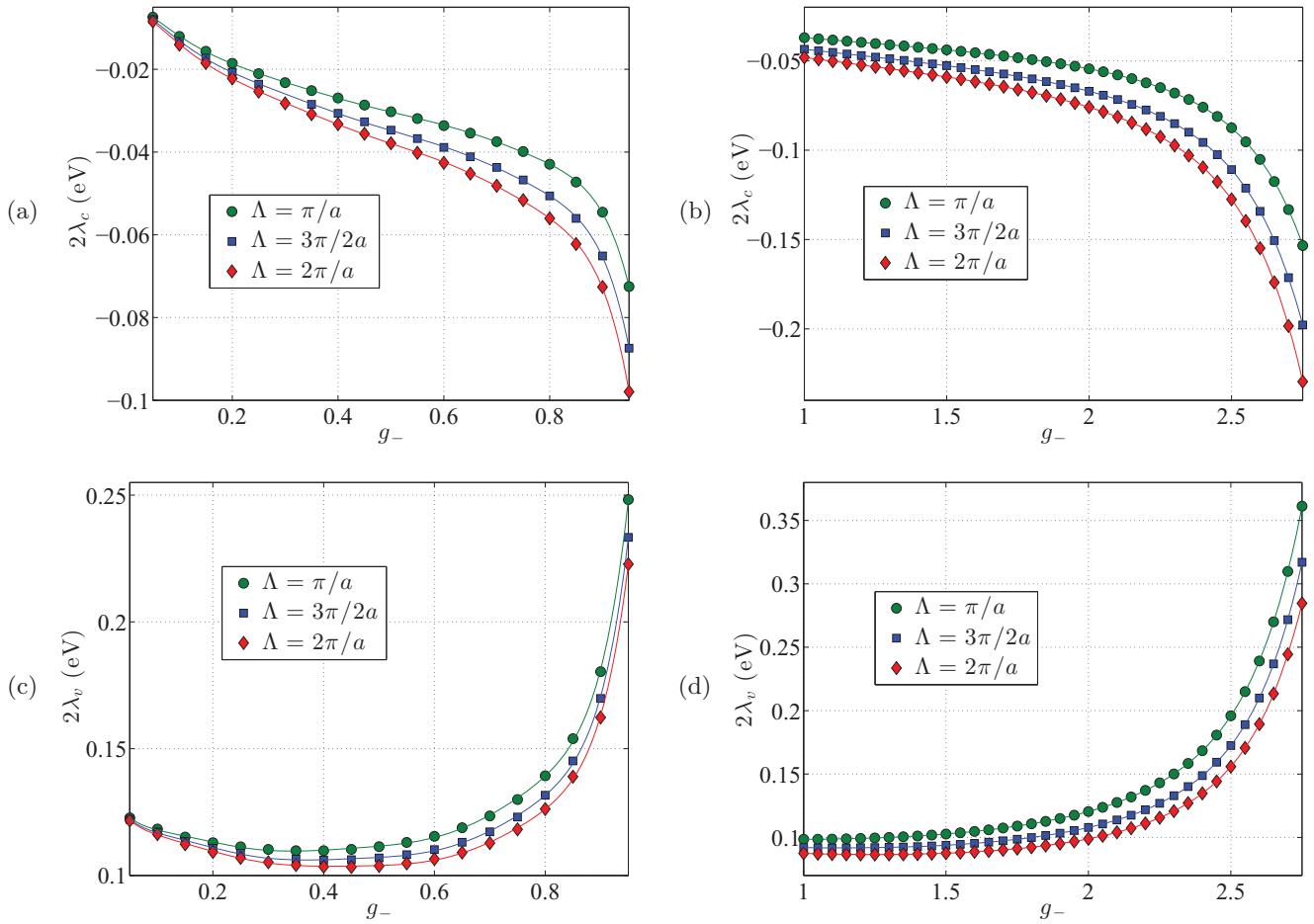

FIG. 1. (Color online) Values for the $\tau = +1$ valley of conduction band splitting [(a),(b)] and valence band splitting [(c),(d)] as a function of the corrected coupling constant for spin down electrons g_-, for three different values of the momentum cutoff (in units of $\hbar$).

From these equations we can obtain the quantum corrections $\delta\Delta, \delta\lambda_{c,v}, \delta v_\pm$ as functions of the bare parameters $\Delta^0, \lambda^0_{c,v}, v^0_\pm$, and the cutoff Λ.

IV. MATCHING THE EXPERIMENTAL DATA

To eliminate the dependence of the quantum corrections on the bare parameters and the cutoff one needs to impose renormalization conditions, which should be obtained from experiments. In the case of single layer TMDC semiconductors some of the most relevant data are the energies of two excitonic peaks A, B found in absorbance experiments in MoS_2 [2,4,17,18], which provide two renormalization conditions.

We will focus our attention on MoS_2, as this is the most studied compound of the family of TMDCs, both theoretically and experimentally. For MoS_2 on a quartz substrate, the excitonic peaks A, B found in absorbance experiments are centered at energies of $E_A = 1.85$ eV and $E_B = 1.98$ eV [17]. The absorption energy difference between these two peaks is a direct consequence of the splitting of the spin up and spin down bands. *Ab initio* calculations give a very small conduction band splitting of approximately $2|\lambda_c| \sim 3$ meV [6,7,10,19–22]. Hence, according to first-principles-based calculations, the difference between the optical absorption energies of the peaks A and B is related almost entirely to a large value of the valence band splitting [10,21,22]. Even analytical calculations of the excitonic properties of MoS_2 use as an input the parameter values obtained by *ab initio* calculations [23].

The optical absorption energies of the excitonic bound states are obtained by solving the two particle problem for the Dirac equation. The expression for the optical absorption energies of the excitons is [24,25]

$$E_s = m_s \left(1 + \frac{n + \sqrt{j^2 - g_s^2/4}}{\sqrt{g_s^2/4 + \left(n + \sqrt{j^2 - g_s^2/4}\right)^2}} \right), \qquad (14)$$

where $n = 0, 1, 2 \ldots$ is the principal quantum number and $j = \pm 1/2, \pm 3/2 \ldots$ is the angular quantum number. The two lowest energy excitonic configurations are $n = 0, |j| = 1/2$ and $n = 0, |j| = 3/2$. The case $|j| = 1/2$ is valid for $g_\pm < 1$ while the case $|j| = 3/2$ is valid for $g_\pm < 3$, as for larger values of the coupling constant the energies would become imaginary and an ultraviolet regularization would be needed to deal with the singularity of the Coulomb potential [25–27]. By

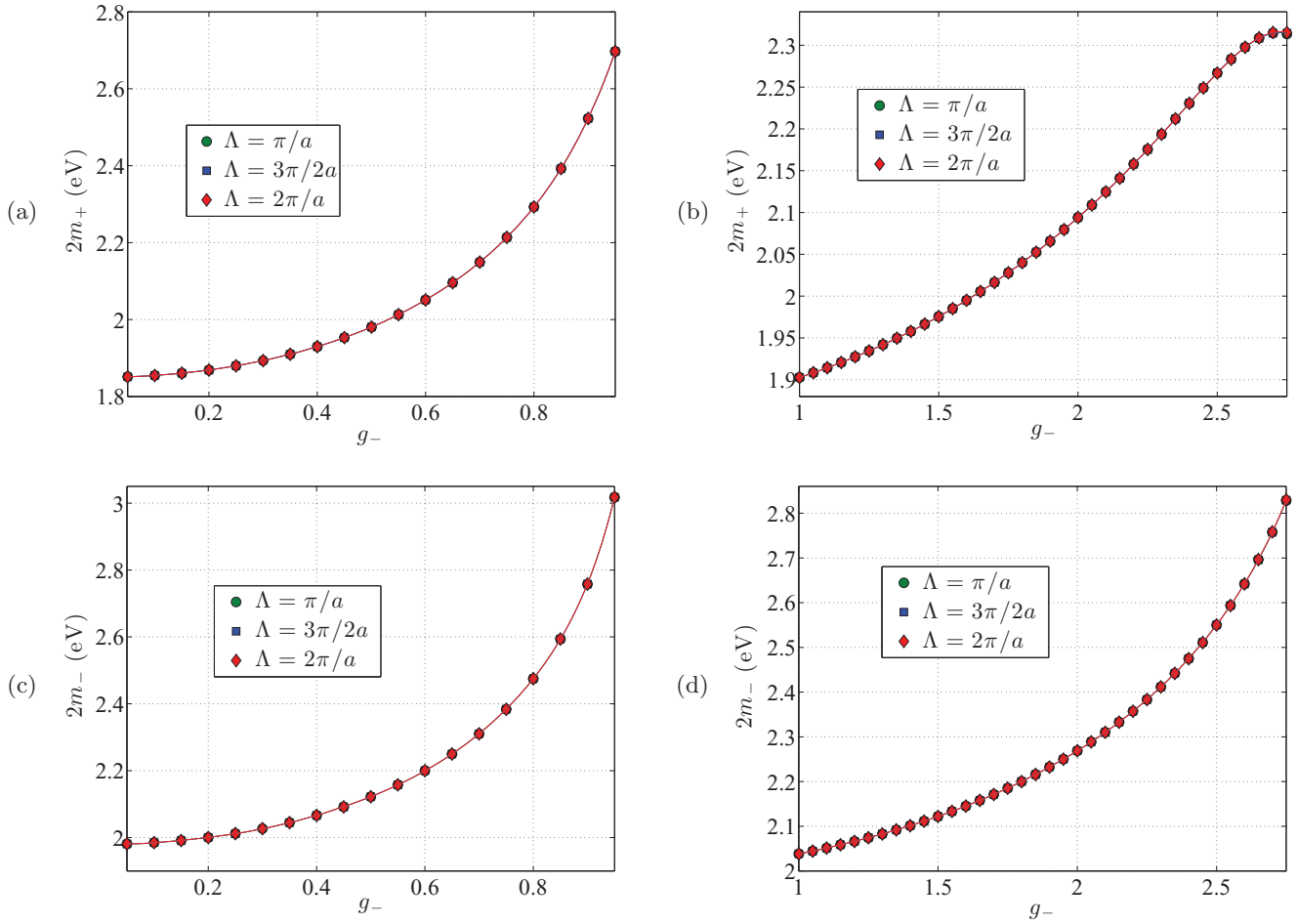

FIG. 2. (Color online) Values for the $\tau = +1$ valley of the gap for the spin up electrons [(a),(b)] and gap for the spin down electrons [(c),(d)] as a function of the corrected coupling constant for spin down electrons g_-, for three different values of the momentum cutoff (in units of $\hbar$).

introducing this regularization, it can be seen that in the strong coupling regime [that in which the optical absorption energies of the excitons given by Eq. (14) become imaginary] the excitonic bound energies become negative and the excitonic bound states ultimately merge with the continuum [25,27].

This dramatic decrease of the excitonic energies in the strong coupling regime means that for $1 < g_\pm < 3$, the lowest excitonic state corresponding to the excitonic peaks A, B seen in the experiments should no longer be $n = 0, |j| = 1/2$, but actually be the second lowest energy configuration $n = 0, |j| = 3/2$. Hence, we have a scenario in which for the small coupling regime, $g_\pm < 1$, the observed peaks A, B correspond to the state $n = 0, |j| = 1/2$, while for the strong coupling regime $1 > g_\pm < 3$ they correspond to the state $n = 0, |j| = 3/2$:

$$E_{A,B} = E_{+,-}(n = 0, |j| = 1/2) \quad g_\pm < 1 \tag{15}$$

$$E_{A,B} = E_{+,-}(n = 0, |j| = 3/2) \quad 1 < g_\pm < 3. \tag{16}$$

It has already been proposed in a previous work [28] that the lowest bright excitons correspond to $|j| = 3/2$ in the strong coupling regime $g_\pm > 1$. In that paper the ground state is claimed to be the lowest excitonic bound state $n = 0, |j| = 1/2$, and the transition from the ground state to the bright excitonic states is actually a transition between proper excitonic states. They concluded that only transitions to states with $|j| = 3/2$ are allowed in the strong coupling regime.

Equations (15) and (16) give two experimental conditions that have to be fulfilled by the renormalized parameters $\Delta, \lambda_{c,v}, v_\pm$. The dielectric permittivity ϵ that enters in the coupling constant $g_\pm$ can be written as $\epsilon = \epsilon_0(1 + \epsilon_s)/2$, ϵ_0 being the dielectric permittivity of the vacuum and ϵ_s the dielectric constant of the substrate. As the experimental absorption energies are obtained using a quartz substrate, we have $\epsilon_s = 3.9$. Notice that Eq. (14) assumes equal hole and electron effective masses.

As we already said, the energies in Eq. (14) are obtained by solving the two particle problem [17]. This is a sensible approach since we are working in the instantaneous approximation, so the self consistent solution of the Schwinger-Dyson equations provides no term proportional to the frequency p_0 in Eq. (9). This implies that there is no wave function renormalization Z_ψ, and there is no loss of electronic coherence [29]. This fact, together with the absence of any imaginary part in $\Sigma_\tau(p)$, means that the poles in the full two-particle propagator will coincide with the ones in the noninteracting two particle

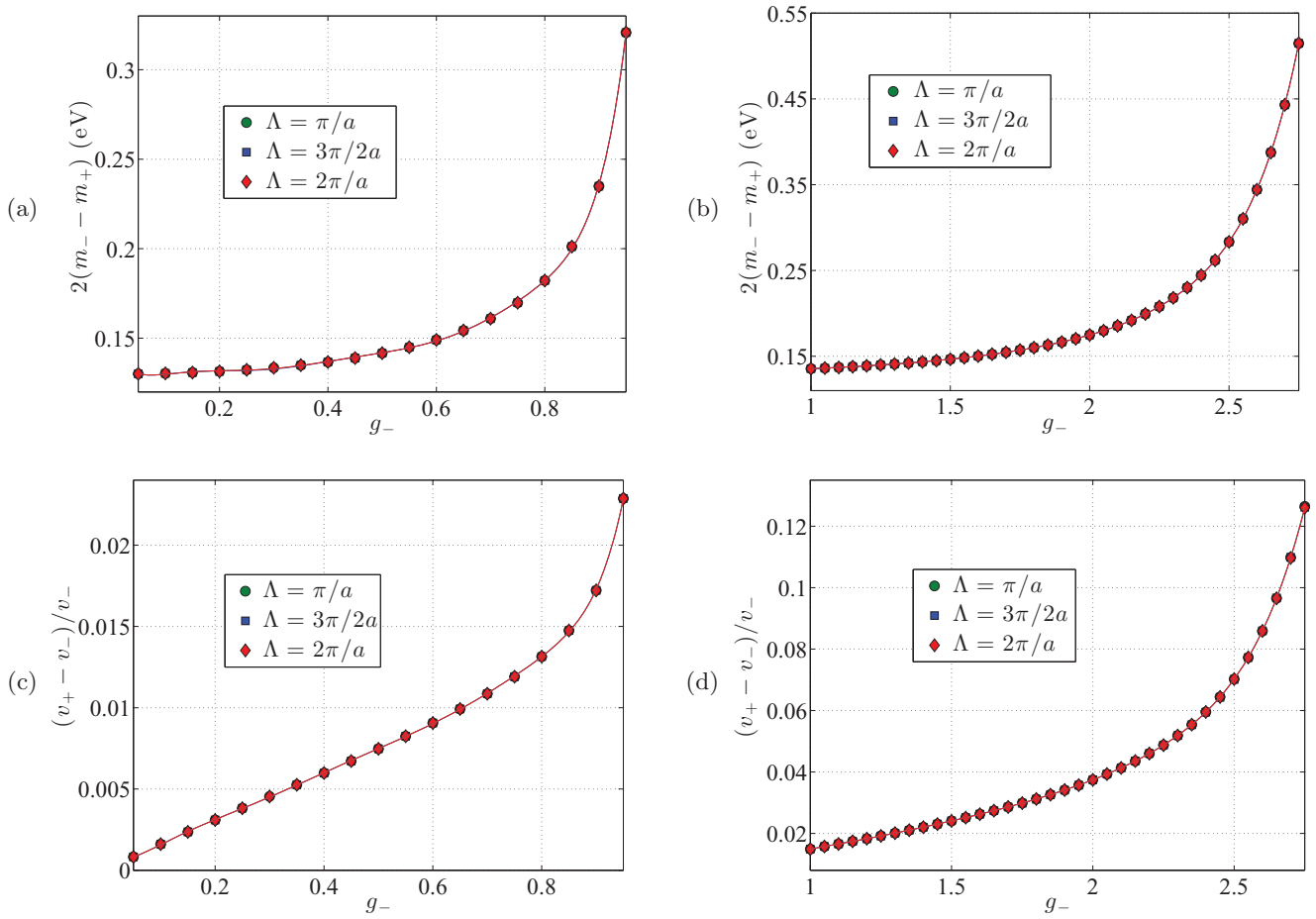

FIG. 3. (Color online) Values for the $\tau = +1$ valley of the gap difference between spin down and up electrons [(a),(b)] and normalized Fermi velocity difference between spin up and down electrons [(c),(d)], as a function of the corrected coupling constant for spin down electrons g_-, for three different values of the momentum cutoff (in units of $\hbar$).

propagator, but dressed with the renormalized parameters in the Green functions [30].

Since the excitonic data are not enough to fully execute the renormalization program, we are forced to impose two additional conditions so that the renormalized parameters will depend only on one bare parameter and the cutoff. At very small interactions (at very high dielectric permittivity $\epsilon \to \infty$), we will force a zero conduction band splitting $\lambda_c = 0$ and equal Fermi velocities for both spin projections $v_+ = v_-$. The motivation for this choice comes from the fact that for $\epsilon \to \infty$ quantum corrections are negligible (assuming a finite physical cutoff), and the conduction band should remain (approximately) degenerate in spin due to the nature of the wave functions [5], while the hopping parameters should be insensitive to spin. In this limit the conditions on the renormalized parameters translate to conditions on the bare parameters: $\lambda_c^0 = 0$ and $v_+^0 = v_-^0$.

Since we have imposed two extra conditions, we still have two free parameters: v_+^0/v_-^0 and the momentum cutoff Λ. We will solve the Schwinger-Dyson equations for different values of the cutoff and the Fermi velocity bare parameter, and give the results as a function of the renormalized coupling constant g_-.

V. SOLUTION OF THE SCHWINGER-DYSON EQUATIONS

We will present the results for one of the two valleys ($\tau = +1$). The values for the other valley are obtained by changing the sign of $\lambda_{c,v}$, and consequently interchanging the values of the masses ($m_+ \leftrightarrow m_-$) and the Fermi velocities ($v_+ \leftrightarrow v_-$).

In Figs. 1–3 the values of different renormalized parameters as functions of g_- are plotted for three different values of Λ, and for the two regimes $g_- < 1$ and $1 < g_- < 3$. The general behavior when g_- approaches the critical values $g_-^c = 1$ and $g_+^c = 3$ will be modified with a proper regularization of the Coulomb potential. This regularization will make the calculations more involved, but this treatment is possible within the presented theoretical framework. Also, this regularization allows for a more accurate computation of the critical value of g_- corresponding to the point when the excitonic states will merge to the continuum, and the observed excitonic peaks are no longer expected to correspond to the lowest energy state $|j| = 1/2$, but rather to the first excited state $|j| = 3/2$. Also let us remember that all the plotted values are constrained to match the experimental energies of the excitonic peaks E_A and E_B. As an example, for a coupling constant $g_- = 2$ and a physical momentum cutoff $\Lambda = 2\hbar\pi/a$ (the lattice constant

is taken to be $a = 3.193$ Å [3]), we have a scenario with a conduction band splitting $2|\lambda_c| \approx 75$ meV, fully compatible with the measured optical absorption energies of the excitonic peaks A, B.

Both the gaps and the difference between spin up and down Fermi velocities are cutoff independent. For the Fermi velocity difference, the independence on the cutoff Λ can be derived from Eqs. (10b) and (13). The correction to the Fermi velocity is given by $\delta v_s = v_s I_s$, and if we do $\delta v_+ - \delta v_-$, the two logarithms which give the explicit dependence on Λ are subtracted, so the explicit dependence vanishes. There is however an implicit dependence on Λ coming from v_s and m_s. From conditions of Eqs. (15) and (16) we obtain m_s as a function of v_s, so all the implicit dependence on the cutoff lies in v_s. With the extra condition $v_+^0 = v_-^0$, we can write $v_+ = v_- + \delta v_+ - \delta v_-$, and for any given v_- we have an equation for $\delta v_+ - \delta v_-$ independent of Λ. With the Fermi velocity difference being cutoff independent, from conditions of Eqs. (15) and (16) one automatically obtains cutoff independent masses for each spin.

VI. SUMMARY

Large conduction band and Fermi velocity spin splitting are found due to the effect of Coulomb interactions, fully consistent with optical absorption measurements. The ultimate reason for these splittings is the presence of a different gap for the two spin polarization species, product of spin-orbit interaction, which induces a different renormalization of the gap and Fermi velocities of the two spin projections. To ensure consistency with absorption experiments, we used the values of the measured energies of the excitonic peaks of MoS_2 on a quartz substrate as renormalization conditions.

ACKNOWLEDGMENTS

A.C. gratefully acknowledges conversations with M. A. H. Vozmediano and R. Asgari at the early stages of this project, and with E. Cappelluti. This research is partially supported by CSIC JAE-doc fellowship program and the Spanish MECD Grant Nos. FIS2011-23713 and PIB2010BZ-00512.

APPENDIX: COMPUTATION OF THE FERMIONIC SELF-ENERGY

To obtain the self-energy we need to compute the integral of Eq. (8):

$$\Sigma(p) \equiv \begin{pmatrix} I_+(p) & 0 \\ 0 & I_-(p) \end{pmatrix} = e^2 \int \frac{d^3q}{(2\pi)^3} D(q) G_{+1}(p-q), \tag{A1}$$

with, keeping terms up to first order in p,

$$I_s(p) = -\begin{pmatrix} I_s^{(1)} & 0 \\ 0 & I_s^{(2)} \end{pmatrix} - v_s I_s (\sigma_x p_x + \sigma_y p_y). \tag{A2}$$

First we shall obtain the asymptotic behavior of the scalar field self-energy $\Pi(q)$, given by Eq. (7), in the limits of low and high momenta. We work in the instantaneous approximation $q_0 = 0$. For $v_s|\vec{q}| \ll m_s$ we have

$$\Pi(|\vec{q}|) = \frac{e^2}{3\pi m_r}|\vec{q}|^2, \tag{A3}$$

while in the opposite limit, $v_s|\vec{q}| \gg m_s$:

$$\Pi(|\vec{q}|) = \frac{e^2}{4v_r}|\vec{q}|. \tag{A4}$$

Now, from the low-energy Hamiltonian (1) one can extract the inverse bare fermion propagator. Inverting it and replacing the bare parameters by the renormalized ones, we get the full fermion propagator which enters the integral (A1). Inserting the explicit values of $D(q)$ and $G_{+1}(p-q)$ we have

$$I_s^{(j)} = i2\pi g_s \left(\int_0^{m_s} \frac{d|\vec{q}|}{2\pi} \left(1 + \frac{4g_s}{6m_r}|\vec{q}|\right)^{-1} + (1+\pi g_r/2)^{-1} \int_{m_s}^{\Lambda v_s} \frac{d|\vec{q}|}{2\pi} \right) \times \int_{-\infty}^{\infty} \frac{dq_0}{2\pi} g_0^s(q) \left(q_0 + i(-1)^j \frac{\Delta}{2} + s\, i((j-1)\lambda_c + (2-j)\lambda_v) \right), \tag{A5}$$

$$I_s = 2\pi g_s \left(\int_0^{m_s} \frac{d|\vec{q}|}{2\pi} \left(1 + \frac{4g_s}{6m_r}|\vec{q}|\right)^{-1} + (1+\pi g_r/2)^{-1} \int_{m_s}^{\Lambda v_s} \frac{d|\vec{q}|}{2\pi} \right) \int_{-\infty}^{\infty} \frac{dq_0}{2\pi} g_0^s(q) \left(1 - |\vec{q}|^2 g_0^s(q)\right), \tag{A6}$$

with:

$$g_0^s(q) = \left(\left(q_0 + s\,\frac{i}{2}(\lambda_c + \lambda_v) \right)^2 + |\vec{q}|^2 + m_s^2 \right)^{-1}. \tag{A7}$$

Note that we divided the momentum integral in two regions, one for $v_s|\vec{q}| \ll m_s$ and another for $v_s|\vec{q}| \gg m_s$, using the expansions of Eqs. (A3) and (A4). Note also that we introduced a momentum cutoff Λ, as the momentum integrals diverge. When doing the integrals in q_0 one should be careful and expand the results in $|\vec{q}|$ accordingly for each momentum integral region $v_s|\vec{q}| \ll m_s$ and $v_s|\vec{q}| \gg m_s$. Doing the integrals we finally arrive at

$$I_s^{(j)} = (-1)^{j+1} I_s^z, \tag{A8a}$$

$$I_s^z = \frac{3m_r}{4} \ln\left(1 + \frac{2g_s m_s}{3m_r}\right) + \frac{g_s m_s}{2+\pi g_r} \ln\left(\frac{\Lambda v_s}{m_s}\right), \tag{A8b}$$

$$I_s = \frac{3m_r}{4m_s} \ln\left(1 + \frac{2g_s m_s}{3m_r}\right) + \frac{g_s}{4+2\pi g_r} \ln\left(\frac{\Lambda v_s}{m_s}\right), \tag{A8c}$$

which are the expressions used in the main text.

[1] A. H. Castro Neto, F. Guinea, N. M. R. Peres, K. S. Novoselov, and A. K. Geim, Rev. Mod. Phys. **81**, 109 (2009).
[2] K. F. Mak, C. Lee, J. Hone, J. Shan, and T. F. Heinz, Phys. Rev. Lett. **105**, 136805 (2010).
[3] D. Xiao, G.-B. Liu, W. Feng, X. Xu, and W. Yao, Phys. Rev. Lett. **108**, 196802 (2012).
[4] K. F. Mak, K. He, J. Shan, and T. F. Heinz, Nature Nanotechnology **7**, 494 (2012).
[5] H. Ochoa and R. Roldán, Phys. Rev. B **87**, 245421 (2013).
[6] A. Kormányos, V. Zólyomi, N. D. Drummond, P. Rakyta, G. Burkard, and V. I. Fal'ko, Phys. Rev. B **88**, 045416 (2013).
[7] K. Kośmider, J. W. González, and J. Fernández-Rossier, Phys. Rev. B **88**, 245436 (2013).
[8] E. Cappelluti, R. Roldán, J. A. Silva-Guillén, P. Ordejón, and F. Guinea, Phys. Rev. B **88**, 075409 (2013).
[9] H. Rostami, A. G. Moghaddam, and R. Asgari, Phys. Rev. B **88**, 085440 (2013).
[10] D. Y. Qiu, F. H. da Jornada, and S. G. Louie, Phys. Rev. Lett. **111**, 216805 (2013).
[11] M. A. Cazalilla, H. Ochoa, and F. Guinea, Phys. Rev. Lett. **113**, 077201 (2014).
[12] J. González, F. Guinea, and M. A. H. Vozmediano, Phys. Rev. B **59**, R2474 (1999).
[13] F. J. Dyson, Phys. Rev. **75**, 1736 (1949).
[14] J. Schwinger, PNAS **37**, 452 (1951).
[15] T. W. Appelquist, M. Bowick, D. Karabali, and L. C. R. Wijewardhana, Phys. Rev. D **33**, 3704 (1986).
[16] A. N. Redlich, Phys. Rev. D **29**, 2366 (1984).
[17] A. Splendiani, L. Sun, Y. Zhang, T. Li, J. Kim, C.-Y. Chim, G. Galli, and F. Wang, Nano Lett. **10**, 1271 (2010).
[18] K. F. Mak, K. He, C. Lee, G. H. Lee, J. Hone, T. F. Heinz, and J. Shan, Nature Materials **12**, 207 (2013).
[19] E. S. Kadantsev and P. Hawrylak, Solid State Communications **152**, 909 (2012).
[20] K. Kośmider and J. Fernández-Rossier, Phys. Rev. B **87**, 075451 (2013).
[21] T. Cheiwchanchamnangij and W. R. L. Lambrecht, Phys. Rev. B **85**, 205302 (2012).
[22] A. Molina-Sánchez, D. Sangalli, K. Hummer, A. Marini, and L. Wirtz, Phys. Rev. B **88**, 045412 (2013).
[23] G. Berghäuser and E. Malic, Phys. Rev. B **89**, 125309 (2014).
[24] V. R. Khalilov and C.-L. Ho, Modern Physics Letters A **13**, 615 (1998).
[25] A. S. Rodin and A. H. Castro Neto, Phys. Rev. B **88**, 195437 (2013).
[26] D. S. Novikov, Phys. Rev. B **76**, 245435 (2007).
[27] V. M. Pereira, V. N. Kotov, and A. H. Castro Neto, Phys. Rev. B **78**, 085101 (2008).
[28] T. Stroucken and S. W. Koch, arXiv:1404.4238.
[29] C. Popovici, C. S. Fischer, and L. von Smekal, Phys. Rev. B **88**, 205429 (2013).
[30] O. V. Gamayun, E. V. Gorbar, and V. P. Gusynin, Phys. Rev. B **80**, 165429 (2009).